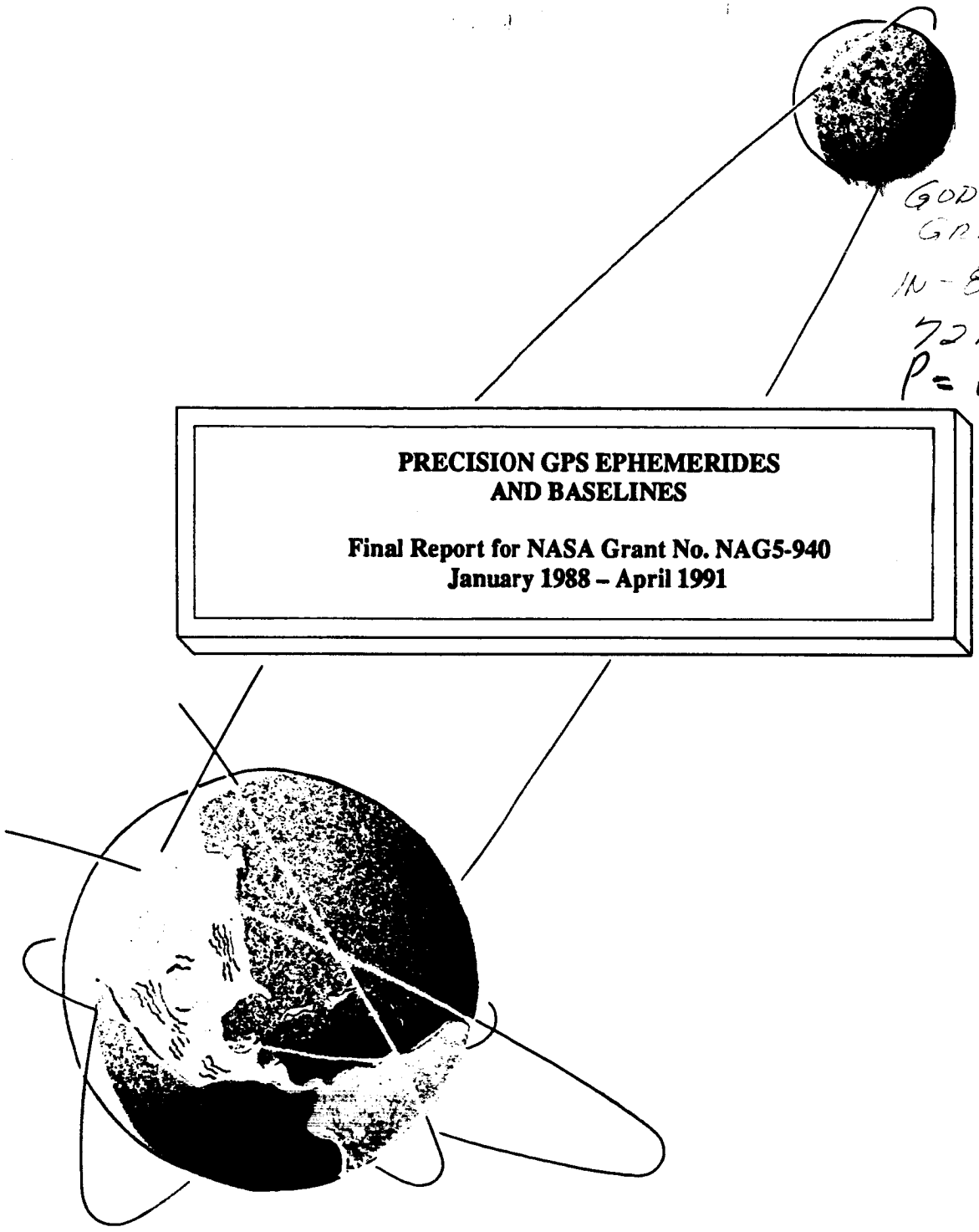

PRECISION GPS EPHEMERIDES AND BASELINES

Final Report for NASA Grant No. NAG5-940
January 1988 – April 1991

CENTER FOR SPACE RESEARCH

THE UNIVERSITY OF TEXAS AT AUSTIN AUSTIN, TEXAS

PRECISION GPS EPHEMERIDES AND BASELINES
NASA GRANT NO. NAG5-940

FINAL REPORT
JANUARY 1988 – APRIL 1991

Introduction

The NAVSTAR Global Positioning System (GPS) satellites are being used in a wide range of civilian applications besides their intended use for navigation by the Department of Defense's military applications. Applications can be divided into two broad categories, namely, navigation and static positioning (absolute or relative). Knowledge of the position of the satellites is fundamental to all the applications of GPS. The required knowledge of the GPS satellite position accuracy can vary depending on a particular application. Application to relative positioning of receiver locations on the ground to infer Earth's tectonic plate motion requires the most accurate knowledge of the GPS satellite orbits. Research conducted at the University of Texas Center for Space Research (CSR) under the NASA grant NAG5-940 was directed towards improving and evaluating the accuracy of GPS satellite orbits. This reports summarizes the activities of CSR in improving GPS satellite orbits, during the grant period from Jan 1988 to April 1991. Major focus was on the understanding and modeling of the forces acting on the satellites besides paying close attention to reference frame, time system, measurement modeling, parameterization and other aspects of orbit determination. Gravitational forces were modeled by truncated versions of extant gravity fields such as, GEM-L2, GEM-T1 or TEG-2 and third body perturbations due to Sun and Moon. Nongravitational forces considered were the solar radiation pressure, and perturbations due to thermal venting and thermal imbalance. At the GPS satellite orbit accuracy level required for crustal dynamic applications, models for the nongravitational perturbations play a critical role, since the gravitational forces are well understood and are modeled adequately for GPS satellite orbits. With these considerations,

CSR's activities during the grant period were in the following areas:

1. Computation and distribution of weekly GPS satellite ephemerides
2. Global versus regional orbit comparison
3. Signal multipath effects
4. CASA UNO campaign data analysis
5. Southwest Pacific campaign data analysis
6. Reference frame comparison
7. Modeling of thermal imbalance force perturbation
8. Eclipsing satellite orbit prediction error
9. Effects of mixed receiver types
10. Effects of selective availability (SA)

In the following, each of the above topics will be described briefly, and relevant publication/meeting presentation will be quoted.

1. Weekly Ephemerides

Pseudo-range measurements from all the GPS satellites collected at the CIGNET sites (three in late 1986 expanding to nine by 1988) were processed routinely to produce precise ephemerides of the satellites. The ephemerides were written in the 'NGS Format' and were distributed to the participants of data collection and the sponsors of the network, namely, NGS at Rockville, Maryland, USGS at Menlo Park, California, Texas State Highway Department at Austin, Texas, CGS at Ottawa, Canada, (through NGS to) Institut fuer Angewandte Geodaesie (IFAG), Germany, and the Norwegian Geodetic Survey at Tromso, Norway. Apart from regular weekly distribution of the GPS ephemerides to the above agencies, from time to time requests for precise ephemerides for specific GPS weeks by other institutes in the U.S. (CCAR, UNAVCO etc.), England and Australia

were fulfilled. Precise ephemerides computed using GPS carrier phase measurements were distributed for specific weeks covering GPS campaigns. For examples of characteristics of orbits distributed see Appendix I.

2. Comparison of Orbits Obtained Using Data From Global and Regional Network

The Cooperative International GPS Network (CIGNET) started with three ground stations in the continental U.S. and with time expanded in the U.S. and to Europe, Japan and Australia. Since the accuracy of GPS satellite ephemerides is fundamental to baseline computation applications, effects of changing the ground station network distribution on the orbit accuracy is an important aspect to be considered. At the time of this analysis the distribution of stations contributing data for routine GPS orbit computation was not really global, but were restricted to U.S. and northern Europe. Five stations in the north American continent (Yellowknife, Mojave, Westford, Richmond, Austin) and three in Europe (Wettzell, Onsala, Tromso) were considered in orbit determination experiments using only the pseudo-range observations. Solutions for several weeks were computed using data from the five stations in the North American continent only or from all the eight stations mentioned above. Trajectories were computed for individual GPS satellites using solutions of these two cases and compared in order to find any common characteristics that be present. Depending on the relative amounts of data and the geometry of coverage, the differences between the ephemeris determined using data from North American stations only and using data from all the eight stations, varied from about 4 meters to about 40 meters. Although these numbers are not the accuracies of the orbits, they are an indication of the effects of network distribution, geometry and the amount of data. Orbit accuracy itself could be inferred through baseline estimates or through comparison to orbits with known accuracy computed by other organizations. However, during the period of this analysis such evaluations were not attempted. Details of this study were reported in a Master's Thesis by Vince Pollmeier, and the summary and conclusions of this thesis are presented in Appendix II.

3. Signal Multipath and Choke Ring Experiment

Degradation of accuracy of the GPS measurements, namely, pseudo-range and carrier phase, due to signal multipath is an aspect that has been treated with considerable importance in the hardware (receiver and antenna) design and in the data analysis. Measurement accuracy directly impacts the orbit accuracy and hence every attempt is made to improve accuracy of GPS measurement. Signal multipath is a phenomenon in which the radio waves coming directly from the GPS satellite are corrupted by their reflections off of any nearby surfaces which can reflect radio waves. Since the P-code pseudo-ranges are computed by time correlation of the P-code signal with that generated at the receiver, its accuracy is affected by multipath much more than that of carrier phase which involves only the measuring of the phase of the carrier. The difference could be as high as two orders of magnitude. Although in geodetic applications only carrier phase is used as the measurement of choice due to its precision, the pseudo-range is essential to one or more of the following necessities of data processing, namely, phase ambiguity resolution, cycle-slip detection and fixing, measurement time-tag correction. In order for the pseudo-range to be effective in its above mentioned uses, its accuracy should be as high as possible; higher the accuracy, lesser would be be the averaging time needed. Pseudo-range accuracy level that is less than the wavelength of its carrier is desirable. For this reason several antenna designs have been studied and experimented by JPL. One of the experiments conducted by JPL was to use a choke ring antenna in place of the regular TI-4100 antenna to collect data at the Mojave CIGNET site for a few days. This data set was analyzed at CSR, and some of the results were presented at the GPS Workshop held at JPL during the Spring of 1988. A part of the presentation is included in Appendix III. CSR also cooperated with personnel at USGS Menlo Park, California, in their experiments and analysis of data to determine the effect of multipath error on accuracies of baseline determinations. The abstract of the paper presented by USGS personnel at the spring 1989 meeting of the American Geophysical Union at Baltimore,

Maryland, is included in Appendix III.

4. CASA UNO Data Analysis

During January and February of 1988, the Jet Propulsion Laboratory, in cooperation with other agencies (national and international), conducted an epoch measurement experiment in South America and in South Pacific. Data were collected from stations in North and South America, Hawaii, South Pacific and Australia in conjunction with the CIGNET stations (in terms of tracking scenario and collection interval). The campaign period was about three weeks during the 'GPS Weeks' 419, 420 and 421. Precise GPS ephemerides using pseudo-range and phase measurements and baselines between various sites were determined using this data set. Extensive analysis has been performed at CSR using this data set over the past two years concentrating on various aspects of determining precise GPS satellite orbits and accurate baselines between tracking sites. Force model fidelity, numerical integration accuracy, proper reference frame for geodetic applications of GPS and estimation strategies were some of the topics that were scrutinized closely, using this and other data sets. Results of analysis of which this data set formed a major part were published in various forms (meeting presentations, journal article, thesis, dissertation) part or whole of which are included in Appendix IV.

5. Southwest Pacific Campaign Data Analysis

Tonga Trench in the southwest Pacific region is considered to be one of the most active fault zones in the world, and GPS campaigns (sponsored jointly by NSF, NASA and UNAVCO) were conducted during three consecutive summers of 1988, 1989 and 1990, to study plate motion around this zone. CSR participated in the campaign planning and preparation and in data processing. Precise GPS ephemerides were computed for selected weeks during each of these campaign periods. These include weeks 444,445 in 1988, weeks 498 to 501 in 1989 and weeks 549 to 551 in 1990.

Extensive analysis of some of the baselines in this region and evaluation of GPS satellite orbit accuracy have been performed using these data sets and are being continued. Although neither SLR nor VLBI measurements of baselines in this region is available for comparison with GPS determinations, orbit accuracies can be inferred by considering the baseline repeatabilities and other criteria. Results of experiments performed at CSR using these data sets were presented in various meetings and have published in symposium proceedings. Copies of some of the publications are included in Appendix V.

6. Reference Frame Comparisons

Most of the GPS applications including some researchers involved in geodetic applications use the GPS ephemerides broadcast from the satellites as their source. Consequently, the solutions (absolute or relative positions) are defined in the coordinate system of the GPS ephemerides used which is the WGS-84. Often such results (especially geodetic) are compared with solutions obtained in other coordinate systems such as defined by SLR or VLBI. These coordinate systems should be coincident for comparisons to be meaningful or their relative orientation must be known in order to account for differences that may be present in the results. In order to facilitate such comparisons or to transform solution in one system to other a set of seven parameter transformation was estimated. This was performed using two sets of tracking data.

1. The first experiment used tracking data from the five Operational Control Segment (OCS) stations and data from CIGNET sites collected during the CASA UNO campaign (weeks 419 to 421). The data type used in the analysis was pseudo-range since that was the only type available from the OCS stations. The coordinates of the OCS stations were available in the WGS-84 reference frame whereas those of the CIGNET sites were available in a reference frame defined by SLR and VLBI systems. Holding few of the CIGNET sites fixed, coordinates of the OCS sites (along with other parameters) were estimated which were in the

SLR/VLBI system. Comparing these to the coordinates of the OCS sites given in WGS-84 system, the seven parameter transformation set was determined using least-squares technique.

2. This same procedure was repeated in a second experiment, but using carrier phase GPS data from the five Defense Mapping Agency (DMA) sites whose coordinates were available in the WGS-84 system, and from the CIGNET sites augmented by a global set of stations. The data used in this experiment were part of those collected during 1989 south west pacific campaign, namely, the weeks of 499 and 500.

Results of these experiments were presented in various meetings and published in symposium proceedings. Abstracts/summaries of these publications are provided in Appendix VI.

7. Thermal Imbalance Perturbation

When the surfaces of the GPS satellite directly exposed to the Sun are heated up, most of the energy is radiated back into the space. The surface away from the Sun also gains temperature due to conduction and then radiates the energy away into space. Depending on the conductive properties of material between the surfaces and the radiation characteristics of both the surfaces the satellite as a whole may or may not be in thermal equilibrium and as a result may experience a small force if there is a thermal imbalance. During the transient phase when the satellite enters or exits the Earth's shadow, a thermal nonequilibrium and hence a net force is certainly possible. Depending on the characteristics of the transient phase (rate of heating/cooling) and the duration of the shadow period, the magnitude of this perturbation could be significant. Simulation experiments were performed at CSR to determine effects of such thermal imbalance perturbations on satellite orbits assuming such simple models as flat plates or rectangular boxes for the satellites. Such simple 'satellites' were assumed to be in orbits of full Sun or maximum shadow configurations and the heat equation (second order partial differential equation) was considered in one dimension only. The major

difficulty in including this perturbation in orbit computation is due to the fact that the second order ordinary and the partial differential equation (finite difference or finite element techniques) have to be integrated simultaneously. Some of these aspects were studied closely but complete implementation of this perturbation for a typical satellite has not been achieved (mainly due to the difficulty mentioned above). Results of this study have been reported in Masters Thesis and in presentations at conferences. Appropriate summaries are presented in Appendix VII.

8. Eclipsing Orbits

Solar radiation pressure is one the most important nongravitational perturbations acting on the GPS satellites. Because of the altitude of the satellite, the magnitude of this perturbation is high (being of the order of 10^{-7} m/sec/sec) and hence play a major role in the accurate computation of the GPS satellite orbits. Its modeling is critical to achieving orbit accuracies needed for geodetic applications. Acceleration due to this perturbation is computed using the "ROCK4" models when the satellite is exposed to the Sun and is assumed to be zero when the satellite is in the shadow of the Earth (or the Moon). Thus when the orbit geometry is in such eclipsing configuration, computed acceleration due to SRP has a large jump in its time history, at the shadow crossing points (entering and leaving the shadow). Such large discontinuities in the acceleration values cause considerable error in the values of satellite state computed using constant step numerical integrators such as the KSG method. Manifestation of this problem has been clearly identified in situations where GPS satellite orbit predictions were performed in order to evaluate ephemeris accuracy. Variable step integrators such as the Runge-Kutta method are computationally expensive and need restarting of the numerical integration algorithm at such discontinuities. The approach taken to remedy this deficiency is to perform special operations at times when the satellite enters or leaves the shadow. This point usually occurs within the interval of a numerical integration step and hence the acceleration function values used by the integrator at the ends of this step have a large jump. To

avoid this discontinuity, the function values are assumed to be valid beyond the shadow crossing, on either side of it. In other words, when the satellite enters the shadow, the SRP acceleration value computed before shadow is assumed to be valid up to the first nodal point (of the integrator) after shadow boundary, and SRP acceleration value of zero is assumed backward up to the first nodal point before the shadow boundary. With this assumption the "back-difference table" of the KSG numerical integration algorithm is modified and appropriate corrections to the satellite state at these nodal points are made. This procedure is called the "modified back-difference table" (MBD) approach. Information on more details about this approach and on the improvements obtained in the prediction accuracy of satellite orbit can be found in Appendix VIII and the references thereof.

9. Effect of Mixed Receiver Types

The earlier tracking sites of the Cooperative International GPS Network (CIGNET), namely, Mojave, Westford, Austin, Wettzell and Richmond, used the TI-4100 (dual frequency P-code) receivers. Later in 1989, additional CIGNET sites collected data using Mini-Mac 2816-AT (dual frequency codeless) receivers. Further, NGS started replacing the TI-4100 receivers with the Mini-Macs. As a result, for a period of time data from two types of receivers had to be processed simultaneously for orbit determination. The differences in the data types and especially in way the time tag of observations were handled in both of these receivers had a considerable impact on preprocessing procedures and on the accuracy of the estimated orbits. In order to evaluate the impact of such mixed receiver data type on orbit accuracy a limited experiment was conducted. This was considered important since some of the field campaigns (such as the South West Pacific Campaign) used more than two types of receivers to collect data and if orbit accuracy is affected due to mixed receiver data, it could impact the baseline estimates.

During specific weeks at Mojave and at Wettzell data were collected, as part of CIGNET tracking, simultaneously from both the TI-4100 and the Mini-Mac receivers. Several orbit

determination experiments were performed using these data sets. In one experiment, only TI-4100 receiver data collected at Mojave would be used along with data from other sites (all TI) Mojave would be replaced by Mini-Mac data collected at Mojave during the same period, thus providing a mixed data set. Orbits determined in these two cases were compared and in addition were used in determining a known baseline. The rms of orbit differences was as much as 4 meters for some satellites; however, the impact on accuracy of the particular baseline tested, was not significant. Results of this study were presented in meetings and were published in meeting proceedings, copies of which are included in Appendix IX.

10. Effects of Selective Availability (SA)

The influence of Selective Availability (SA) on geodetic positioning was presented at the Fall 1990 meeting of the American Geophysical Union ("Observations of SA and the Effect on Precision Geodesy"). An example of SA is given in Appendix X, which illustrates phase residuals obtained by removing the effect of the orbit, the ionosphere and the troposphere. The examples shown were taken simultaneously from different locations and receivers. The similarity of the residuals indicates that the source of the variation was common and not produced by local effects, such as clock variations. In fact, the effect is SA and is characterized by a spectrum of frequencies with periods of several minutes. It was also demonstrated that SA is common to L1 and L2; thus the effect cancels in L1 minus L2 differencing. Double difference phase residuals on a zero baseline, i.e., Trimble 4000SST and TI4100 receivers were operated with the same antenna. During the period of the experiment, Week 549, SA was active on Block II satellites. As a consequence, double differences formed with the zero baseline using only Block I satellites can be characterized by white noise residuals. However, because of the data recording offset between the Trimble and TI receivers (the TI recorded 0.92 sec prior to the Trimble), the effect of SA does not cancel in the differencing process, and residuals that exhibit SA-induced periodicities remain. Other results, using baselines of

1000 km, showed that if the receivers record at nearly the same time (to within a few milliseconds), the effect of SA can essentially be removed.

APPENDIX I

1. Report on GPS orbit determination for Week 378 using pseudo-range data
2. Report on GPS orbit determination for Week 378 using double differenced phase data

REPORT ON GPS ORBIT DETERMINATION

GPS WEEK 378
APRIL 5 TO APRIL 11, 1987
(DAYS 95 - 101)

RELEASE:
EW378V4.EPH

PREPARED
FOR
U. S. GEOLOGICAL SURVEY
MENLO PARK, CA

BY
CENTER FOR SPACE RESEARCH
UNIVERSITY OF TEXAS AT AUSTIN

WITH THE COOPERATION
OF
TEXAS STATE DEPARTMENT OF HIGHWAYS AND PUBLIC TRANSPORTATION
AUSTIN, TX

NATIONAL GEODETIC SURVEY
ROCKVILLE, MD

CANADIAN GEODETIC SURVEY
OTTAWA, CANADA

For further information:
Dr. B. E. Schutz or Dr. P. Abusali
Center for Space Research
The University of Texas at Austin
Austin, Texas 78712

Telephone:
(512) 471-4267
FTS 770-5240
Telex:
704265 CSRUTX UD
BITNET:
AOVS751 @ UTCHPC
SPAN:
UTSPAN::UTCSR::SCHUTZ

ARPANET:
SCHUTZ%UTCSR.DECNET@CHPC.BRC.UTEXAS.EDU

GPS Week : 378

Contributing Stations :

Location	ID	Receiver	Reference Oscillator	Agency
Austin, TX	A	TI-4100	Cesium	SDHPT
Kauai, HI	K	TI-4100	H-Maser	UNAVCO
Mojave, CA	M	TI-4100	H-Maser	CSR
Westford, MA	W	TI-4100	H-Maser	NGS
Yellowknife, NWT	Y	TI-4100	Cesium	CGS

NOTE: SDHPT - State Department of Highways and Public Transportation (Texas)
CSR - Center for Space Research
NGS - National Geodetic Survey
CGS - Canadian Geodetic Survey
USGS - U. S. Geological Survey
UNAVCO- University Navstar Consortium

MODELS:

Gravity
MERIT Standard (GEM-L2, modified)
Luni-solar from DE-200

Nongravitational
Constant area, estimate reflectivity, estimate y-bias

Polar Motion, UT1
Lageos derived, reported on GE Mark III

Station Coordinates

Location	x (m)	y (m)	z (m)	Reference
Austin:	-743773.949	-5460643.710	3200347.492	Mader [1987b]
Kauai:	-5543817.634	-2054588.618	2387854.437	Mader [1987a]
Mojave:	-2356214.421	-4646733.994	3668460.630	Mader [1987b]
Westford:	1492233.223	-4458091.535	4296045.911	Mader [1987a]
Yellowknife:	-1224064.162	-2689834.572	5633432.720	McArthur [1987]

The Conventional Terrestrial System is defined by the NGS VLBI-defined frame.

References

Mader, G. L., "GPS Antenna Connections to VLBI Reference Points at Kokee Park and Westford," NGS Memo, July 17, 1987a.

Mader, G. L., "GPS Antenna Connection to VLBI Reference Point at Mojav and the Position of Austin GPS," NGS Memo, October 13, 1987b.

McArthur, D., "Yellowknife GPS Monitor Site," CGS Memo, February 4, 19

Data Distribution :

DAY		Satellite PRN 3	6	9	11	12	13
	A		X	X	X	X	X
	K		X	X	X	X	X
Sunday	M	X	X	X	X	X	X
	Y	X	X	X	X	X	X
	A		X	X	X	X	X
	K		X	X	X	X	X
Monday	M	X	X	X	X	X	X
	Y	X		X	X	X	X
	A		X	X	X	X	
	K		X	X	X	X	X
Tuesday	M	X	X	X	X	X	X
	Y	X	X	X	X	X	X
	A		X	X	X	X	X
	K		X	X	X	X	X
Wednesday	M	X	X	X	X	X	X
	Y	X	X	X	X	X	X
	A		X	X	X	X	X
	K		X	X	X	X	X
Thursday	M	X	X	X	X	X	X
	Y	X	X	X	X	X	X
	A		X	X	X	X	X
	K		X	X	X	X	X
Friday	M						
	Y	X	X	X	X	X	X
	A		X	X	X	X	X
	K						
Saturday	M						
	Y	X	X	X	X	X	X

NOTES:

- The locations, e.g., M, are defined on the preceding page in the column labelled ID.
- Data from the Westford receiver suggests that the receiver was operated on the internal oscillator instead of the hydrogen maser; consequently, Westford data were not used in this ephemeris release.

SOLUTION CHARACTERISTICS (NORMAL POINT DATA):

Satellite PRN	RMS (m) A	K	M	Y	Over-all	Sig	NP Meas. Processed A	K	M	Y	TOTAL
3	-	-	0.94	1.26	1.18	11	-	-	55	142	197
6	1.85	1.21	1.05	1.36	1.42	3	117	84	86	195	482
9	2.29	0.90	1.18	1.38	1.58	2	172	150	96	198	616
11	1.51	1.17	1.01	1.27	1.30	4	182	71	99	220	572
12	2.29	1.24	1.54	1.35	1.75	3	169	70	78	178	495
13	2.06	1.36	1.58	1.30	1.63	3	188	96	121	207	612

NOTES: The column labelled "Sig" is the formal standard error based on the trace of the satellite position estimate variances, using a measurement standard deviation of 1 m. It reflects the tracking geometry and the amount of data available.
The normal point (NP) data were obtained from the raw data by compressing the 30 second interval data into 15 minute bins.

STATE COMPARISON:

The following table provides a comparison in the epoch positition vector. The differences in position are obtained from the position vector reported in the EW378V1 solution distributed earlier and the current solution, EW378V4. The values in the table correspond to differences at the initial epoch only. The primary differences in the two solutions are as follows:

- Different station coordinates: analysis has shown difference in the two coordinate sets of less than two meters in individual components
- Use of Kauai data instead of Haleakala: although the amount of data from the two Hawaiian sites is very similar, the Kaua coordinates are more internally consistent with the other coordinates.

Epoch: 5 April 1987 00:00:00 GPS
Week 378

Satellite PRN	Epoch Difference (m) (EW378V4 minus EW378V1) X	Y	Z	One Week Difference (m) (EW378V4 minus EW378V1) Mean	RMS
3	0.6	10.9	12.0	16.5	17.0
6	-1.5	-5.7	8.4	5.7	6.0
9	-5.1	-4.7	1.6	6.2	6.3
11	-17.0	15.4	7.0	18.7	19.4
12	-5.1	-12.6	-5.2	15.1	16.0
13	-5.4	-0.6	4.5	4.3	4.2

REPORT ON GPS ORBIT DETERMINATION

GPS WEEK 378
APRIL 5 TO APRIL 11, 1987
(DAYS 95 - 101)

DIFFERENCED PHASE
RELEASE A
(EW378D1.EPH)

PREPARED
BY
CENTER FOR SPACE RESEARCH
UNIVERSITY OF TEXAS AT AUSTIN

Sponsored by:

U. S. Geological Survey
National Aeronautics and Space Administration
National Science Foundation

For further information:
Dr. B. E. Schutz or Dr. P. Abusali
Center for Space Research
The University of Texas at Austin
Austin, Texas 78712

Telephone:
(512) 471-4267
FTS 770-5240
Telex:
704265 CSRUTX UD
BITNET:
SCHUTZ @ UTADNX
SPAN:
UTSPAN::UTADNX::SCHUTZ

GPS Week : 378

Contributing Stations :

Location	ID	Receiver	Reference Oscillator	Agency
Austin, TX	A	TI-4100	Cesium	SDHPT
Mojave, CA	M	TI-4100	H-Maser	CSR
Kokee Park, HI	K	TI-4100	H-Maser	UNAVCO
Westford, MA	W	TI-4100	H-Maser	NGS
Yellowknife, NWT	Y	TI-4100	Cesium	CGS

NOTE: SDHPT - State Department of Highways and Public Transportation (Texas)
CSR - Center for Space Research
NGS - National Geodetic Survey
CGS - Canadian Geodetic Survey
USGS - U. S. Geological Survey
UNAVCO- University Navstar Consortium

MODELS:

Gravity
GM = 398600.440 km**3/s**2
Earth radius = 6378137.0 m
MERIT Standard (GEM-L2, modified)
Luni-solar from DE-200

Nongravitational
Solar radiation reflectivity estimated
y-bias estimated

Polar Motion, UT1
Lageos derived, reported on GE Mark III

Center of Mass:
Phase center in spacecraft axes with origin at center of mass
x=0.21 m; y=0.0 m; z=0.854 m

Measurement Model:
Daily values of zenith delay are estimated for each site.
Relativity correction included.

Station Coordinates
System defined by Lageos Laser Ranging [SSC(CSR)88 L 01].
VLBI coordinates [SSC(GSFC)88 R 01] rotated into SLR system through ties at Wettzell, Westford, Ft. Davis and Mojave.
Both sets of coordinates are given in the BIH Annual Report for 1987. The coordinates of the L1 phase center used in the solution are:

Site	x (m)	y (m)	z (m)
Kokee Park:	-5543817.866	-2054588.143	2387854.349
Mojave:	-2356214.840	-4646733.811	3668460.544
Westford:	1492232.844	-4458091.718	4296045.914
Yellowknife:	-1224064.507	-2689832.995	5633432.550

The location of the Kokee Park VLBI reference point (1311) in this system is:

Kokee VLBI:	-5543846.014	-2054563.735	2387813.666

The tie between the GPS antenna location and the VLBI was determined by Mader, as described in an NGS memorandum dated July 17, 1987.

OLUTION SUMMARY:

otes:

All full-rate data were collected at a 30 second interval unless otherwise noted.
Solution for PRN 3 was not computed due to sparcity of data.
Austin data were not included until final coordinate solution is performed.
The report for the pseudo-range orbit determination (EW378V1.EPH) contains information on the data distribution.
Full-rate phase data were edited and corrected for cycle slips.
Solution was obtained with double differences only for entire week.
File EW378D1.EPH is the ephemeris of the respective spacecraft center of mass.

Number of Double Differences: 9521

RMS of Double Differences: 0.031 m

STATE ADJUSTMENT:

The following table provides the adjustment in the epoch positition vector. The differences in position are obtained from the position predicted from the preceding week solution to the epoch of this report. The values in the table correspond to differences between the position vectors at the last time in the ephemerides reported for the preceding week and the first vectors of the current week, that is, the point of commonality between the current week and the preceding week.

Epoch: 5 April 1987 00:00:00 GPS
Week 378

Satellite	Position Difference (m) (Week 378 epoch minus last point of Week 377)		
PRN	R	T	N
6	2.04	6.43	3.08
9	1.57	5.82	-0.29
11	3.97	10.89	-1.02
12	0.40	-2.97	-1.13
13	1.23	0.75	0.74

R - Radial
T - Along-track, transverse
N - Cross-track, normal

APPENDIX II

Pollmeier, V. M., "A Comparison of GPS Orbits Estimated Using Observations From North America and Europe," Masters thesis, The University of Texas at Austin, December 1988 (Summary and Conclusions)

A COMPARISON OF GPS ORBITS ESTIMATED USING OBSERVATIONS FROM NORTH AMERICA AND EUROPE

by

Vincent M. Pollmeier, B.S.

THESIS

Presented to the Faculty of the Graduate School of
The University of Texas at Austin
in Partial Fulfillment
of the Requirements
for the Degree of

MASTER OF SCIENCE IN ENGINEERING

THE UNIVERSITY OF TEXAS AT AUSTIN

December, 1988

CHAPTER 8

SUMMARY/CONCLUSIONS

The results of the comparison of the N. American/European estimates with those of the N. American estimates show that there is some consistent and significant differences between the two sets of estimates in terms of the initial condition estimates, the estimated parameters (y-bias and solar radiation), the week long trajectories, or the coincident point offsets. The points of note are that the transverse components of most of the differences are the largest components. This suggest the possible existence of some type of unmodeled phenomena that is causing an effect in the along-track direction. This unmodeled force is probably non-gravitational, in nature.

The N. American formal standard errors are 54% larger on the average than the corresponding errors for the N. American/European estimate. It is possible that this increase in the formal standard error is attributable to the fewer number of normal point observations used in the N. American estimate as opposed to the N. American/European estimate. However, it seems unlikely that this would result in this large a change and that some portion of the difference in the formal standard error must be due to the larger range of coverage afforded by the inclusion of the European observations. A future examination to

determine just what part of this reduction in the formal standard error is attributable to the better coverage could be performed by reprocessing the N. American/European solutions with an observation set somehow reduced to an equal size of N. American solution may be in order, but is impossible to include here.

The large differences in orbit solutions that were possibly indicated by the earlier experiment (Stolz, *et al.*, 1987), were not apparent. The largest differences between the two sets of estimates were those for Satellite 8. This is not surprising due to the nature of Satellite 8's clock and the behavior of other values for this satellite. The solutions did not consistently show any significant differences that would indicate a major departure in the solution. Inclusion of GPS observations from other locations which are even more globally distributed than those discussed herein, is likely to improve the orbits even further.

It does appear that there is some unmodeled force acting on the GPS satellites. Its exact cause is not apparent, however. It is possible that it is a clock related problem. If this is the case, a thorough examination of the estimated clock parameters (not discussed in any depth here, due to time and length considerations) is in order.

APPENDIX III

1. "GPS antenna performance comparison," presented at the Third Annual Workshop on GPS Geodesy, Jet Propulsion Laboratory, Pasadena, Calif., March 1988
2. "How much does multipath affect the TI-4100 antenna, and how much difference does it make?" presented at the Spring Meeting of the American Geophysical Union, Baltimore, Maryland, May 1989 (Abstract)

GPS Antenna Performance Comparison

P. A. M. ABUSALI

CENTER FOR SPACE RESEARCH
UNIVERSITY OF TEXAS
AUSTIN, TEXAS

THIRD ANNUAL WORKSHOP ON GPS GEODESY
JET PROPULSION LABORATORY
PASADENA CALIFORNIA
21 MARCH 1988

COMMENTARY

The antenna experiment at Mojave was done February 6–12, 1988 (GPS week 422). The data for February 9 and 10 (days 40 and 41) and also for two days in the previous week, February 2 and 3 (days 33 and 34) of week 421, were analyzed. Table-1 shows, for all the satellites, the comparison between the pseudo-range noise rms of day 33 and day 40. Although it is not a one-to-one comparison, the rms of noise is less on day 40 than that on day 33, for all satellites. Table-2 shows similar comparison for days 34 and 41.

Figures 1 and 2 show the pseudo-range noise for PRN-3 for two consecutive days in week 421. The time origins of the plots were adjusted for the 4-minute delay in day-to-day repeatability of GPS, so that the figures can be laid one on top of another. When that is done, there is a clear indication of multipath effect. This is not the case in week 422 as indicated by comparison of Figures 3 and 4. Further, comparison of Figures 1 and 3 and Figures 2 and 4 shows the reduction in rms and the change in structure of the noise in pseudo-range measurements.

TABLE-1

Comparison of Pseudo Range Noise RMS (m)

SV-PRN	Week 421 (D 33)		Week 422 (D 40)	
	NOBS	RMS	NOBS	RMS
3	404	2.1772	705	0.8867
6	328	1.7731	208	0.6996
8	375	2.8333	397	0.9792
9	94	2.0175	390	0.7288
11	598	2.3963	539	1.1271
12	351	2.0352	306	0.7472
13	541	2.7715	565	0.9764

TABLE - 2

Comparison of Pseudo Range Noise RMS (m)

SV-PRN	Week 421 (D 34)		Week 422 (D 41)	
	NOBS	RMS	NOBS	RMS
3	712	2.2571	234	0.7812
6	540	2.5029	458	0.7037
8	509	3.3297	319	0.9709
9	430	1.8462	314	0.5983
11	635	2.3624	330	0.9215
12	428	1.9442	305	0.6441
13	570	2.9104	436	1.0248

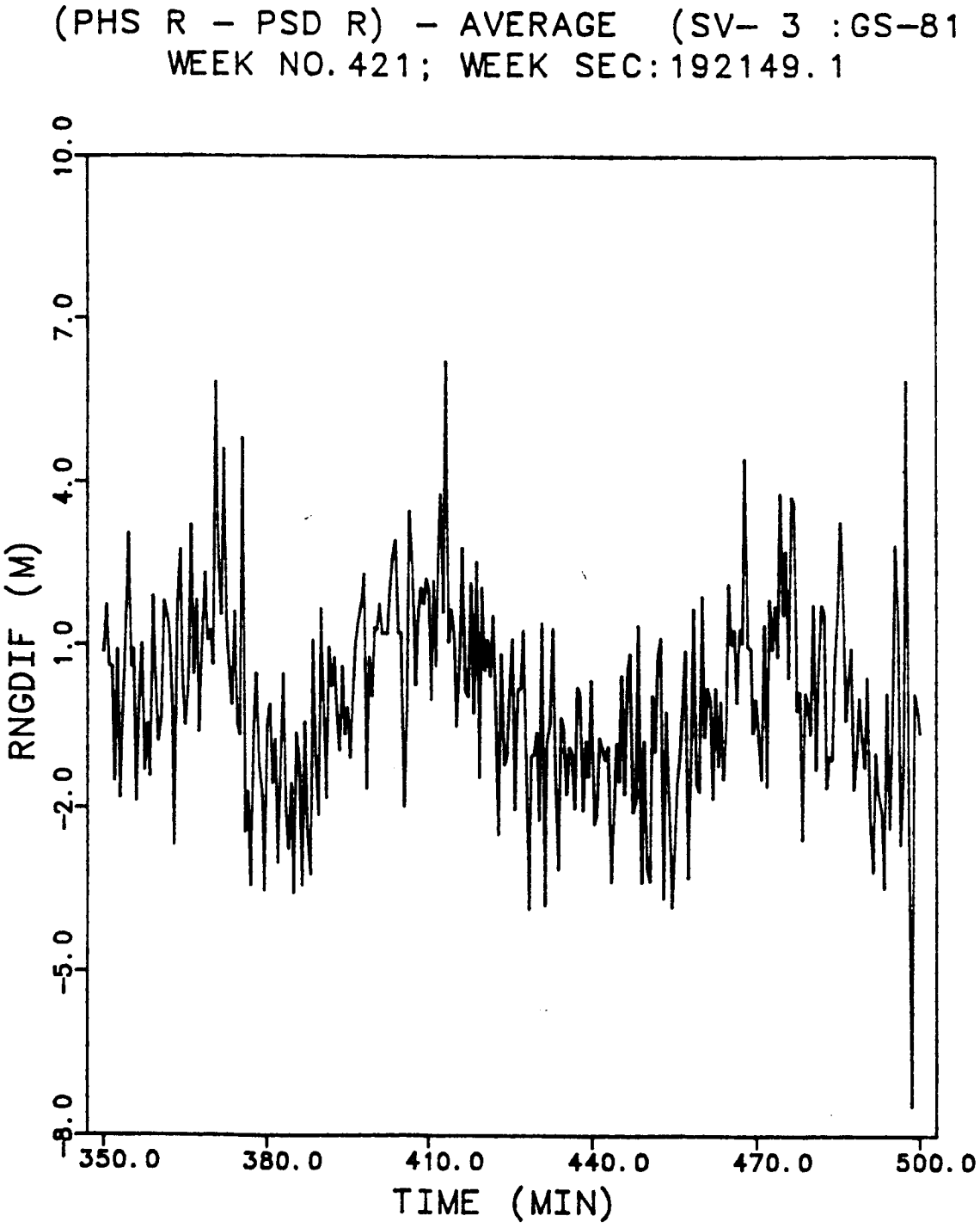
(PHS R - PSD R) - AVERAGE (SV- 3 : GS-81
WEEK NO. 421; WEEK SEC: 192149. 1
RNGDIF (M)
10.0
7.0
4.0
1.0
-2.0
-5.0
-8.0
350.0
380.0
410.0
440.0
470.0
500.0
TIME (MIN)

Figure - 1

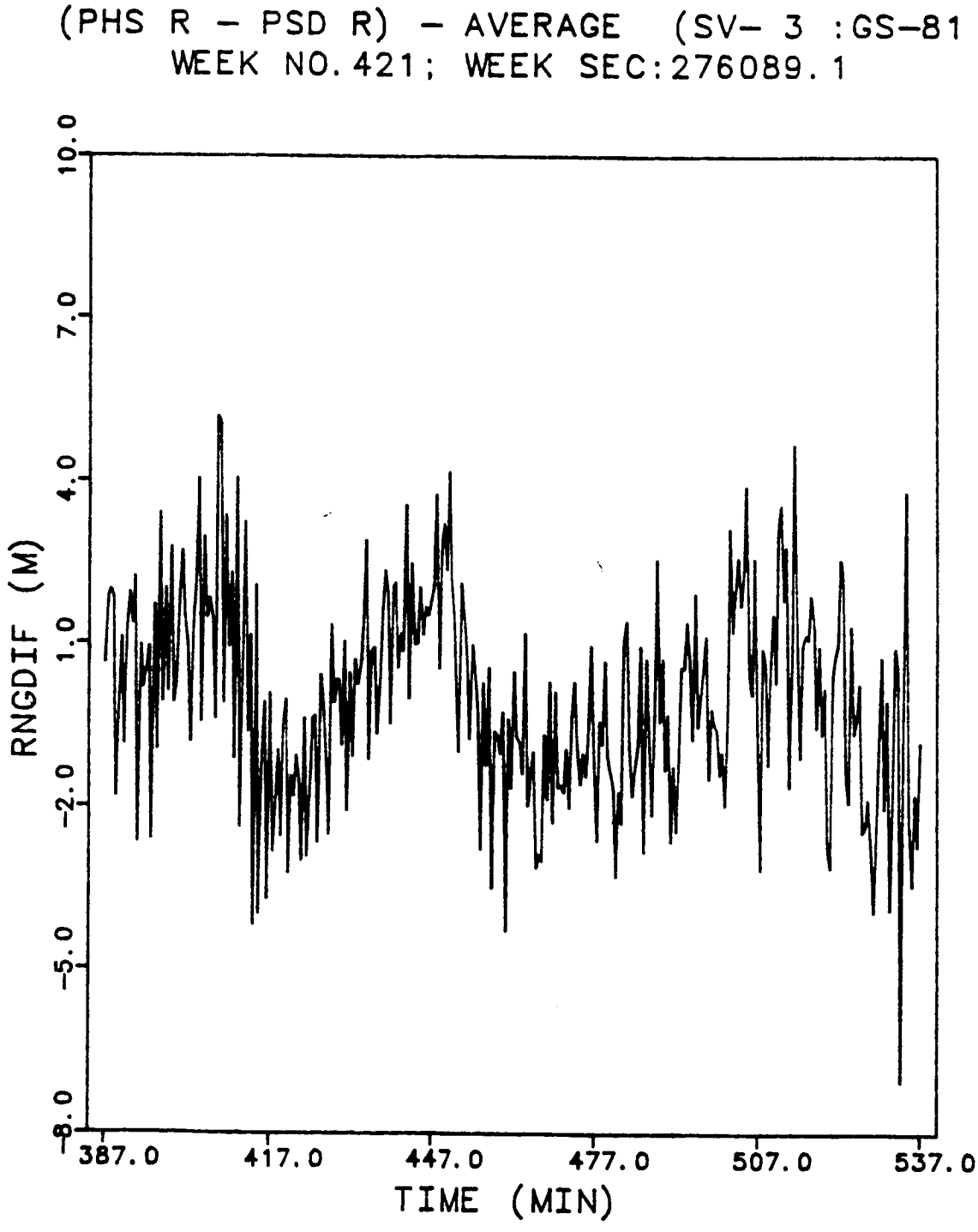
(PHS R – PSD R) – AVERAGE (SV– 3 :GS–81
WEEK NO. 421; WEEK SEC: 276089. 1
RNGDIF (M)
10.0
7.0
4.0
1.0
–2.0
–5.0
–8.0
387.0
417.0
447.0
477.0
507.0
537.0
TIME (MIN)

Figure – 2

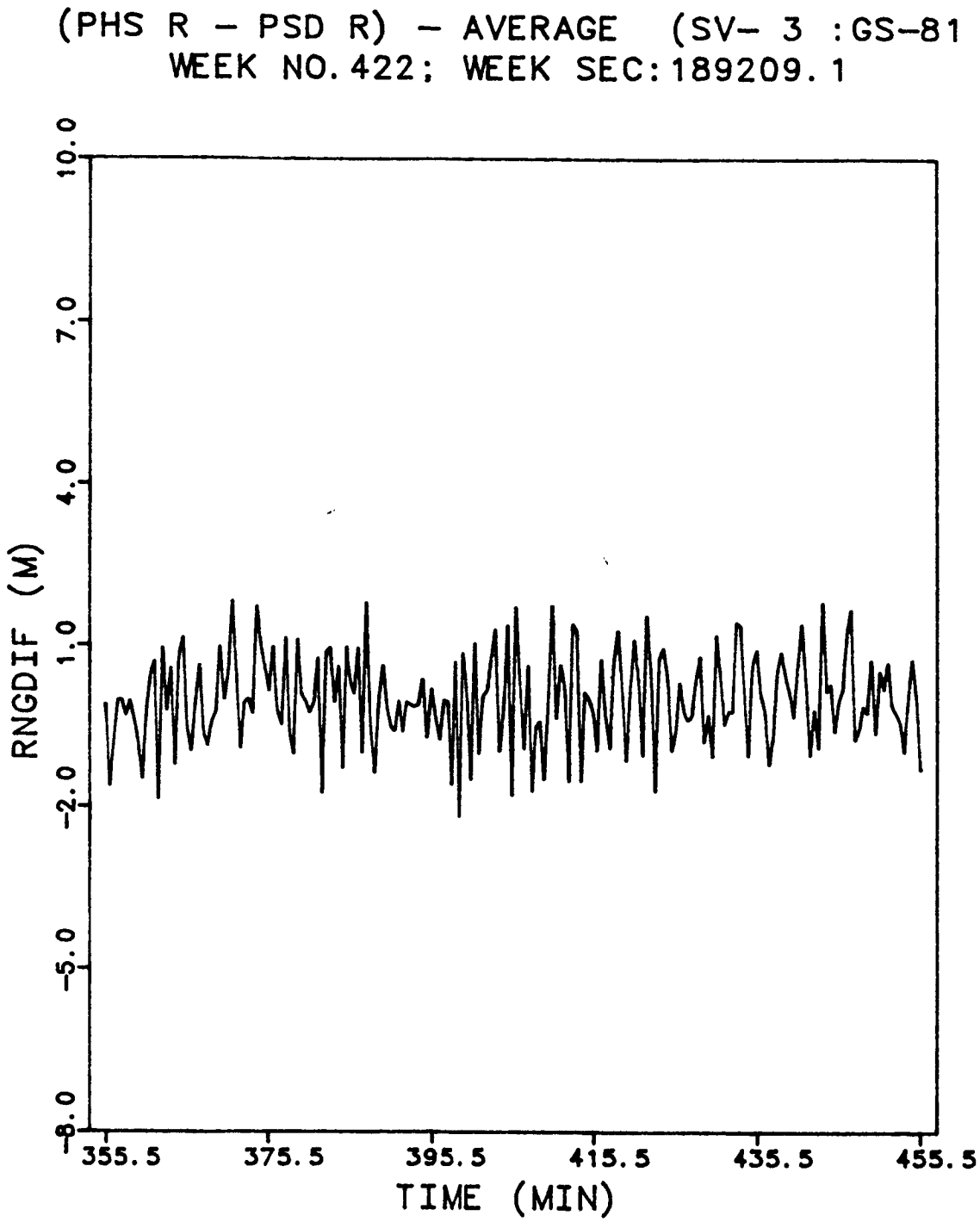
(PHS R - PSD R) - AVERAGE (SV- 3 :GS-81
WEEK NO. 422; WEEK SEC: 189209. 1
10.0
7.0
4.0
1.0
-2.0
-5.0
-8.0
RNGDIF (M)
355.5
375.5
395.5
415.5
435.5
455.5
TIME (MIN)

Figure - 3

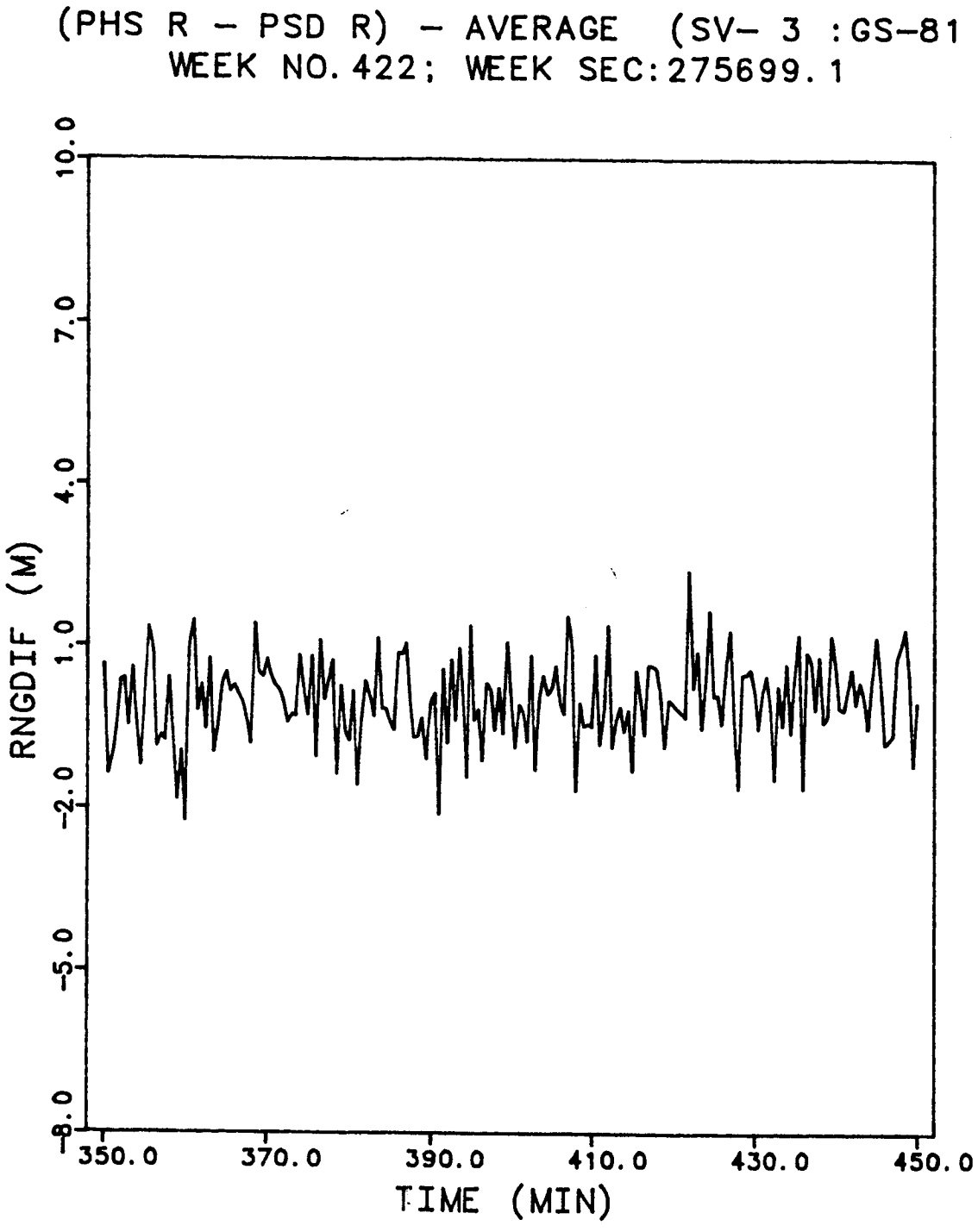
(PHS R - PSD R) - AVERAGE (SV- 3 :GS-81
WEEK NO. 422; WEEK SEC: 275699. 1
10.0
7.0
4.0
1.0
-2.0
-5.0
-8.0
RNGDIF (M)
350.0
370.0
390.0
410.0
430.0
450.0
TIME (MIN)

Figure - 4

made GPS measurement at several triangulation sites with observations as early as 1857. The map below shows the more important triangulation sites. Filled triangles are sites where we have made high-accuracy GPS measurements, while open circles show sites to be measured in March 1989. Results will reveal the extent of convergence and right lateral shear across the Los Angeles basin in the last century.

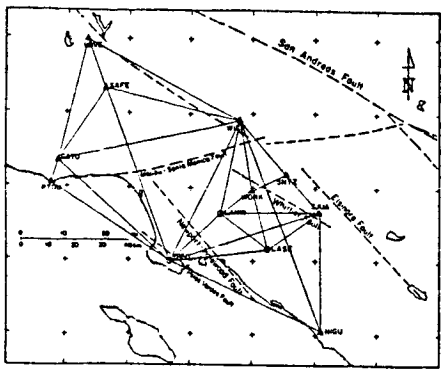

G32A-14 1645H

How Much Does Multipath Affect the TI-4100 Antenna, and How Much Difference Does it Make?

JL Svarc (U.S. Geological Survey, 345 Middlefield Road, MS/977, Menlo Park, CA 94025; Phone 415-329-4832; Bitnet address WPRESCOTT@USGSRESV)
PAM Abusali (University of Texas, Center for Space Research/WRW 402, Austin, TX 78712; 512-471-5573)
L Young (JPL/Mail Stop 238-600, 4800 Oak Grove Dr., Pasadena, CA 91109; 818-354-5018)
WH Prescott, JL Davis (also at USGS, Menlo Park)

We have studied the effect of several Global Positioning System (GPS) antenna/backplane configurations on P-code multipath, and the effect of multipath on relative positions obtained from carrier phase data. Two experiments were conducted at the National Geodetic Survey tracking station located at Mojave, California. A third experiment was conducted near the town of Parkfield, California. Data were collected using a standard TI-4100 antenna, a Fixed Radiation Pattern Antenna (FRPA-2), a Rogue antenna/"choke-ring" assembly, and a TI-4100 antenna surrounded by microwave-absorbing foam. In the table below, we present estimates of pseudorange noise determined by differencing the phase and pseudorange measurements. The primary contributors to this noise are random pseudorange measurement error and P-code multipath. We have established a test network on the roof of a USGS building in Menlo Park, California. Even though this network appears to be in a high multipath environment, the relative positions of the roof stations are correctly determined to less than 1 mm. The difference between lengths determined by GPS and Geodolite (a high precision laser distance measuring device) is 0.6 ± 0.5 mm. Although there are applications where very accurate pseudorange measurements are needed, we conclude that the effect of multipath on relative positions determined by carrier phase is at the level of 1 mm.

Antenna Configuration	RMS (m)
TI antenna ("good" location - brushy area at Mojave)	0.52
TI antenna ("bad" location - roof at USGS)	0.87
FRPA-2 antenna (roof at Mojave)	0.58
TI antenna with absorbing foam (Parkfield)	0.59
TI antenna (roof at Mojave)	0.77
Rogue antenna/choke rings (roof at Mojave)	0.34

Tectonics of the Mediterranean and Circum-Mediterranean-I (G41A)

Chesapeake III THURS AM
R Reilinger, MIT
K Kastens, L-DGO
Presiding

G41A-01 0845H

1988 Global Positioning System (GPS) Crustal Deformation Measurements in Turkey

R Reilinger (1) M N Toksoz (1) A Barka (1) E Kasapoglu (2) P Wilson (3) H Seeger (3) J Stowell (4) B Stephens (4)
(1)Earth Resources Laboratory, M.I.T., Cambridge, MA 02139; (2) Dept. of Geological Engineering, Hacettepe Univ., Ankara, Turkey; (3) IFAG, Frankfurt, Fed. Rep. Germany; (4) UNAVCO, Univ. of Colorado, Boulder, CO

A multi-institutional experiment involving scientists from the United States, Germany, England, Turkey, Greece, and Italy was begun in September-October 1988 to directly monitor present-day deformation throughout the eastern Mediterranean region. The September observations included establishing a network of 18 GPS sites in Turkey, 4 of which were observed previously by Satellite Laser Ranging (SLR) under the WEGENER/MEDLAS Project. Continuous GPS observations were maintained at 3 SLR sites in Greece (Dionysos, Askites, Rhodes), 1 in southern Italy (Matera), and 3 in northern Europe (Wettzell, Onsala, Tromso) throughout the Turkey Campaign.

The 18 sites established in Turkey were observed during a 23 day period using 4 TI-4100 dual frequency receivers provided by the University Navstar Consortium (UNAVCO). The GPS site at Ankara (Hacettepe University) was monitored continuously throughout the Turkey Campaign, while most other sites in Turkey were observed a minimum of 3 days each. Sites in Turkey were located to monitor broad scale plate tectonic movements and intraplate deformations, deformations along the western and central parts of the North Anatolian fault (including strain accumulation, fault creep near Karabuk, and the distribution of strain where the fault bifurcates in northwest Turkey), and lithospheric extension in the Aegean Trough region of Southwest Anatolia. The GPS network will be extended into eastern Turkey during the Fall of 1989 to begin monitoring deformation associated with collision of the Arabian Plate with Eurasia. Selected baselines will be reobserved yearly, with a complete reoccupation every 2 years.

G41A-02 0900H INVITED

Continental extension on sets of parallel faults

Rob Westaway (Department of Geological Sciences, University of Durham, South Road, DURHAM DH1 3LE, England)

Regions of distributed continental extension, such as Italy, central Greece and western Turkey, typically comprise an upper-crustal brittle layer containing sets of parallel active faults that bound blocks that are rectangular in plan view and like tilted dominoes in cross-section. Evolution of such regions can be quantitatively predicted as a function of extensional strain rate E_1 and vertical vorticity χ_z beneath the brittle layer. The ratio $\chi_z/(2E_1)$, or i, is a dimensionless parameter, Holmes number, which describes relative importance of extensional strain and rotation around vertical axes during evolution of such regions. $H=\cot(\gamma)$, where γ is the angle between strike and common slip vector azimuth for faults in a parallel set.

In central Italy, H~-0.15, and clockwise rotation during extension over the past ~2 Myr has been negligible. H~-0.7 in central Greece and ~+0.7 in western Turkey. This inplies that the present active fault generation in both regions has taken up ~10° rotation during the past ~2 Myr whilst the region has extended by ~1.2. A single previous fault generation took up ~30° rotation during the previous ~5 Myr, whilst the region extended by ~1.7. Thus, observed paleomagnetic rotation of ~40° clockwise in Greece and ~40° anticlockwise in Turkey during the past 7 Myr can be explained as a consequence of vertical vorticity causing oblique slip on two generations of parallel fault sets.

Financial support is being provided by UK Natural Environment Research Council grant GR3/6966

G41A-03 0915H

Kinematics of Mediterranean tectonic deformation

Rob Westaway (Department of Geological Sciences, University of Durham, South Road, DURHAM DH1 3LE, England)

Mediterranean active tectonics are dominated by northward convergence of the African plate relative to Europe. It is well known that this convergence is taken up in the eastern Mediterranean by subduction of Africa beneath Greece and Turkey, and in the western Mediterranean by shortening of the continental lithosphere in NW Africa. Recent work in Italy and adjacent regions of Africa has enabled the plate boundary position in the central Mediterranean and the sense of deformation along it to be deduced for the first time. Deformation within the African plate in Tunisia and northern Libya deflects its local direction of motion from northward towards the NE, consistent with the observed sense of extension in southern Italy. Relative motion between the Adriatic Sea, central and northern Italy and Yugoslavia can be regarded as anticlockwise rotation of the rigid Northern Adriatic microplate relative to Europe.This model is summarised in the map below, in which dots and crosses denote regions that are extending or shortening.

Financial support is being provided by UK Natural Environment Research Council grant GR3/6966.

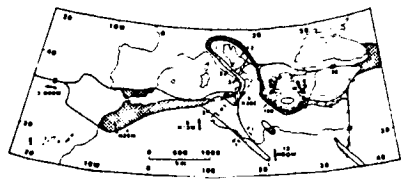

G41A-04 0930H INVITED

Mediterranean Geodynamics from Satellite Laser Ranging

D.E. Smith, R. Kolenkiewicz (Laboratory for Terrestrial Physics, NASA/GSFC, Greenbelt, MD 20771)
M. H. Torrence, P. J. Dunn, R. G. Williamson, S. M. Klosko, J. W. Robbins (ST Systems Corp, Lanham, MD 20706)
E. C. Pavlis (Univ. of Maryland-Astronomy Program, NASA/GSFC, Greenbelt, MD 20771)
S. K. Fricke (RMS Technologies, Lanham MD 20706)

The Mediterranean campaign, conducted by three transportable laser systems tracking the Laser Geodynamic Satellite (LAGEOS) since 1985, has provided accurate epoch positions for sites in Italy, Greece and Turkey. These three-dimensional locations can be set in a European reference frame defined by fixed tracking instruments. The fixed sites in Italy, France, Austria, Germany and England have been tracking LAGEOS for as long as five years, enabling the determination of their inter-station baseline values to an accuracy of 5 mm/year. The most significant deviation from rigidity assumptions for the European plate is a compressive motion at Matera, Italy towards its neighbors to the north. The accuracy of baselines between the Mediterranean sites and Matera reaches approximately 3 cm in each of three dimensions for an annual solution. Similar levels of accuracy are obtained for relative distances between any pair of locations occupied by the transportable systems.

G41A-05 0945H

Kinematic Evolution of the Mediterranean Region

W L Helman and J F Dewey (Department of Earth Sciences, University of Oxford, Oxford, OX1 3PR, England)
(Sponsor: Kim Kastens)

Convergent motion of Africa, Adria, and Eurasia has long been recognized as the cause of the Alpine orogeny (sensu lato), but the amount and direction of the motion could only be suggested by geology of the orogenic belt until the significance of oceanic magnetic anomalies and fracture zones was recognized. The vector (finite) difference between the independent seafloor spreading systems of the Central Atlantic (Africa-North America separation) and the North Atlantic (North America-Eurasia separation) is the relative motion between Africa and Eurasia.

The relative motion of Africa with respect to Eurasia has been the object of several studies since the early 1970's. Sharp, sudden changes in the direction of relative motion characterize the earliest of these. Such changes have since been recognized as the result of the misinterpretation or lack of data. More recent studies have tended to show a smoother path, with more gradual changes in direction and general agreement on parts of the relative motion path; e.g., Late Jurassic-Early Cretaceous ESE directed, sinistral strike-slip and Tertiary northward directed compression. Other aspects of Africa's motion are less widely agreed upon. These include the change to NE compression in the Cretaceous, the possibility of E-W dextral strike-slip in the mid-Tertiary, and NW directed motion from the Late Miocene.

Parts of Africa's motion path can be directly correlated with geologic data from the Mediterranean area, whereas other parts are at odds with the geologic evidence, particularly kinematic indicators from the Alps. This suggests the importance of other factors (microplates, gravity spreading) in the evolution of this region.

G41A-07 1015H INVITED

Reactivation of Convergence Structures and Seismogenesis in the Trans-tensional Regime of the Apennines of Central Italy

Leonardo Seeber (Lamont-Doherty Geol. Obs. Palisades, NY 10964), and Peter A. Geiser (Dept. of Geol.and Geophy., Univ of Connecticut, Storrs, CT 06268)

The Apennines of central Italy are dominated by thrusts and folds that accommodated a large amount of shortening in the Neogene. Although aspects of the depth extrapolation of some of these structures is still controversial, subsurface data from oil exploration and structural mapping strongly suggest that shallow-angle bedding-parallel thrusts with large displacements are the controlling structures in the upper crust. The current tectonic regime in the central Apennines is characterized by extension, as expressed by several large and often destructive earthquakes with large normal faulting component and by range-

APPENDIX IV

1. "CASA UNO GPS orbit and baseline experiments," *Geophysical Research Letters, 17*(5), 643–646, April 1990
2. "GPS orbit determination: Experiments and results," Proc. Fifth International Geodetic Symposium on Satellite Positioning, Las Cruces, New Mexico, March 1989
3. Ho, C. S., "Precision Orbit Determination of Global Positioning System Satellites," Ph.D. dissertation, The University of Texas at Austin, August 1990 (Abstract)

GEOPHYSICAL RESEARCH LETTERS, VOL. 17, NO. 5, PAGES 643-646, APRIL 1990

CASA UNO GPS ORBIT AND BASELINE EXPERIMENTS

B. E. Schutz, C. S. Ho, P.A.M. Abusali, and B. D. Tapley

Center for Space Research, The University of Texas at Austin

Abstract. CASA UNO data from sites distributed in longitude from Australia to Europe have been used to determine orbits of the GPS satellites. The characteristics of the orbits determined from double difference phase have been evaluated through comparisons of two-week solutions with one-week solutions and by comparisons of predicted and estimated orbits. Evidence of unmodeled effects is demonstrated, particularly associated with the orbit planes that experience solar eclipse. The orbit accuracy has been assessed through the repeatability of unconstrained estimated baseline vectors ranging from 245 km to 5400 km. Both the baseline repeatability and the comparison with independent space geodetic methods give results at the level of 1–2 parts in 10^8. In addition, the Mojave/Owens Valley (245 km) and Kokee Park/Ft. Davis (5409 km) estimates agree with VLBI and SLR to better than 1 part in 10^8.

Introduction

The purposes of the CASA UNO experiment have been described in detail by Kellogg et al. [1989]. Although the primary goal was to make epoch measurements in areas subjected to significant crustal motions from which strain information could be ultimately inferred, the experiment also offered an exceptional opportunity to study other phenomena. The establishment of a global network of stations to track the Global Positioning System (GPS) satellites in support of the experiment provided a data set from civilian sites that could be used for assessment of GPS orbit accuracy and force model fidelity. Such studies are important for the application of GPS to the accurate measurement of intersite vectors of hundreds or thousands of kilometers in length.

Even though the GPS satellites orbit at high altitude and, as a consequence, are less influenced by errors in the modeling of both gravitational and nongravitational forces than lower altitude satellites, the orbits are still influenced by forces that are not completely understood. The well-known "y-bias" force [Fliegel et al., 1985], which is defined along the solar panel axis to account for observed orbit characteristics is possibly caused by thermal radiation or misaligned solar panels. Such effects are small, approximately 10^{-9} m/s^2 in magnitude, but the complete time history and precise directions of the force (or forces) have not been established. These characteristics, among others, can limit the accuracy of the determined satellite ephemerides which, in turn, can limit their application to determination of intersite vectors used for geophysical studies.

The purposes of this paper were to examine the fidelity of the models used for the analysis of CASA UNO data and to assess the resulting orbit accuracy. The evaluation process was based on various criteria, including the comparison of estimated vector baselines with those determined by other space geodetic techniques and the repeatability of GPS-determined baselines. Furthermore, ephemerides resulting from different arc lengths have been compared and information about the model fidelity has been inferred.

Paper number 90GL00177
0094-8376/90/90GL-00177$03.00

Data and Site Descriptions

The CASA UNO experiment was conducted in the period from January 18 through February 5, 1988, corresponding to GPS Weeks 419 through 421. A significant portion of the global tracking data was provided by the Cooperative International GPS Network (CIGNET). Although CIGNET has been augmented since the CASA UNO experiment, the network consisted of the sites shown in Table 1 during the experiment. Several additional sites in Table 2 were used to extend the global coverage offered by CIGNET as well as to provide coverage to support evaluation and assessment of results.

TABLE 1. CIGNET Sites: January 1988

Site	Instrument/Software	Oscillator
Austin, TX	TI-4100/CORE	Cesium
Mojave, CA	TI-4100/CORE	Hydrogen Maser
Onsala, Sweden	TI-4100/CORE	Hydrogen Maser
Richmond, FL	TI-4100/CORE	Hydrogen Maser
Tromso, Norway	TI-4100/CORE	Cesium
Westford, MA	TI-4100/CORE	Hydrogen Maser
Wettzell, FRG	TI-4100/CORE	Hydrogen Maser
Yellowknife, NWT	TI-4100/CORE	Cesium

TABLE 2. Extended Network

Site	Instrument/Software	Oscillator
American Samoa	TI-4100/GESAR	Rubidium
Black Birch, NZ	TI-4100/GESAR	Cesium
Ft. Davis, TX	TI-4100/GESAR	Hydrogen Maser
Kokee Park, HI	TI-4100/GESAR	Hydrogen Maser
Owens Valley, CA	TI-4100/GESAR	Crystal
Tidbinbilla, Australia	TI-4100/GESAR	Hydrogen Maser

The fiducial concept has been adopted for the study in which coordinates from the space geodetic techniques of satellite laser ranging (SLR) and very long baseline interferometry (VLBI) were used to establish the coordinates of the GPS sites. Both SLR and VLBI have been demonstrated to have internal consistencies of a few centimeters and the comparison of mutual sites have suggested comparable accuracy. Most CIGNET sites have been established in the vicinity of VLBI sites and local

surveys have been performed to enable determination of the GPS receiver coordinates in a VLBI system. The relative vectors used for this study between the respective VLBI reference points and the GPS ionospherically corrected (L1/L2) phase centers are given in Table 3. The specific markers used for GPS were RM4 at Ft. Davis, BP ARIES 3 at Owens Valley and NM/C/194 at Tidbinbilla. Because of problems encountered with processing of data collected at Richmond and Austin, these sites were not used in the analysis reported in this paper.

TABLE 3. Relative Position Vectors

VLBI/SLR Marker		Vector from VLBI/SLR to L1/L2 Phase Center (m)		
		x	y	z
Ft. Davis	7216	18.751	−38.199	−74.106
Kokee Park	1311	6.868	−24.034	−3.930
Mojave	7222	−43.667	21.844	−10.209
Onsala	7213	53.521	−40.269	−42.432
Owens Valley	7207	−43.025	79.840	36.259
Tidbinbilla	1642	−80.923	−45.438	81.976
Westford	7209	26.296	38.824	30.409
Wettzell	7224	6.213	90.527	−29.829
Yellowknife	7285	59.992	−302.568	−122.822

Although Kokee Park became a regular CIGNET site in April 1988, the site used for CASA UNO was a different location (JPL Marker 3028-S). To establish the Kokee Park position with respect to the VLBI shown in Table 3, an additional experiment was conducted during GPS Week 441. The regular CIGNET site coordinates were determined during GPS Week 431 by the National Geodetic Survey (NGS). The Week 441 experiment was conducted by JPL and the USGS to determine the CASA UNO coordinates with respect to the CIGNET coordinates, from which the relative coordinates of the CASA UNO site were inferred as given in Table 3.

The site at American Samoa was located near a previously occupied SLR geodetic marker (7096). However, the marker 7096 could not be occupied by the GPS instrument and the local survey from the GPS location to the marker has not been performed. The site at Tromso was occupied in July 1989, with a mobile VLBI system but the results are not yet available. The New Zealand site was previously occupied with a doppler system, but uncertainty exists in relating the reference frames. These considerations resulted in the treatment of these three sites as nonfiducial sites that were estimated simultaneously with other parameters.

Recent results of Prescott et al. [1989] that demonstrate the dependency of the L2 phase center on the model of the TI-4100 antenna were used to establish the relative vectors in Table 3. In particular, the height of the L1/L2 phase center above the L1 phase center was 3.9 cm for TI-4100 Series 100 antennas and 2.3 cm for Series 4000.

Further information concerning the local site surveys is given in the CSTG GPS Bulletin. Details concerning local vectors between the VLBI or SLR geodetic markers and other local markers can be found in NASA Technical Reference 1198 [1988].

The phase data collected by the receivers were used in a double difference mode to eliminate most of the influence of satellite and receiver clock variations. Pseudo-range data were used to ensure an accuracy of one microsecond with respect to GPS time in the phase time tag. Preliminary orbits were generated from the pseudo-range data to support editing and correction of cycle slips. All solutions for one or two-weeks began at Sunday 00:00:00 of the respective week and the data were collected at 30-second intervals.

Reference System and Models

A reference system with origin at the Earth center of mass was used to describe the GPS satellite ephemerides. Since the VLBI system is insensitive to the center of mass, a system defined by SLR was used to establish the appropriate origin. Using sites that are common to both VLBI and SLR solutions, a seven parameter transformation was determined (translation, rotation and scale) between selected VLBI and SLR solutions. The approach was similar to a technique used by Kolenkiewicz et al. [1985] and Murray and King [1988]. The adopted VLBI system was produced at the Goddard Space Flight Center, labeled GLB484 [C. Ma and J. Ryan, private communication, 1989], and the SLR solution was obtained at The University of Texas at Austin, labeled CSR 8901 and based on analysis of the LAGEOS satellite [R. Eanes and M. Watkins, private communication, 1989]. These solutions were generated for an epoch of January 1, 1988, and the coordinates were adopted for the CASA UNO period with no further adjustment. After application of the transformation parameters, the common VLBI and SLR sites agree below 3 cm RMS in all three components [J. Ray et al., in preparation, 1990]. The resulting GPS site coordinates for the L1/L2 phase center were obtained by adding the relative vectors in Table 3 to the VLBI/SLR coordinates. The result for the GPS coordinates is in Table 4, identified as FSC-4.

TABLE 4. FSC-4 GPS Site Coordinates (m)

Site	x	y	z
Ft. Davis	−1324192.413	−5332061.177	3232044.361
Kokee Park	−5543839.212	−2054587.748	2387810.010
Mojave	−2356214.813	−4646733.808	3668460.510
Onsala	3370659.923	711877.022	5349788.065
Owens Valley	−2409643.917	−4478269.461	3838639.584
Tidbinbilla	−4461015.908	2682720.628	−3674299.714
Westford	1492232.872	−4458091.687	4296045.902
Wettzell	4075546.502	931825.518	4801599.280
Yellowknife	−1224064.474	−2689832.978	5633432.538

Most models adopted for GPS analysis have been used extensively with SLR analysis of the LAGEOS satellite [Tapley et al., 1985]. The gravitational force model included the MERIT Standards [Melbourne et al., 1983], with GM = 398600.440 km^3/s^2 and the GEM-L2 gravity field truncated at degree and order 8. The nongravitational force model used the ROCK4 solar radiation pressure model and included a y-bias force [Fliegel et al., 1985]. Polar motion and UT1 were based on LAGEOS analysis [Schutz et al., 1988]. The Chao [1974] troposphere model was used and the ionosphere corrections were applied using the dual frequency measurements. The satellite phase center with respect to the center of mass was $x = 0.21$ m, $y = 0.0$ m and $z = 0.854$ m. The results have been obtained with a multi-satellite derivative of the University of Texas Orbit Processor (UTOPIA) [Schutz and Tapley, 1980]. Various parts of the data analysis have been accomplished using VAXstation 2000, VAX 8200, CDC Cyber 170/750 and Cray X-MP/24 computers.

Results

As previously noted, several sites did not have antenna coordinates available in the adopted VLBI/SLR coordinate system, thereby precluding their use as fiducial sites in the strict sense. These sites included Black Birch, American Samoa and Tromso. Although the Owens Valley and the Ft. Davis coordinates were known in the adopted system, they were treated as unknown to enable their use for evaluation purposes. With these considerations, all sites were fixed to the coordinates in Table 4, except Black Birch, American Samoa, Tromso, Owens Valley and Ft. Davis which were adjusted in the estimation process without constraints.

Regardless of the arc length used, the epoch position and velocity vectors were estimated at Sunday 00:00:00 GPS time of the appropriate week. In addition, a scale parameter for the ROCK4 solar radiation pressure model [Fliegel et al., 1985] and one or more *y*-bias parameters were estimated for each satellite. A zenith troposphere delay parameter was estimated for each three hour interval at each station during the observing periods. In all cases, the orbit was determined from double difference phase measurements, with pseudo-range measurements used to correct phase time tags to GPS time. A bias parameter was estimated also for each respective combination of two satellites and two ground stations in the double difference mode. No a priori constraints were applied to any estimated parameter, i.e., all parameters were completely free to simultaneously adjust.

One-week solutions, or one-week arcs, were computed for each respective week of the experiment. In addition, two-week arcs were computed using Weeks 419 and 420 as well as 420 and 421. The double difference (DD) residual root-mean-square (RMS) and the number of measurements in each week are given in Table 5. The statistics include cases resulting from the modeling of multiple *y*-bias parameters for the two-week arcs. The one week arcs used a single *y*-bias for each satellite. The higher RMS in the two-week arcs compared to the one-week arcs is indicative of remaining unmodeled effects. The experiments with increased number of *y*-bias parameters demonstrate that the unmodeled force cannot be satisfactorily explained by a force along the solar panel axis, the spacecraft-fixed *y*-direction, since only modest reduction in the RMS was achieved. Although the DD RMS level for the two-week arcs is at the 5 cm level, experience has shown that the error distribution represented by this magnitude can adversely affect baseline vector estimates.

TABLE 5. Solution Statistics

Week No.	Number of Double Differenced Phase Measurements	DD Residual RMS (m)
419	82,039	0.0297
420	91,115	0.0327
421	78,632	0.0277
Two-week cases, one *y*-bias for the arc*:		
419/420	141,812	0.09702
420/421	134,785	0.05645
Two-week cases, two *y*-bias for the arc*:		
419/420	141,812	0.05567
420/421	134,785	0.05252
Two-week cases, four *y*-bias for the arc*:		
419/420	141,812	0.05208
420/421	134,785	0.05047

*The number of *y*-bias parameters applies to each satellite. The two-week arcs did not include Owens Valley and Tromso.

The characteristics of the solutions described in Table 5 were further investigated by comparing the two-week solutions with the individual one-week orbit solutions. The two-week solutions in which two *y*-bias parameters per satellite were estimated were chosen for the comparison. As expected, the differences exhibit a behavior characterized by a twelve-hour period (once per revolution). The two-week orbit determined for Weeks 419 and 420 was compared to the one-week solution for Week 419. The differences for all satellites were confined to the range of ± 10 m, however, satellites with the PRN identity of 3, 8, 11 and 13 also exhibited either a long period (>14 days) or quadratic trend in the along-track direction in addition to the once per revolution periodicity. It is presumed that the one-week orbit is a more accurate representation of the actual orbit, hence, the differences are one illustration of problems in force model fidelity on the two-week arc.

Another approach to the assessment of the orbit accuracy and model fidelity is to use the estimated parameters from one-week for the prediction of the orbit into the next week. The predicted orbit can be compared with the orbit estimate for the second week. Errors in either the state estimates or the force model will introduce errors in the predicted states. The orbits determined for Week 419 were predicted into Week 420 and compared with the determined orbit for Week 420. While PRN 6, 9 and 12 exhibit differences bounded by ± 5 meters with a periodicity of once per revolution, the other satellites exhibit a quadratic-like growth in the along-track component reaching 50–100 m after one week. The satellites share the common characteristic that PRN 3, 8, 11 and 13 experience eclipsing of the Sun by the Earth and the other satellites do not. As a consequence, it is tentatively concluded that an effect associated with the eclipse season remains unmodeled.

The one-week orbits described in the preceding paragraphs were evaluated further with applications to the estimation of baseline vectors, the essential test of geodetic accuracy. In some cases, the assessment was based on the repeatability of the baseline estimate from different experiments. While this is a necessary test for accuracy, it is not sufficient. Still other cases allow a comparison with values determined by independent techniques such as SLR or VLBI which are subjected to different error sources.

The site solutions obtained for each individual week are given in Table 6 as the vector relative to the fixed site used for forming the double differences. The solution is given as the average of the three weeks and the repeatability from week to week is indicated by the RMS. The results indicate length repeatability at the level of one or two parts in 10^8, except for Tidbinbilla to American Samoa which is about four parts in 10^8. It should be noted that if the Week 419 estimate for American Samoa is eliminated, the remaining two solutions agree at the level of one or two parts in 10^8.

As noted previously, only the Kokee Park/Ft. Davis and Mojave/Owens Valley have been independently determined by another technique, namely, VLBI and SLR. Table 7 shows the comparison of the estimated baseline (Table 6) with VLBI/SLR vectors determined from Table 4, resolved into longitude, latitude and height differences. Both cases show agreement with the independent determination of one part in 10^8 or better in the baseline magnitude. These results have been determined without a priori constraints in solutions that were allowed to freely adjust to a converged solution. The quality of the 245 km baseline results is

TABLE 6. Estimates Averaged from One Week Solutions (m)

Baseline	Δx	Δy	Δz	Length
TI to AS	−1638933.040	−3680013.690	2105673.934	4545598.419
RMS	0.044	0.144	0.101	0.177
TI to BB	−278055.991	−2168360.092	−551140.618	2254519.151
RMS	0.005	0.072	0.020	0.066
ON to TR	−1267718.477	9692.532	608405.800	1406186.936
RMS	0.023	0.029	0.026	0.011
KO to FD	4219646.772	−3277473.446	844234.346	5409249.735
RMS	0.024	0.047	0.022	0.048
MO to OV	−53429.130	168464.348	170179.065	245348.370
RMS	0.012	0.033	0.026	0.007

AS-American Samoa BB-Black Birch FD-Ft. Davis
KO-Kokee Park MO-Mojave ON-Onsala
OV-Owens Valley TI-Tidbinbilla TR-Tromso

TABLE 7. Difference (m) of Table 6 with Table 4

Baseline	Longitude	Latitude	Height	Length
MO to OV	−0.014	−0.007	0.004	0.000
KO to FD	−0.013	−0.008	0.017	0.012

consistent with results of other investigators [Blewitt, 1989; Dong and Bock, 1989].

Conclusions

Evidence has been presented for the existence of unmodeled GPS force characteristics that may, in part, be associated with eclipse season. While understanding these forces is important, results have been obtained for vector baselines that demonstrate 1–2 parts in 10^8 repeatability and comparison with SLR and VLBI determinations. Compensation of the error sources by stochastic techniques or improved understanding of the nature of the forces could contribute to further improvements in the baseline results.

Acknowledgments. This study was supported, in part, by NASA and the USGS. The data preprocessing was done by Dano Carroll. Use of The University of Texas at Austin Computation Center and The University of Texas System Center for High Performance Computing facilities are gratefully acknowledged. The local survey ties at Tidbinbilla were provided by J. Steed, Australian Lands and Information Group. Numerous institutions contributed time and effort in conscientiously collecting the data used in the analysis, as acknowledged by Kellogg et al. [1989].

References

Blewitt, G., Carrier phase ambiguity resolution for the Global Positioning System applied to geodetic baselines up to 2000 km, *J. Geophys, Res., 94*(B8), 1187–1203, August 1989.

Chao, C. C., The troposphere calibration model for mariner Mars 1971, *Technical Report 32-1587*, Jet Propulsion Laboratory, Pasadena, California, March 1974.

CSTG (International Coordination of Space Techniques for Geodesy and Geodynamics), *GPS Bulletin, 2*(1), published by NGS, January–February 1989.

Dong, D., and Y. Bock, Global Positioning System network analysis and phase ambiguity resolution applied to crustal deformation studies in California, *J. Geophys. Res, 94*(B4), 3949–3966, April 1989.

Fliegel, H. F., W. A. Feess, W. C. Layton and N. W. Rhodus, The GPS radiation force model, *Proceedings of the First International Symposium on Precise Positioning with Global Positioning System*, NOAA, Rockville, Maryland, 1985.

Kellogg, J., T. Dixon and R. Neilan, Central and South America 1988 GPS geodesy campaign - CASA UNO, *Eos Trans. AGU, 70*(24), 649–656, June 1989.

Kolenkiewicz, R., J. Ryan and M. H. Torrence, A comparison between LAGEOS laser ranging and very long baseline interferometry determined baseline lengths, *J. Geophys. Res., 90*(B11), 9265–9274, 1985.

Melbourne, W., R. Anderle, M. Feissel, R. King, D. McCarthy, D. Smith, B. Tapley and R. Vicente, Project MERIT Standards, U.S. Naval Observatory, Circular No. 167, 1983.

Murray, M. and R. King, SV-3 coordinates of GPS receivers, MIT Internal Memorandum, 1988.

NASA Crustal Dynamics Project Staff, Crustal Dynamics Project: Catalog of site information, *NASA Reference Publication 1198*, March 1988.

Prescott, W., J. Davis and J. Svarc, Height of L2 phase center for TI antennas, *CSTG-GPS Bulletin, 2*(2), published by NGS, March–April 1989.

Schutz, B., B. Tapley, R. Eanes and M. Watkins, Earth rotation from LAGEOS laser ranging, *Annual Report for 1987*, D-51 to D-56, Bureau International de l'Heure, Paris, 1988.

Schutz, B. and B. Tapley, UTOPIA: University of Texas orbit processor, *TR 80-1*, Center for Space Research, University of Texas, Austin, Texas, 1980.

Tapley, B., B. Schutz and R. Eanes, Station coordinates, baselines and Earth rotation from LAGEOS laser ranging: 1976–1984, *J. Geophys. Res., 90*(B11), 9235–9248, 1985.

P.A.M. Abusali, C. S. Ho, B. E. Schutz, and B. D. Tapley, Center for Space Research, The University of Texas, Austin, TX 78712.

(Received November 20, 1989;
accepted January 10, 1990.)

To appear in the proceedings of the Fifth
International Geodetic Symposium on Satellite Positioning

GPS ORBIT DETERMINATION: EXPERIMENTS AND RESULTS

B. E. Schutz, B. D. Tapley, C. S. Ho, H. J. Rim, and P. A. M. Abusali,
University of Texas, Center for Space Research
Austin, Texas 78712, U.S.A.

ABSTRACT

Experiments have been conducted with GPS data collected during the CASA UNO campaign (January, 1988). This campaign collected data from an enhanced CIGNET by including data from Australia, New Zealand and American Samoa. The experiments have focused on the model fidelity associated with one and two week arcs computed during the campaign period. The orbit accuracy was evaluated, in part, through comparison of the satellite positions at the time point common to adjacent one week arcs and by examining the week to week consistency of station coordinate/baseline estimates. Based on the consistency tests and the comparison of baseline estimates with those determined by other techniques, the accuracy has been estimated at a few parts in 10^8.

INTRODUCTION

Since the last Geodetic Symposium held in Austin, TX, in 1986, significant progress has been made in the organization of a civilian network of GPS receivers, primarily dedicated to regular tracking of the GPS Block I constellation. In September, 1986, with the sponsorship of the U.S. Geological Survey (USGS), The University of Texas at Austin Center for Space Research (CSR) organized a cooperative network of three TI-4100 receivers. This network consisted of the following locations and cooperating agencies:

- Mojave, CA: receiver owned by CSR, operated by National Geodetic Survey (NGS) using a hydrogen maser frequency reference;
- Austin, TX: receiver owned and operated by the Texas State Department of Highways and Public Transportation using a cesium reference;
- Westford, MA: receiver owned and operated by the NGS using a hydrogen maser reference.

This network was used to support regional geodetic applications and orbit determination.

Through the efforts of the NGS, an expanded and more global network has been organized. This network of cooperating stations, the Cooperative International GPS Network (CIGNET) now consists of the sites given in Table 1 (CSTG Bulletin, 1989).

Early orbit determination studies were limited by the regional nature of the Continental U.S. network. In the presence of no model errors and precise measurements, accurate orbits can be determined using such a regional network. However, in the presence of complex GPS clock variation and uncertainties in force models, a regional network is inadequate for orbit determination. Some difficulties can be diminished by use of a global tracking network which allows observation of the satellite over a greater portion of the orbit, thereby providing enhanced information about the model error characteristics and enabling improved averaging of model errors. Nevertheless, model errors continue to exist and are also dependent on the temporal data span, or arc length. It is generally acknowledged that as the arc length is lengthened, the effects of model errors will become more pronounced. On the other hand, the pronounced effect can be used to study the phenomena

and, hence, improve the modeling and understanding of it.

The purpose of this paper is to examine the fidelity of the models through the use of GPS tracking data in different arc lengths. The evaluation process uses various criteria, including the arc to arc consistency for selected baseline estimations and the differences in orbits for two adjacent arcs. This paper is not intended to be an exhaustive treatment, but instead to document interim results obtained from a selected set of cases in an ongoing study.

DATA

For the study described in this paper, the CASA UNO Campaign (Kellogg, et al., 1989) was chosen to augment the regular TI–4100 data set of the CIGNET. This campaign was conducted for a period of almost three weeks and used sites which enhanced the global distribution. The additional sites, which used TI-4100 receivers, are given in Table 2. While the purpose of this campaign was to obtain a set of epoch measurements in Central and South America, additional global tracking contributions were organized to provide improved orbit determination support. It should be noted that the CIGNET site at Kauai (Kokee Park) was not in operation during CASA UNO, however, a TI-4100 receiver was operated in the vicinity of the permanent CIGNET site which was installed about three months after the campaign.

The results described in this paper used the first two weeks of the CASA UNO, namely, GPS Week 419 (January 17-23, 1988) and Week 420 (January 24-30, 1988). All stations used GESAR or a closely related product (CORE) developed by the Applied Research Laboratory of the University of Texas at Austin. The CIGNET sites used either hydrogen maser or cesium frequency standards and collected data at 30 sec intervals.

The pseudo-range data were used from all sites to determine preliminary orbits for phase editing and determination of receiver time tag corrections. Phase processing required several steps, including the tasks of locating and fixing cycle slips. The phase data were used in a double difference mode for orbit and parameter estimation.

The arcs considered in this paper were one or two weeks in duration. All arcs began at Sunday 00:00:00 GPS Time of the respective week.

REFERENCE SYSTEM

Most of the sites listed in Table 1 are near Very Long Baseline Interferometry (VLBI) or Satellite Laser Ranging (SLR) sites whose coordinates have been determined to an accuracy of a few centimeters. Local surveys, performed with classical and GPS techniques, provide the tie between the GPS antenna and the VLBI or SLR reference point. Since VLBI is insensitive to the Earth center of mass required for the description of satellite orbits, a combination of the VLBI/SLR reference frames was used for the GPS reference frame.

An analysis similar to a technique described by Kolenkiewicz et al., (1985) and Murray and King (1988) was applied to obtain the GPS reference frame. In the approach used in this paper, the SLR coordinates SSC (CSR) 88L01 (Schutz et al., 1988) were mapped to an adopted epoch of January 1, 1988, using the tectonic motion model of Minster and Jordan (1978). Similarly, the Earth-fixed VLBI coordinates of Goddard Space Flight Center, GLB206 (Ryan et al., 1988) were mapped to the same epoch. Although the GLB206 was replaced by the solution GLB223, the differences between the two solutions at the sites of interest is small.

Several mutual or nearby collocations of SLR and VLBI exist. The sites used for this study and the corresponding geodetic markers are given in Table 3. The relative locations of appropriate geodetic markers were obtained from NASA Tech. Ref. 1198 (1988). By adding the marker relative position vector to the VLBI coordinates, a set of coordinates for the SLR sites expressed in the VLBI reference frame was formed.

The SLR coordinates expressed in the VLBI system were compared with those derived from SLR analyses and a seven parameter transformation set was obtained. This transformation was applied to other VLBI coordinates in order to map them into the SLR reference frame. The resulting differences between the coordinates of the VLBI sites transformed into the SLR system compared to the SLR coordinates are given in Table 4.

Analysis documented by Chin (private communication, 1989) for the local ties was used to obtain the GPS antenna coordinates after the use of the transformation parameters. The resulting GPS coordinates for the fixed (unadjusted) CASA UNO L1-phase centers, identified as CSR Fiducial Station Coordinates, FSC-2, are given in Table 5. The coordinates for the special CASA UNO fixed sites used operator measurements of the antenna height above the respective geodetic marker. Additional information on local surveys at the Tidbinbilla site was provided by the Australian Lands and Information Group (Steed, personal communication, 1988). The Tidbinbilla site was the marker identified as NM/C/194. The Ft. Davis and Owens Valley sites refer to markers RM-4 and BP Aries-3, respectively, and the coordinates of these markers with respect to VLBI sites can be found in NASA Tech. Ref. 1198 (1988).

MODELS

The models used for the GPS analysis were based primarily on experience derived from Lageos laser ranging investigations (Tapley et al., 1985) and the adoption of the SLR geocentric coordinate system described in the preceding section. The adopted force model for GPS analysis is given in Table 6. To a large extent, the models have been used and validated on several satellites, including SLR targets and radiometric satellites.

The orbit analysis software, MSODP, has been developed at the University of Texas at Austin, partly derived from UTOPIA (Schutz and Tapley, 1980). Various parts of the computations have been done on a VAX 8200, CDC Cyber 170/750 and a Cray X-MP/24.

RESULTS

For the two weeks examined, most data collected with the enhanced CIGNET was of good quality, although some sites experienced excessive cycle slips at some times. Only one site (Richmond) experienced significant problems that resulted in little usable data.

During the CASA UNO, several sites did not have antenna coordinates available in the adopted VLBI/SLR coordinate system. These sites were Black Birch, American Samoa, Kauai and Tromso. Although Owens Valley coordinates were known in the adopted system, the site coordinates were treated as unknown to enable use of the site for evaluation purposes. During Week 446, a local GPS survey was conducted that enabled determination of the CASA UNO Kauai site in the adopted system. A VLBI occupation of the Tromso site is planned for summer, 1989, thus enabling assessment of the coordinates given later in this paper.

Regardless of the arc length, the epoch position and velocity vectors of each satellite were estimated. In addition, a scale parameter on the ROCK4 model and one or more y-bias parameters were

estimated also. A zenith delay parameter was estimated for each three hour interval during observing periods. In all cases, double differenced phase measurements were used to estimate the parameters of interest. These measurements require estimation of a bias parameter for each respective combination of two satellites and two ground stations.

The solution statistics obtained for Weeks 419 and 420 are given in Table 7. As readily seen from this table, over 65,000 double differenced measurements were used in the one week arcs. The respective one week residual RMS is a little more than 3 cm. In the case where the arc length is extended to two weeks, the residual RMS increases by almost a factor of two, although the signal level expected to cause such an increase is a little more than the RMS, namely 4 cm. The cause of the increase is under investigation, but the nongravitational forces are suspected of being major factors.

The orbit position differences at the common time point between the arcs of Weeks 419 and 420 are given in Table 8. While the differences at common time are not a definitive assessment of the orbit accuracy, they are an indicator of the level at which unmodeled effects still exist. Even though the two week arc will remove this common time difference, the comparison at the initial and final epochs demonstrates several meter differences.

Another means of assessing the orbit quality is by examining the week to week consistency of the baseline estimates and the comparison of baselines with VLBI/SLR determined coordinates, where available. Table 9 illustrates the week to week comparisons for the coordinates of the sites estimated in the one week arc experiments. In this table, the second site was estimated and the first held fixed to the coordinates given in Table 5. With the exception of American Samoa, the week to week consistency is at the level of a few centimeters on baselines as long as 5409 km, or a few parts in 10^8. The behavior of the American Samoa estimate requires further investigation.

In some cases the ability to estimate accurate three-dimensional coordinates using a long baseline is of interest. With the local survey performed at Kauai during Week 441 by JPL and USGS, the coordinates in the FSC-2 system have been determined and can be compared with the estimates obtained with the analysis of Weeks 419 and 420. The results are given in Table 10. While differences between the estimates and the survey are about 10 cm, the differences are consistent with a few parts in 10^8. Nevertheless, the discrepancy is under further investigation.

With the VLBI determination of Tromso coordinates planned for summer, 1989, the GPS determined coordinates of Tromso can be assessed. The results from Weeks 419 and 420 are given in Table 11 relative to Onsala. These coordinates refer to the GPS receiver antenna phase center which will have to be corrected to an appropriate reference mark for comparison with VLBI.

CONCLUSIONS

Comparison of the Week 419 and 420 orbit solutions at a common time point shows differences at a few meter level, even for PRN 8 which is difficult to handle because of the clock modeling required with pseudo-range. It has also been shown that the baseline week to week consistency is a few parts in 10^8 for baselines up to 5400 km. The two-week solution, as well as the common point differences, suggest the existence of remaining unmodeled effects, possibly caused by nongravitational forces. Comparison of the three-dimensional coordinates of Kauai with a later GPS local survey shows agreement at a few parts in 10^8 from a 5000 km baseline. Tromso coordinate estimates are given for future comparison with a VLBI determination.

Future analyses will focus on the third week of CASA UNO as well as the fidelity of the force model required on two and three week arcs. It is believed that the results of the long arc analyses will contribute to the short arc results through improved understanding of the forces and development of improved models.

ACKNOWLEDGEMENTS

This work was supported by the USGS and NASA. Use of the University of Texas at Austin Computation Center and the University of Texas System Center for High Performance Computing facilities is gratefully acknowledged.

REFERENCES

CSTG (International Coordination of Space Techniques for Geodesy and Geodynamics), GPS Bulletin, Vol. 2, No. 1, published by NGS, January-February 1989.

Kellogg, J., T. Dixon and R. Neilan, Central and South America 1988 GPS Geodesy Campaign - CASA UNO, To appear in EOS, 1989.

Kolenkiewicz, R., J. Ryan and M. H. Torrence, A Comparison Between LAGEOS Laser Ranging and Very Long Baseline Interferometry Determined Baseline Lengths, *J. Geophys. Res.*, 90(B11), 9265-9274, 1985.

Melbourne, W., R. Anderle, M. Feissel, R. King, D. McCarthy, D. Smith, B. Tapley and R. Vicente, Project MERIT Standards, U.S. Naval Observatory Circular No. 167, 1983.

Minster, J. B., and T. H. Jordan, Present-day Plate Motions, *J. Geophys. Res.*, 83(B11), 5331-5354, 1978.

Murray, M. and R. King, SV-3 Coordinates of GPS Receivers, MIT Internal Memorandum, 1988.

NASA Crustal Dynamics Project Staff, Crustal Dynamics Project: Catalog of Site Information, NASA Reference Publication 1198, March 1988.

Ryan, J., C. Ma and E. Himwich, SOLVE Global Solution GLB206, GSFC Memo, March 1988.

Schutz, B., B. Tapley, R. Eanes and M. Watkins, Earth Rotation from LAGEOS Laser Ranging, Annual Report for 1987, D-51 to D-56, Bureau International de l'Heure, Paris, 1988.

Schutz, B. and B. Tapley, UTOPIA: University of Texas Orbit Processor, TR 80-1, Center for Space Research, 1980.

Tapley, B., B. Schutz and R. Eanes, Station Coordinates, Baselines and Earth Rotation from LAGEOS Laser Ranging: 1976-1984, *J. Geophys. Res.*, 90(B11), 9235-9248, 1985.

TABLE 1. CIGNET TI–4100 SITES (JANUARY, 1989)	
Kokee Park, Kauai, HI	Tromso, Norway
Mojave, CA	Westford, MA
Onsala, Sweden	Wettzell, FRG
Richmond, FL	Yellowknife, NWT

TABLE 2. ADDITIONAL CASA UNO SITES (TI-4100)
Black Birch, New Zealand
Canberra (Tidbinbilla), Australia
Ft. Davis, TX
Owens Valley, CA
Pago Pago, American Samoa

TABLE 3. VLBI/SLR TRANSFORMATION SITES		
Location	VLBI Mark	SLR Mark
Ft. Davis, TX	7216	7086
Mojave, CA	7222	7265
Westford, MA	7209	7091
Wettzell, FRG	7224	7834

TABLE 4. TRANSFORMATION SITE DIFFERENCES AFTER APPLICATION OF 7-PARAMETER TRANSFORMATION				
Location	SLR Mark	Differences (m)		
		Δx	Δy	Δz
Ft. Davis, TX	7086	0.020	–0.071	0.050
Mojave, CA	7265	0.025	–0.001	–0.018
Westford, MA	7091	–0.087	0.071	0.054
Wettzell, FRG	7834	0.043	0.002	0.022
	RMS	0.051	0.050	0.039

TABLE 5. FSC-2 COORDINATES (m)			
Site	x	y	z
Mojave, CA	–2356214.8400	–4646733.8110	3668460.5440
Westford, MA	1492232.8440	–4458091.7180	4296045.9140
Yellowknife, NWT	–1224064.5070	–2689832.9950	–5633432.5500
Wettzell, FRG	4075546.3550	931825.4590	4801599.1700
Onsala, Sweden	3370659.8770	711876.9860	5349788.1050
Ft. Davis, TX	–1324192.4360	–5332061.1350	3232044.3480
Owens Valley, CA	–2409643.9260	–4478269.4230	3838639.5860
Canberra, Australia	–4461015.8080	2682720.5220	–3674299.5410
Epoch: January 1, 1988	Coordinates refer to phase center		

TABLE 6. GPS FORCE KINEMATIC AND MEASUREMENT MODELS

Gravitational Force:

Earth

GM = 398600.440 km^3/s^2

R = 6378137.0 m

GEM-L2, MERIT Standards (Melbourne, et al., 1983) truncated at degree and order 8, with the value of J2 corrected for the permanent tide

Other Bodies

Sun and Moon from DE-200

Nongravitational Force:

Radiation Pressure

Direct solar, ROCK 4 model, scale factor estimated

Other

y-bias, estimated parameter in spacecraft *y*-axis

Kinematic Models:

Precession, Nutation

IAU (see MERIT Standards)

Earth Rotation

UT1 tide variations (see MERIT Standards)

Polar motion and UT1, determined by LAGEOS SLR (reported weekly on GE Mark 3)

Measurement Models:

Relativity

Chao troposphere model, zenith delay estimated for each day

Ionosphere correction applied from dual frequency

Phase center in spacecraft axes with respect to center of mass:

$x = 0.21$ m; $y = 0.0$ m; $z = 0.854$ m

TABLE 7. SOLUTION STATISTICS		
Week	Number of Double Differenced Measurements	Residual RMS(m)
419	66,735	0.03127
420	75,077	0.03447
419/420	141,812	0.05223

TABLE 8. POSITION DIFFERENCES AT COMMON TIME							
	Satellite PRN						
Component	3	6	8	9	11	12	13
x	2.58	6.04	0.43	2.48	0.25	2.01	1.96
y	0.36	−1.79	−1.87	−1.22	−1.89	0.72	−4.18
z	0.08	−3.16	1.01	−2.36	0.56	0.87	0.87

TABLE 9. WEEKS 419 AND 420 COMPARISONS				
	Week 420–419(m)			
Baseline	Δx	Δy	Δz	Δb
Canberra/A. Samoa b = 4545598m	−0.147	−0.212	+0.087	0.265
Canberra/Black Birch b = 2254519m	−0.012	−0.070	+0.045	0.048
Ft. Davis/Kauai b = 5409249m	−0.006	+0.085	−0.038	0.062
Mojave/OVRO b = 245348m	−0.040	−0.030	0.034	0.011
Onsala/Tromso b = 1406186m	−0.021	−0.027	−0.023	−0.009

TABLE 10. WEEKS 419 AND 420 KAUAI ESTIMATION			
	x	y	z
Week 419	−5543839.250	−2054587.639	2387809.937
Week 420	−5543839.256	−2054587.554	2387809.899
Week 441 Survey	−5543839.248	−2054587.750	2387810.051
Ft. Davis/Kauai Baseline:			
Week 419		5409249.809m	
Week 420		5409249.871m	
Week 441 Survey		5409249.722m	

TABLE 11. WEEKS 419 AND 420 TROMSO ESTIMATION				
Week	Coordinates in FSC-2(m)			
	x	y	z	
419	2102941.481	721569.546	5958193.990	
420	2102941.460	721569.519	5958193.967	
Week	Coordinates Relative to Onsala (m)			
	Δx	Δy	Δz	b
419	−1267718.396	9692.560	608405.885	1406186.900
420	−1267718.417	9692.533	608405.862	1406186.909
All coordinates refer to antenna phase center.				

PRECISION ORBIT DETERMINATION OF GLOBAL POSITIONING SYSTEM SATELLITES

by

CHING-SHUN HO

Center for Space Research

The University of Texas at Austin

August 1990

CSR-90-2

This report was prepared with the support of

Contracts NAG5-940 and USGS 14-08-0001-A-00358

under the direction of

Byron D. Tapley and Bob E. Schutz

PRECISION ORBIT DETERMINATION OF
GLOBAL POSITIONING SYSTEM SATELLITES

Precise geodetic measurement can provide an excellent study of plate tectonic motion. The potential of Global Positioning System (GPS) has been shown in determining the precise baseline. The precise GPS satellite orbit is one key to high-accuracy long baseline (>200 km) solutions. This study examines GPS orbit determination using two L-band signals transmitted by GPS satellites.

The research concentrates on the analysis of the pseudo-range and phase data collected during the CASA UNO campaign. The fidelity of the applied force and derived observation models has been tested by processing the tracking data from the campaign with the unconstrained (i.e., no *a priori* state covariance) batch estimation approach. The orbit accuracy has been assessed through the baseline solution and the orbit comparison.

Based on the results from the tracking data experiments, the precise GPS orbit resulted in baseline accuracy of a few parts in 10^8 can be obtained by using a weekly data set from a globally distributed tracking network. In addition, the potential that the precise baseline can be independently determined has been demonstrated if a global orbit is available. Evidence has been shown for the existence of unmodeled GPS force characteristics that is, in part, associated with Earth shadowing. The approach with several subarcs to model the acceleration in satellite body-fixed Y-direction improves the multi-week orbit quality, especially of eclipsing orbits.

APPENDIX V

1. "Analysis of southwest Pacific campaign data: July 1988," Proc. Fifth International Geodetic Symposium on Satellite Positioning, Las Cruces, New Mexico, March 1989
2. "Precision orbit determination for GPS," Proc. Second International Symposium on Satellite Positioning Using GPS, Ottawa, Canada, September 1990

ANALYSIS OF SOUTHWEST PACIFIC CAMPAIGN DATA: JULY 1988

B. E. Schutz and C. S. Ho
Center for Space Research
The University of Texas
Austin, Texas 78712, U.S.A.

M. Bevis
Marine, Earth and Atmospheric Sciences
North Carolina State University
Raleigh, NC 27695, U.S.A.

ABSTRACT

In July 1988, four TI-4100 receivers occupied sites in the Southwest Pacific to collect epoch measurements for tectonic studies. Three UNAVCO receivers operated for about ten days at Upolu (Western Samoa), Rarotonga (Cook Islands) and Vava'u (Tonga). A TI ROM receiver on loan to UNAVCO was operated at Tongatapu (Tonga). Other sites were occupied for a period of two days. Fiducial station support was provided with the operation of a receiver at Orroral, Australia, and a Mini-Mac receiver operated at Tsukuba, Japan. The CIGNET sites provided data from locations in the United States, Canada, Federal Republic of Germany, Sweden and Norway. The Southwest Pacific baselines vary in length; the longest baseline is about 1600 km. This paper describes the overall quality of the first six days of the 1988 Campaign data and presents the results of geodetic analyses of these data. Various cases have been considered and the internal consistency of the baselines was found to be a part in 10^8 on 1600 km baselines.

INTRODUCTION

In July 1988, a GPS campaign was conducted in the Southwest Pacific to collect epoch measurements to be used for crustal motion studies in the plate boundary complex of the Tonga region. In this region where the Indo-Australian and Pacific plates create a complex crustal deformation, the relative plate velocities are expected to be in the vicinity of 18 cm/yr.

The epoch measurements of July 1988 were collected at sites which are a subset of sites planned for occupation in the Main Campaigns of 1989, 1990 and 1992. The Main Campaigns will extend from Rarotonga on the Pacific Plate to New Caledonia on the Indo-Australian Plate. The purposes of the 1988 Campaign were:

- Collect epoch measurements at a few selected sites
- Gain experience in Southwest Pacific logistics, GPS data collection and data analysis
- Use experience to plan the Main Campaign.

The 1988 Campaign was conducted during July 11-21 (Days 193-203) and the participating institutions are given in Table 1. The sites visited in 1988 are illustrated in Fig. 1. Further information on details of the July 1988 Campaign are given by Bevis (1989) who serves as the Project Coordinator.

The purpose of this paper is to summarize analysis and results of data collected during the first six days of the 1988 Campaign corresponding to GPS Week 444. The analysis includes an examination of the sensitivity of the results to various parameters.

DATA

Data collected by the CIGNET (CSTG Bulletin, 1989) played an important role in the 1988 Campaign for the determination of GPS orbits. These data were augmented by equally important contributions from Orroral, Australia, and Tsukuba, Japan. Further information concerning the fiducial sites and the field sites are given in Table 2 and the global distribution of sites is illustrated in Fig. 2. In the studies performed, Tromso was not treated as a known, fixed site but was allowed to adjust in the same manner as the field sites.

In general, most receivers performed excellently during the the campaign. One receiver (Richmond, FL) experienced problems and contributed little data. Occasional problems were experienced at some CIGNET sites. Because of a software problem, the TI ROM receiver located at Tongatapu recorded data for some periods that was out of time synchronization with the other receivers by nine seconds.

The pseudo-range data from all sites were used to provide corrections to the phase time tag. Phase data were used in a double difference mode from the current operating Block-I satellites, namely, PRN 3, 6, 8, 9, 11, 12 and 13.

MODELS AND REFERENCE FRAME

The force and kinematic models used in the analysis of the July 1988 Campaign are described by Schutz, et al. (1989). The technique used to obtain the reference frame and the resulting fiducial coordinates can be found in the same source. The adopted coordinates for the Southwest Pacific campaign, identified as FSC-2, are given in Table 3. Information provided by AUSLIG (Steed, private communication, 1988) and GSI (M. Tsuji, private communication, 1988) enabled establishment of the Orroral and Tsukuba coordinates in the FSC-2 system.

The set of estimated parameters associated with the dynamical description of the satellite motion are given in Table 4. In addition, coordinates of all experiment sites in the Southwest Pacific were estimated in addition to the coordinates of Tromso, Norway. A priori constraints were not used with any estimated parameters, i.e., the a priori covariance on estimated parameters was infinite.

RESULTS

A single orbital arc spanning the entire Week 444 was used to determine the GPS orbits for analysis of the field sites. Experiments were performed to investigate the sensitivity of the results to force model characteristics and data contributions. Consideration of data contributions included the influence of the Tongatapu receiver synchronization which was investigated by treating the data with less than one second synchronization as a separate and independent "site" from the data collected with a nine second synchronization offset. The cases considered are summarized in Table 5.

The three-dimensional coordinates for the field sites were estimated, but the results are given in terms of the intersite distance (baseline) from the "base" station, Rarotonga, in Table 6. Rarotonga was chosen as the base station because of its distant location on the Pacific plate. Although the orbit changes from case to case by a few centimeters to several meters, the 1500 km baselines show changes at the one to two centimeter level or better than a part in 10^8.

To demonstrate the influence of the fiducial coordinates, the fixed coordinates of Kauai were changed by about 10 cm and Case A was repeated. This change in the coordinates produced a change in the absolute length of the baseline of two centimeters. The other cases produced comparable shifts in the absolute value and the same level of internal consistency from case to case as shown in Table 6.

The estimated three-dimensional coordinates of Tromso are shown in Table 7. For comparison, the estimate is compared with a result obtained for GPS Week 419, as given by Schutz, et al. (1989). The comparison between Weeks 419 and 444 show agreement at the few centimeter level in all three components for a 1400 km baseline. As a further comparison, the Case A orbit, which excluded Tromso in the orbit determination, was held fixed and the Tromso coordinates were estimated. The result is in less agreement with the cases in which Tromso simultaneously contributed to the orbit determination and the estimation of the site coordinates, although the baseline length is consistent.

CONCLUSIONS

Based on the analysis of available CIGNET and field data collected during GPS Week 444, the results presented in this paper show internal consistency on the 1500 km intersite baselines at the level of 1-2 cm, corresponding to a part in 10^8. No external standard is currently available in this region to serve as a comparison. Although in a different region of the world, a determination of Tromso, Norway, was performed that produced a result in good agreement with determinations from CASA UNO data. A VLBI visit scheduled for summer, 1989, will enable an evaluation of the Tromso results.

Lack of receiver synchronization at the 10 second level produced a small difference in baseline length (3 cm) when compared to results obtained with less than one second time synchronization. Other factors may have contributed to the 3 cm difference, such as the influence of data loss from fiducial stations, especially Kauai, experienced during some intervals.

Future analysis will focus on the remaining data in Week 445, which comprises about 40% of the total data set. Some differences exist in the global tracking in the remaining data sets, such as no available data from Onsala. Further refinements will be completed in the processing of Week 444, such as the use of fiducial coordinates mapped to July, 1988, rather than the coordinates for January 1, 1988, used in the analysis described in this paper. It is expected that the absolute values of the baselines will slightly change with the modified fiducial coordinates, but the internal consistency is expected to be unchanged.

ACKNOWLEDGEMENTS

Many individuals made invaluable contributions in the field campaign. They are identified by Bevis (1989). It is the case that without their dedicated efforts, the results given in this paper would not have been possible. The support of NSF, NASA and The University of Texas at Austin is gratefully acknowledged.

REFERENCES

Bevis, M., Southwest Pacific GPS Project Newsletter #3, North Carolina State University, January, 1989.

CSTG (International Coordination of Space Techniques for Geodesy and Geodynamics), GPS Bulletin, Vol. 2, No. 1, published by NGS, January-February 1989.

Schutz, B. E., B. D. Tapley, C. S. Ho, H. J. Rim, and P.A.M. Abusali, GPS Orbit Determination: Experiments and Results, proceedings of the 5th. Geodetic Symposium, University of Texas, April, 1989.

TABLE 1
INSTITUTIONS AND AGENCIES PARTICIPATING IN THE SOUTHWEST PACIFIC GPS PROJECT
North Carolina State University (USA)
University of Colorado (USA)
University of Texas at Austin (USA)
ORSTOM (France, New Caledonia
National Geodetic Survey (USA)
Cornell University (USA)
Jet Propulsion Laboratory (USA)
Institut Géographique National (France)
University of New South Wales (Australia)
Australian Surveying and Land Information Group (Australia)
Department of Survey and Land Information (New Zealand)
Department of Lands and Survey (Western Samoa)
Ministry of Lands, Survey and Natural Resources (Tonga)
Lands and Survey Branch (Niue)
Mineral Resources Department (Fiji)
Topographic Service (Vanuatu)
Service Topographique (New Caledonia)
Geographical Survey Institute (Japan)

TABLE 2. DATA		
Fiducial Sites		
Orroral, Australia	TI4100/GESAR	Cesium
Tsukuba, Japan	Mini-Mac	Cesium
Kauai, HI	TI4100/CORE	H-Maser
Mojave, CA	TI4100/CORE	H-Maser
Yellowknife, NWT	TI4100/CORE	Cesium
Westford, MA	TI4100/CORE	H-Maser
Richmond, FL	TI4100/CORE	H-Maser
Wettzell, FRG	TI4100/CORE	H-Maser
Onsala, Sweden	TI4100/CORE	H-Maser
Tromso, Norway	TI4100/CORE	Cesium
Field Sites		
Rarotonga (Cook Islands)	TI4100/GESAR	Crystal
Upolu (Western Samoa)	TI4100/GESAR	Crystal
Vava'u (Tonga)	TI4100/GESAR	Crystal
Tongatapu (Tonga)	TI4100/ROM	Crystal
Rubidium used on occasion at field sites.		

TABLE 3. FSC-2 COORDINATES (m)			
Site	x	y	z
Mojave, CA	−2356214.8400	−4646733.8110	3668460.5440
Westford, MA	1492232.8440	−4458091.7180	4296045.9140
Yellowknife, NWT	−1224064.5070	−2689832.9950	−5633432.5500
Wettzell, FRG	4075546.3550	931825.4590	4801599.1700
Onsala, Sweden	3370659.8770	711876.9860	5349788.1050
Kauai, HI	−5543818.2778	−2054582.7942	2387858.4651
Orroral, Australia	−4446476.5730	2678105.1735	−3696262.2145
Tsukuba, Japan	−3957193.3880	3310191.6530	3737733.3390

TABLE 4. ESTIMATED PARAMETERS
Arc Length: 7 days
Epoch position, velocity of each satellite
Scale parameter for ROCK4 radiation pressure for each satellite
y −bias, one for each satellite
Troposphere zenith delay (3 hour) for each station
Station coordinates (selected)
Double difference biases

TABLE 5. STUDY CASES	
Case	Description
A	Excluded data: Tsukuba, Tongatapu, Tromso
B	Same as Case A, except three y −bias parameters estimated instead of one
C	Excluded data: Tsukuba, Tromso
D	Excluded data: Tromso, Tongatapu
E	Excluded data: Tsukuba, Tongatapu
Estimated parameters are defined in Table 4, except as noted.	

TABLE 6. BASELINE RESULTS*

			Distance (m): Rarotonga to			
Case	DD RMS(m)	No. of DD	Vava'u 1509181+	W. Samoa 1527539+	Tongatapu-1 1605588+	Tongatapu-2 1605588+
A	0.03696	63,370	0.635	0.105	-	-
B	0.03594	63,370	0.649	0.116	-	-
C	0.03729	70,997	0.630	0.105	0.575	0.541
D	0.03737	63,834	0.635	0.105	-	-
E	0.03572	75,797	0.637	0.092	-	-

* Phase center to phase center, not reduced to geodetic mark

Note: Case to case orbits change by up to 3 meters
Tongatapu 1 synchronized < 1 sec
Tongatapu 2 synchronized < 10 sec
DD = Double Difference
RMS = Root Mean Square

TABLE 7. OTHER COMPARISONS

Onsala/Tromso Baseline:

Case E: 1406186.915m
Case A orbit, fixed: 1406186.918m
CASA UNO 419: 1406186.900

Three-dimensional Onsala/Tromso:

	Case E	Case A orbit fixed	Week 419
Δx	−1267718.414	−1267718.350	−1267718.396
Δy	9692.512	9692.563	9692.560
Δz	608405.882	608406.024	608405.885

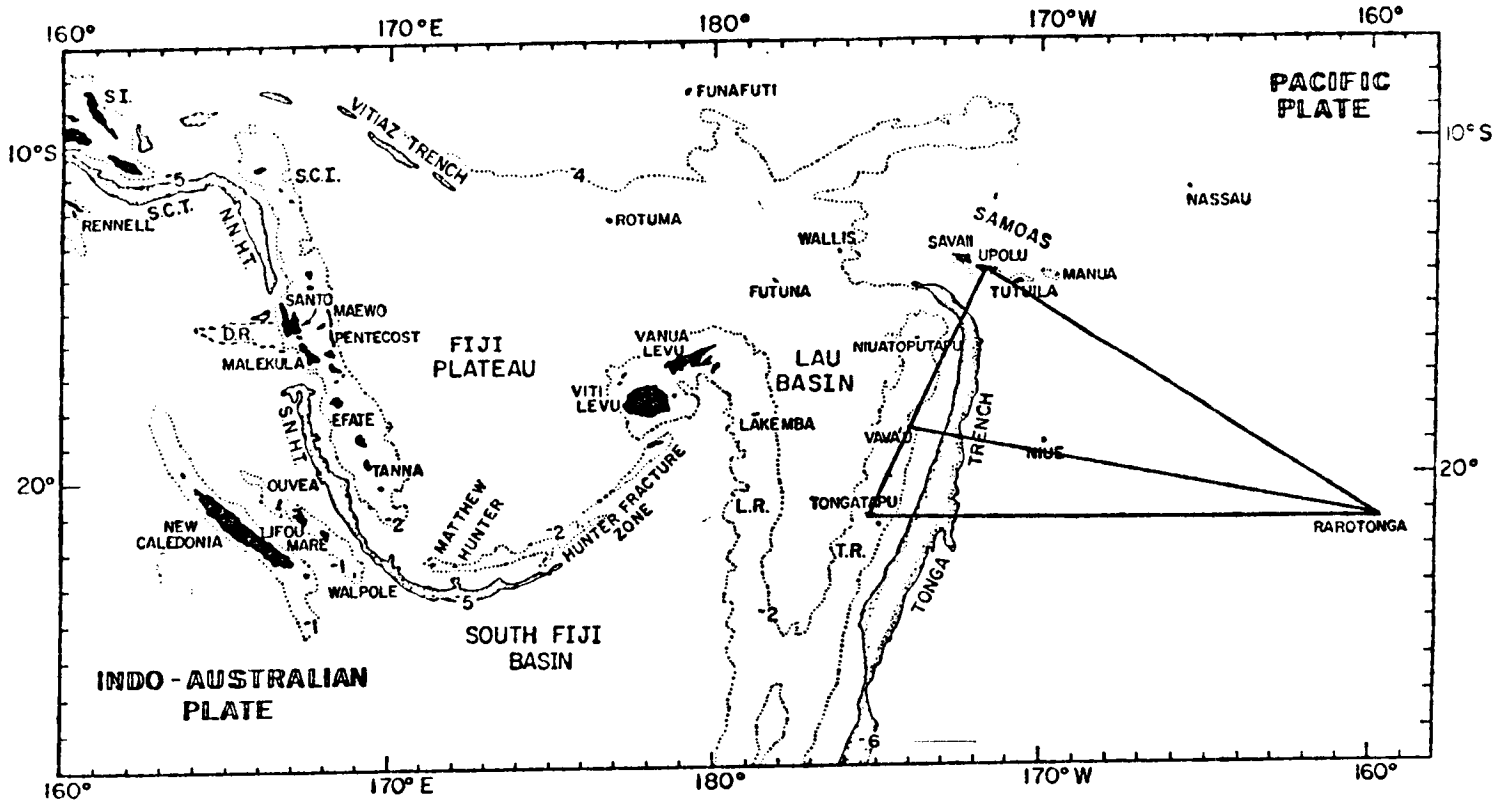

Figure 1. Southwest Pacific Network: 1988

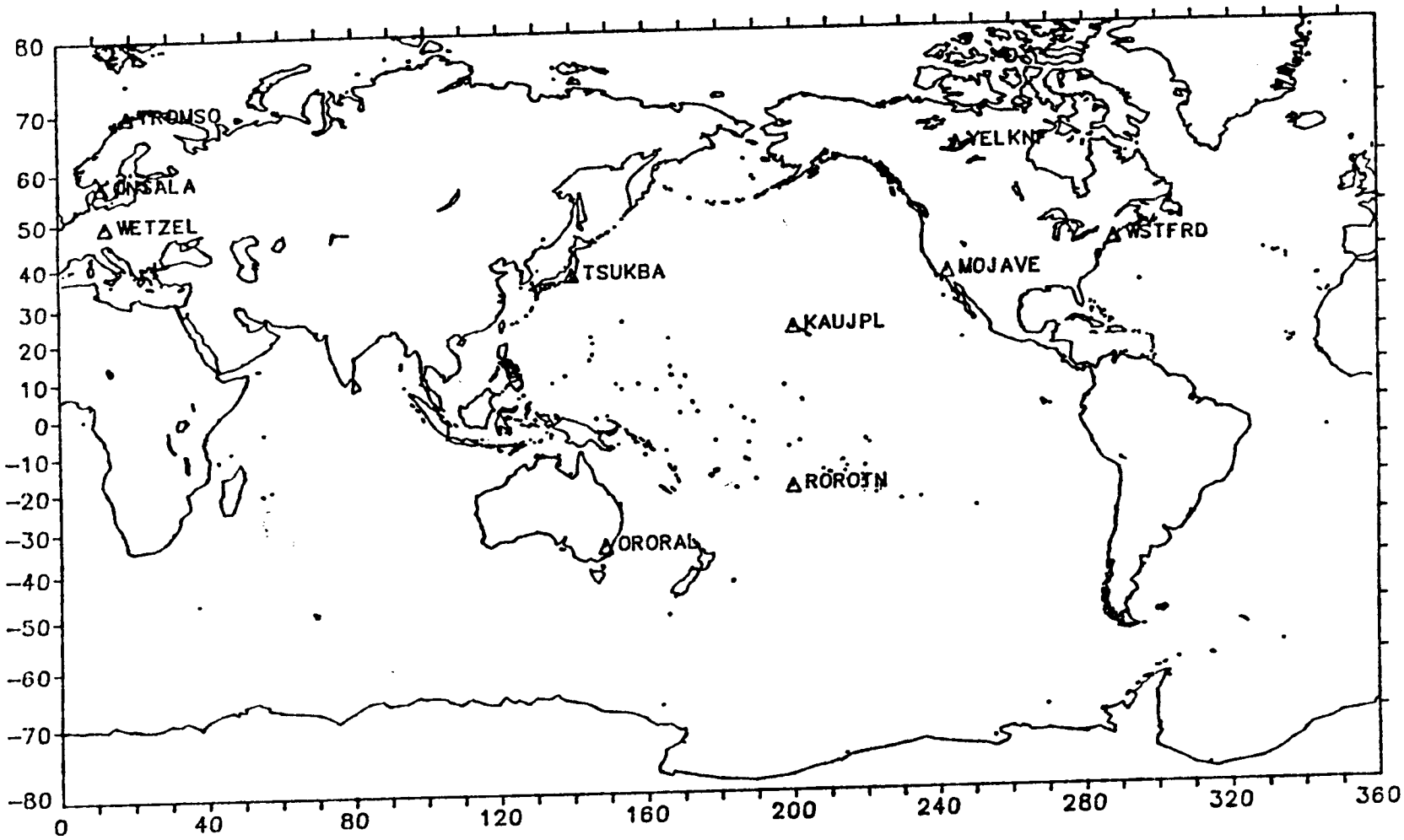

Figure 2. 1988 Southwest Pacific Campaign Global Sites

PRECISION ORBIT DETERMINATION FOR GPS

B. Schutz, C. Ho, P. Abusali, B. Tapley
Center for Space Research
University of Texas at Austin
Austin, TX 78712-1085
Tel (512) 471-5573, Fax (512) 471-3570

Nearly global distribution of GPS data have been collected to support several campaigns in recent years, e.g., the CASA UNO and GOTEX experiments. Such campaigns are becoming increasingly characterized by the use of a variety of receiver types as the abundance of new receivers increases. It is not uncommon for the global data set collected at the CIGNET sites to be augmented with data from global data outside the geographical area of the campaign. As the networks have become more global and as the number of available GPS satellites has grown, both opportunities and difficulties have been presented to the analyst community. The opportunities presented by the global data sets include an improved understanding of the nature of nongravitational forces acting on the satellites. Such improved understanding could contribute to concomitant improvements in baseline determinations through improved ephemerides. Results obtained from specific campaigns are described based on double difference measurements. The results show evidence of unmodeled effects on the orbits and possible sources are discussed. Evaluation of the orbits is conducted through orbit comparisons and assessment of baselines derived from the use of those orbits, where possible. For example, a recent comparison of the Onsala/Tromso baseline with recently released VLBI results shows agreement at a level of better than 2 parts in 10^8 on the 1406 km baseline.

INTRODUCTION

The importance of accurate orbits to support applications of GPS is widely recognized. Yet the orbit accuracy is one of the more difficult characteristics to ascertain in an absolute sense. For the most part, orbit accuracy is assessed in geodetic applications (e.g., positioning) by the ability of the orbit to support the desired accuracy in the application. In fact, for those applications, the orbit could exhibit large errors in an absolute sense and still be tolerated if the orbit is able to produce the desired geodetic accuracy. Even though the orbit accuracy does not always map in a one-to-one manner into geodetic accuracy, it is a readily demonstrated fact that high orbit accuracy is a necessary condition for high geodetic accuracy from satellite techniques.

The orbital position accuracy depends on a variety of factors, including the fidelity of models describing both the forces acting on the satellite as well as the kinematic models. In a complex way, the model fidelity interacts with other characteristics such as the data span, or arc length, and the measurement precision (and accuracy) to influence the orbit accuracy as noted, for example, by Lichten [1990] and Schutz, et al. [1990]. In addition, software accuracy is a factor that cannot be ignored.

From the standpoint of assessing the orbit accuracy, several criteria can be used, such as:

- direct comparison of independently determined orbits using either the same or different data sets
- direct comparison of independent software models
- direct comparison of geodetic results obtained by independent sources

This paper attempts to assess the GPS orbit accuracy for a specific period of time using these criteria. A complete analysis with all criteria has not been conducted, and unequal emphasis is placed on each of the preceding criteria in the following sections.

DATA

In the summer of 1989, a crustal motion campaign with GPS was conducted in the Southwest Pacific. The data collected from the CIGNET stations was augmented with data from several additional sites as well as the Defense Mapping Agency sites. The fiducial sites are given by Abusali, et al. [1990]. The campaign took place in GPS Weeks 496-500, however, the results given in this paper concentrate primarily on Weeks 499 and 500. The coordinates of the fiducial sites were adopted in a reference frame defined by Satellite Laser Ranging (SLR) and Very Long Baseline Interferometry (VLBI) as described by Schutz, et al. [1990].

A mixture of receivers was used at the fiducial sites. For example, the CIGNET sites used MiniMac 2816AT receivers, except for the use of TI-4100 at Kauai, Yellowkinife, Onsala and Tromso. The extended network used TI-4100 at Orroral, Huahine and Ft. Davis, a MiniMac at Kwajalein and a Rogue at Wellington. The DMA sites all used TI-4100 receivers. The field sites in the Southwest Pacific used TI-4100 and Trimble receivers, but these data were not used in the analysis described in this paper.

The phase and pseudo-range data were collected at 30 second intervals and were used in a double difference mode to eliminate most of the influence of satellite and receiver clock variations. Pseudo-range data were used to ensure time tag accuracy of one microsecond with respect to GPS time.

MODELS

The force and kinematic models used were generally consistent with the IERS Standards [McCarthy, 1989], with a few exceptions. These standards have been primarily adopted for the Lageos SLR satellite, but can be readily adjusted to accommodate GPS. The primary gravity differences between the Standards and the GPS model is the truncation of the gravity field at degree and order 8 for GPS. The nongravitational force model used ROCK4 with an estimated scale parameter and a y-bias parameter. A zenith delay was estimated every 3 hours at each tracking site. Ionospherically corrected phase measurements were used in the analysis.

The results have been obtained using the Multi-Satellite Orbit Determination Program (MSODP), a multi-satellite derivative of the single satellite University of Texas Orbit Processor (UTOPIA). The data were pre-processed using IBM PC, VAXstations and a VAX 8200. Final results have been, for the most part, generated on a Cray X-MP/24 computer.

RESULTS

The results obtained used all available Block-I satellites (PRN 3, 6, 8, 9, 11, 12 and 13) and one Block-II satellite (PRN 14). The statistics for one week arcs coincident with Weeks 499 and 500 are given in Table 1. As shown in this table, almost 100,000 double difference phase measurements were used in the solution. The solution for Week 500 shows fewer measurements because not all available data have been merged into the solution process at the present time.

The resulting Block-I Earth-fixed ephemerides for Week 499 were compared with ephemerides produced by the Defense Mapping Agency and the Naval Surface Warfare Center. PRN 8 was not available in the DMA ephemeris set. The results of a direct comparison, without any adjustments in the respective ephemerides, are summarized in Table 2. The differences for PRN 3 are shown in Fig 1 for radial, along-track and cross-track components. As shown in Table 2 and illustrated in Fig. 1, the radial component exhibits a consistent mean value of 1.3 m which is caused by the different values of GM used in WGS-84 (398600.5 km^3/s^2) and the IERS Standards (398600.44 km^3/s^2). The cross-track differences suggest a reference frame source and the along-track components are expected to be dominated by the force model.

Table 1. Solution Summary

	Week 499	Week 500
Number of satellites	8	8
Number of stations	18	16
Number of DD*	97828	82702
RMS of DD (cm)	3.0	3.0
Number of sites estim.	9	7

*DD: Double difference

Table 2. Week 499 Ephemeris Comparison with DMA, Mean (RMS)

Satellite PRN	Radial (m)	Along-Track(m)	Cross-Track(m)
3	-1.3 (1.6)	-1.9 (3.1)	0.5 (4.6)
6	-1.3 (1.6)	-0.3 (2.2)	0.5 (4.2)
9	-1.3 (1.7)	-0.8 (2.4)	0.5 (3.6)
11	-1.3 (1.4)	1.0 (1.8)	0.0 (2.5)
12	-1.3 (1.3)	-2.1 (2.8)	-0.1 (3.8)
13	-1.3 (1.4)	0.5 (1.5)	-0.2 (2.4)

Note: the value in parenthesis is the RMS

The ephemeris differences illustrated in Table 1 and 2 as well as Fig. 1 were further investigated by attempting to ascertain the level of software compatibility. In this investigation, the DMA/NSWC ephemerides were used as "observations" to MSODP and the satellite position, velocity, ROCK4 scale and a y-bias were adjusted for each satellite. While the adjustment reduces the level of differences, residuals at the meter level remain as illustrated in Fig. 2, the along-track component for PRN 3. The source of the remaining differences are expected to be solely caused by software and model differences, including the reference frames and the treatment of nongravitational forces.

A test of model fidelity was conducted in which the solution for Week 499 summarized in Table 1 was predicted forward in time and compared with the ephemeris estimated for Week 500. The results obtained were generally consistent with those reported for the CASA UNO experiment [Schutz, et al., 1990] in which the satellites experiencing eclipsing showed significant degradation in the along-track prediction performance, a strong indicator of model fidelity. The effects of eclipsing have been recently examined by Feulner [1990] and Vigue [1990]. Feulner investigated the influence of numerical integrator performance across the discontinuous shadow boundary and modified the MSODP fixed step integrator to handle the effect. While his results showed that the effect was significant, it did not remove the observed characteristics with real GPS data. In the second study, Vigue solved the partial differential equations for heat conduction and radiation for simplified spacecraft models simultaneously with the orbit equations. She showed that distinctly different temperatures can exist on the solar panel surfaces which can produce a several meter orbit effect over one week. Additional investigation is in progress.

An important question from the geodetic standpoint is the influence of the previously described orbit differences on the recovery of geodetic parameters. Detailed comparisons of such recovery using the ephemerides described in this paper (CSR and DMA/NSWC) are in progress using the field data in the Southwest Pacific. The Onsala/Tromso baseline has been repeatedly used as a verification test, especially since it was measured in 1989 by a VLBI visit to Tromso. Using the double difference phase ephemerides described in this paper, the estimated baseline (without the application of any *a priori* constraints) agrees with the VLBI result at the 1-2 parts in 10^8 level on the 1400 km baseline. This result suggests that the ephemeris differences described above are not a limiting factor at this level. The possibility that the differences are a limiting factor in achieving a part in 10^9 geodesy remains to be determined.

ACKNOWLEDGEMENTS

This study was supported, in part, by NASA, NSF and the University of Texas at Austin. Computational assistance was provided by The University of Texas System Center for High Performance Computing. Numerous organizations have participated and contributed to the Southwest Pacific campaign. These contributions are greatly appreciated.

REFERENCES

Abusali, P. A. M., B. E. Schutz, C. Ho," Relation Between SLR/VLBI and WGS-84 Reference Frames," *Proceedings of Second International Symposium on Precise Positioning with GPS (GPS '90), Ottawa, Ontario, September 3-7,* 1990.

Feulner, M., "The Numerical Integration of Near Earth Satellite Orbits Across SRP Boundaries Using the Method of Modified Back Differences," Masters Thesis, University of Texas at Austin, August, 1990.

Lichten, S. M., "Towards GPS Orbit Accuracy of Tens of Centimeters," *Geophysical Research Letters 17(3),* 215-218, 1990.

McCarthy, D. (ed.), "IERS Standards (1989," IERS Technical Note 3, Observatoire de Paris, Paris, November, 1989.

Schutz, B., C. Ho, P. Abusali and B. Tapley, "CASA UNO GPS Orbit and Baseline Experiments," *Geophysical Research Letters 17 (5),* 643-646, 1990.

Vigue, Y., "Thermal Imbalance Effects on a GPS Satellite," Masters Thesis, University of Texas at Austin, May, 1990.

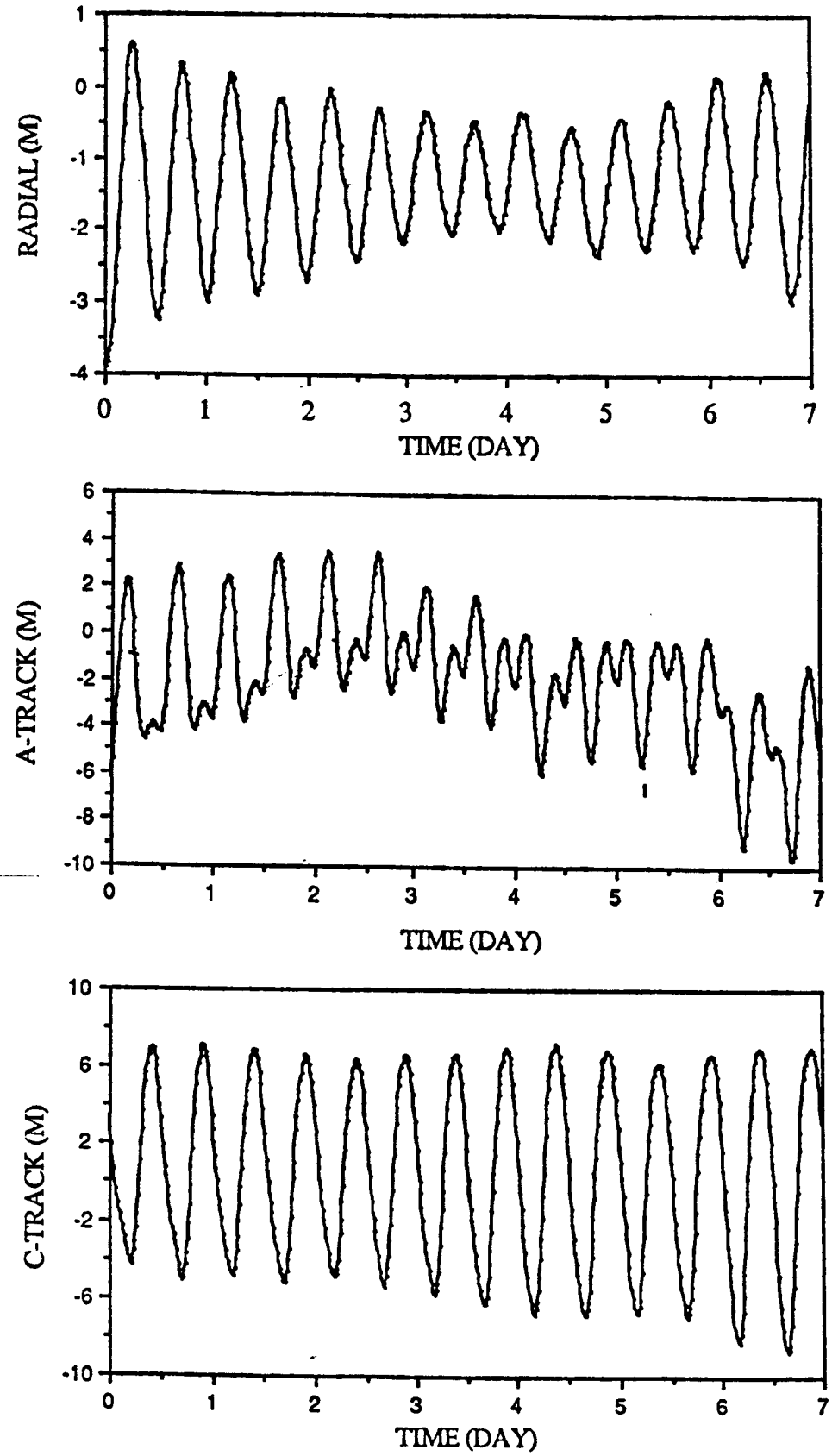

Fig. 1. Week 499 Differences Between DMA/NSWC and CSR Ephemerides (PRN 3)

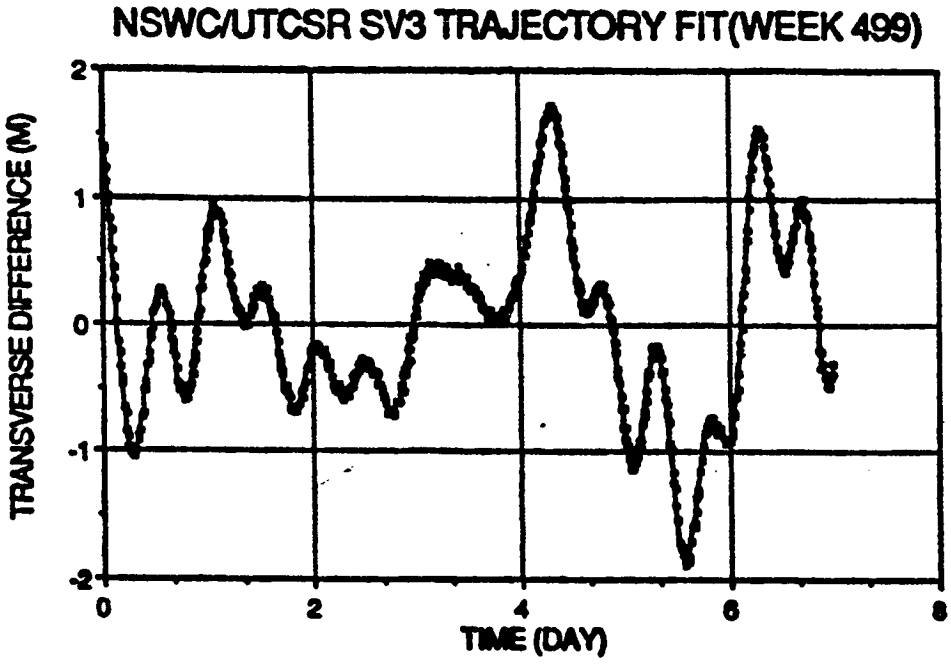

Fig. 2. Week 499 Difference After Orbit Adjust (PRN 3 Along Track)

RELATION BETWEEN SLR/VLBI AND WGS-84 REFERENCE FRAMES

P. A. M. Abusali, B. E. Schutz, C. S. Ho

Center for Space Research

University of Texas at Austin

Austin, TX 78712-1085

Tel (512) 471-5573, Fax (512) 471-3570

In order to establish a relationship between the SLR/VLBI and WGS-84 reference frames, GPS tracking data collected from stations defined in these two frames during a common period have been processed. Previous investigations have used common pseudo-range data from the OCS Monitor Stations and augmented CIGNET sites to determine a longitude rotation of about 1 m. For the investigation reported in this paper, the CIGNET sites have been augmented with TI-4100 data from five DMA sites and were processed in a double differenced phase mode. The coordinates resulting from adjustments of the DMA sites into the SLR/VLBI system used for the CIGNET sites with a priori WGS-84 coordinates, were used to determine the seven parameter transformation set. The characteristics of the transformations have been investigated for selected time periods in 1989 when DMA data were available to support particular experiments.

INTRODUCTION

Several reference frames are in use for geodetic applications, including the WGS-84 [Decker, 1986;White, et al., 1989] and those frames based on Satellite Laser Ranging (SLR) and/or Very Long Baseline Interferometry (VLBI). The reference frame defined by the International Earth Rotation Service (IERS) is based primarily upon SLR and VLBI [Boucher, 1990], known as the IERS Terrestrial Reference Frame (ITRF), and is one of the important products of the IERS.

Since the GPS ephemerides broadcast from the satellites are in the WGS-84 frame, many applications have adopted that frame as the most convenient or appropriate. On the other hand, most applications that require comparison with external techniques, such as VLBI and SLR, or that will continue time series of geodetic measurements that have been obtained by those techniques, will adopt the ITRF or another system based on SLR and VLBI.

Recent results have shown agreement between the SLR and VLBI reference frames at the less than 3 cm level [Ray, et al., 1990]. These results were obtained using sites which have been occupied by both SLR and VLBI at different times as well as those sites where both techniques operate within a few kilometers on a regular basis. This centimeter level demonstration of accuracy supports the notion that a reference frame based on the combined SLR and VLBI systems is capable of supporting high accuracy geodetic applications.

The relationship between the WGS-84 and SLR/VLBI reference frames is required for a variety of applications, especially those applications in which results obtained in one reference frame are to be compared or applied in the other reference frame. Previous studies in which this relationship was investigated include Abusali, et al. [1989] in which the smoothed pseudo-range data from the Operational Control Segment (OCS) were used in combination with data from the Cooperative International GPS Network (CIGNET) to determine the relation between the reference frames. In this study, the data from the OCS were combined with pseudo-range data from the CIGNET. By fixing the OCS coordinates to the WGS-84 values, the orbits and the coordinates of the CIGNET sites were estimated using WGS-84 force model parameters as well. Conversely, the CIGNET sites were fixed to their coordinates in an SLR/VLBI reference frame and the OCS sites were estimated simultaneously with the orbit parameters. With the estimated coordinates in the respective systems, the seven parameter transformation (translation, rotation and scale) was determined. The major conclusion of this study was that there appeared to be an approximately 60 milliarc second longitude rotation between the WGS-84 and the SLR/VLBI reference frames, while little consistency was observed in the other six parameters depending on the estimated parameters. In any case, the observed longitude shift was within the uncertainty assigned to the longitude origin by the Defense Mapping Agency of 200 milliarc seconds (DMA, 1987).

The purpose of this paper is to further examine the relationship between the WGS-84 and a SLR/VLBI reference frame using double differenced phase data and a different data set than used previously. In this case, data from the five DMA sites were used to determine position vectors relative to the CIGNET sites whose coordinates are described in an SLR/VLBI reference frame. By comparing the resulting coordinates with those obtained in the WGS-84 system, the seven parameter transformation parameters can be obtained. The resulting parameters are described and investigated in the following sections.

DATA

While the establishment of the relation between the reference frames is important for the previously de-

scribed reasons, the primary motivation for this study was the need for the DMA data to provide tracking coverage during the Southwest Pacific '89 campaign in which, for various reasons, incomplete geographical coverage was available. The primary purpose of this campaign is the study of crustal motions in an area of the Southwest Pacific ranging from the Tonga region to New Caledonia. A nearly global set of CIGNET sites was further augmented with additional sites in the Pacific as summarized in Table 1, as well as the five DMA sites. The campaign took place during GPS Weeks 496-500, however, the results for this paper concentrate on GPS Week 499.

The coordinates of the CIGNET and augmented network in Table 1 were defined in an SLR/VLBI reference frame using results that differed only slightly from those given by Ray, et al. [1990]. The estimation of the DMA sites was based on the double differenced phase data formed between the sites given in Table 2. As shown in this table, the baselines varied in length from 900 km to 4000 km.

TABLE 1. Contributing Sites

CIGNET	Augmented	DMA
Mojave, CA	Huahine, Fr. Polynesia	Buenos Aires, Argentina
Kokee Park, HI	Orroral, Australia	Quito, Ecuador
Westford, MA	Tanna	Smithfield, Australia
Richmond, FL	Western Samoa	Hermitage, England
Yellowknife, NWT	Kwajalein	Bahrain
Wettzell, FRG		
Onsala, Sweden		
Tromso, Norway		
Tsukuba, Japan		

TABLE 2. Baselines

Reference Site	DMA	Baseline (km)
Orroral	Smithfield	941
Onsala	Hermitage	1078
Richmond	Quito	2841
Wettzell	Bahrain	4050
Quito	Buenos Aires	4252

RESULTS

With the network adopted for this experiment, information about the orbit is given by Schutz, et al. [1990]. To summarize, a one week solution was computed in which the DMA sites were treated as unknowns and a simultaneous solution for orbits, spacecraft y-bias, ROCK4 radiation pressure scale parameter, double difference biases and troposphere parameters were obtained. For this solution, approximately 100,000 double differenced measurements were used and these were fit in the estimation process to about 3 cm.

The resulting estimates for the DMA site coordinates, defined in the SLR/VLBI reference frame, were then compared with coordinates determined in the WGS-84 reference frame. As shown in Table 3, the direct comparison of the coordinates is at the one meter level in all three components. Using these differences to solve for translation, rotation and scale parameters results in differences (after applying the estimated parameters) of less than 0.5 m. As shown in Table 3, a longitudinal rotation (32 mas) is the dominant angular contribution. Furthermore, the scale difference is approximately consistent with the different values of GM (WGS-84: 398600.5 km^3/s^2; SLR: 398600.4404 km^3/s^2).

The longitude rotation deserves additional comment. The observed rotation requires an eastward rotation of 32 mas of the WGS-84 to coincide with the SLR reference meridian. However, an eastward 16 mas rotation was required to make the VLBI meridian coincide with the SLR meridian.

In summary, the VLBI, SLR and WGS-84 reference frames are compatible at the meter level. Based on the results given in Table 3, an eastward longitudinal rotation of 16 mas is required to make the WGS-84 coincident with VLBI and 32 mas is required to be coincident with SLR. Since the choice of longitude origin is arbitrary, these rotations may not be valid for all SLR and VLBI solutions.

ACKNOWLEDGEMENTS

This study was supported, in part, by NASA, NSF and the University of Texas at Austin. Computational assistance was provided by The University of Texas System Center for High Performance Computing. The Southwest Pacific GPS Campaign has been organized by M. Bevis and F. Taylor, and includes numerous contributors whose assistance is greatly appreciated. The authors are grateful to DMA for providing the data from their sites.

REFERENCES

Abusali, P. A. M., B. E. Schutz, H. Fliegel and A. Liu, Coordinate Reference Frame Compatibility Between VLBI/SLR Systems and WGS-84, Proceedings of Fifth International Geodetic Symposium on satellite Positioning, Las Cruces, NM, March 13-17, 1989.

Boucher, C. and Z. Altamimi, The Initial IERS Terrestrial Reference Frame, IERS Technical Note No. 1, 1989.

Decker, B. L., World Geodetic System 1984, Proceedings of Fourth International Geodetic Symposium on Satellite Positioning, Austin, TX, April 28-May 2, 1986.

Defense Mapping Agency, Department of Defense World Geodetic System 1984, DMA Tech. Report 8350-

2-B, September, 1987.

Ray, J., J. Ryan, C. Ma, T. Clark, B. Schutz, R. Eanes, M. Watkins and B. Tapley, Comparison of VLBI and SLR Geocentric Site Coordinates, *Geophysical Research Letters*, to appear, 1990.

Schutz, B., C. Ho, P. Abusali and B. Tapley, Precision Orbit Determination for GPS, Proceedings of the Second International Symposium on Precise Positioning with GPS (GPS '90), Ottawa, Ontario, September 3-7, 1990.

White, H. L., B. L. Decker and M. Kumar, World Geodetic System 1984: A Modern and Accurate Global Reference Frame, Proceedings of the Fifth International Geodetic Symposium on Satellite Positioning, Las Cruces, NM, March 13-17, 1989.

TABLE 3. WGS-84 to VLBI/SLR

Direct Comparison:

Component	RMS (m)
x	1.211
y	1.033
z	0.894

Seven Parameter Transformation:

Component		Std. Error
Origin x (m)	- 0.094	0.12
Origin y (m)	0.281	0.12
Origin z (m)	- 0.436	0.12
Scale (ppm)	- 0.222	0.02
Rotation x (mas)	- 6.018	4.40
Rotation y (mas)	2.279	5.22
Rotation z (mas)	31.700	4.67

Comparison after Transformation:

Component	RMS (m)
x	0.446
y	0.212
z	0.107

APPENDIX VI

1. "Coordinate reference frame compatibility between VLBI/SLR system and WGS84," Proc. Fifth International Geodetic Symposium on Satellite Positioning, Las Cruces, New Mexico, March 1989
2. "Relation between SLR/VLBI and WGS84 reference frames," Proc. Second International Symposium on Satellite Positioning Using GPS, Ottawa, Canada, September 1990
3. "Comparison of SLR/VLBI and WGS84 reference frames," presented at the Fall Meeting of the American Geophysical Union, San Francisco, Calif., December 1990 (Abstract)

RELATION BETWEEN SLR/VLBI AND WGS-84 REFERENCE FRAMES

P. A. M. Abusali, B. E. Schutz, C. S. Ho

Center for Space Research

University of Texas at Austin

Austin, TX 78712-1085

Tel (512) 471-5573, Fax (512) 471-3570

In order to establish a relationship between the SLR/VLBI and WGS-84 reference frames, GPS tracking data collected from stations defined in these two frames during a common period have been processed. Previous investigations have used common pseudo-range data from the OCS Monitor Stations and augmented CIGNET sites to determine a longitude rotation of about 1 m. For the investigation reported in this paper, the CIGNET sites have been augmented with TI-4100 data from five DMA sites and were processed in a double differenced phase mode. The coordinates resulting from adjustments of the DMA sites into the SLR/VLBI system used for the CIGNET sites with a priori WGS-84 coordinates, were used to determine the seven parameter transformation set. The characteristics of the transformations have been investigated for selected time periods in 1989 when DMA data were available to support particular experiments.

INTRODUCTION

Several reference frames are in use for geodetic applications, including the WGS-84 [Decker, 1986;White, et al., 1989] and those frames based on Satellite Laser Ranging (SLR) and/or Very Long Baseline Interferometry (VLBI). The reference frame defined by the International Earth Rotation Service (IERS) is based primarily upon SLR and VLBI [Boucher, 1990], known as the IERS Terrestrial Reference Frame (ITRF), and is one of the important products of the IERS.

Since the GPS ephemerides broadcast from the satellites are in the WGS-84 frame, many applications have adopted that frame as the most convenient or appropriate. On the other hand, most applications that require comparison with external techniques, such as VLBI and SLR, or that will continue time series of geodetic measurements that have been obtained by those techniques, will adopt the ITRF or another system based on SLR and VLBI.

Recent results have shown agreement between the SLR and VLBI reference frames at the less than 3 cm level [Ray, et al., 1990]. These results were obtained using sites which have been occupied by both SLR and VLBI at different times as well as those sites where both techniques operate within a few kilometers on a regular basis. This centimeter level demonstration of accuracy supports the notion that a reference frame based on the combined SLR and VLBI systems is capable of supporting high accuracy geodetic applications.

The relationship between the WGS-84 and SLR/VLBI reference frames is required for a variety of applications, especially those applications in which results obtained in one reference frame are to be compared or applied in the other reference frame. Previous studies in which this relationship was investigated include Abusali, et al. [1989] in which the smoothed pseudo-range data from the Operational Control Segment (OCS) were used in combination with data from the Cooperative International GPS Network (CIGNET) to determine the relation between the reference frames. In this study, the data from the OCS were combined with pseudo-range data from the CIGNET. By fixing the OCS coordinates to the WGS-84 values, the orbits and the coordinates of the CIGNET sites were estimated using WGS-84 force model parameters as well. Conversely, the CIGNET sites were fixed to their coordinates in an SLR/VLBI reference frame and the OCS sites were estimated simultaneously with the orbit parameters. With the estimated coordinates in the respective systems, the seven parameter transformation (translation, rotation and scale) was determined. The major conclusion of this study was that there appeared to be an approximately 60 milliarc second longitude rotation between the WGS-84 and the SLR/VLBI reference frames, while little consistency was observed in the other six parameters depending on the estimated parameters. In any case, the observed longitude shift was within the uncertainty assigned to the longitude origin by the Defense Mapping Agency of 200 milliarc seconds (DMA, 1987).

The purpose of this paper is to further examine the relationship between the WGS-84 and a SLR/VLBI reference frame using double differenced phase data and a different data set than used previously. In this case, data from the five DMA sites were used to determine position vectors relative to the CIGNET sites whose coordinates are described in an SLR/VLBI reference frame. By comparing the resulting coordinates with those obtained in the WGS-84 system, the seven parameter transformation parameters can be obtained. The resulting parameters are described and investigated in the following sections.

DATA

While the establishment of the relation between the reference frames is important for the previously de-

scribed reasons, the primary motivation for this study was the need for the DMA data to provide tracking coverage during the Southwest Pacific '89 campaign in which, for various reasons, incomplete geographical coverage was available. The primary purpose of this campaign is the study of crustal motions in an area of the Southwest Pacific ranging from the Tonga region to New Caledonia. A nearly global set of CIGNET sites was further augmented with additional sites in the Pacific as summarized in Table 1, as well as the five DMA sites. The campaign took place during GPS Weeks 496-500, however, the results for this paper concentrate on GPS Week 499.

The coordinates of the CIGNET and augmented network in Table 1 were defined in an SLR/VLBI reference frame using results that differed only slightly from those given by Ray, et al. [1990]. The estimation of the DMA sites was based on the double differenced phase data formed between the sites given in Table 2. As shown in this table, the baselines varied in length from 900 km to 4000 km.

TABLE 1. Contributing Sites

CIGNET	Augmented	DMA
Mojave, CA	Huahine, Fr. Polynesia	Buenos Aires, Argentina
Kokee Park, HI	Orroral, Australia	Quito, Ecuador
Westford, MA	Tanna	Smithfield, Australia
Richmond, FL	Western Samoa	Hermitage, England
Yellowknife, NWT	Kwajalein	Bahrain
Wettzell, FRG		
Onsala, Sweden		
Tromso, Norway		
Tsukuba, Japan		

TABLE 2. Baselines

Reference Site	DMA	Baseline (km)
Orroral	Smithfield	941
Onsala	Hermitage	1078
Richmond	Quito	2841
Wettzell	Bahrain	4050
Quito	Buenos Aires	4252

RESULTS

With the network adopted for this experiment, information about the orbit is given by Schutz, et al. [1990]. To summarize, a one week solution was computed in which the DMA sites were treated as unknowns and a simultaneous solution for orbits, spacecraft y-bias, ROCK4 radiation pressure scale parameter, double difference biases and troposphere parameters were obtained. For this solution, approximately 100,000 double differenced measurements were used and these were fit in the estimation process to about 3 cm.

The resulting estimates for the DMA site coordinates, defined in the SLR/VLBI reference frame, were then compared with coordinates determined in the WGS-84 reference frame. As shown in Table 3, the direct comparison of the coordinates is at the one meter level in all three components. Using these differences to solve for translation, rotation and scale parameters results in differences (after applying the estimated parameters) of less than 0.5 m. As shown in Table 3, a longitudinal rotation (32 mas) is the dominant angular contribution. Furthermore, the scale difference is approximately consistent with the different values of GM (WGS-84: 398600.5 km^3/s^2; SLR: 398600.4404 km^3/s^2).

The longitude rotation deserves additional comment. The observed rotation requires an eastward rotation of 32 mas of the WGS-84 to coincide with the SLR reference meridian. However, an eastward 16 mas rotation was required to make the VLBI meridian coincide with the SLR meridian.

In summary, the VLBI, SLR and WGS-84 reference frames are compatible at the meter level. Based on the results given in Table 3, an eastward longitudinal rotation of 16 mas is required to make the WGS-84 coincident with VLBI and 32 mas is required to be coincident with SLR. Since the choice of longitude origin is arbitrary, these rotations may not be valid for all SLR and VLBI solutions.

ACKNOWLEDGEMENTS

This study was supported, in part, by NASA, NSF and the University of Texas at Austin. Computational assistance was provided by The University of Texas System Center for High Performance Computing. The Southwest Pacific GPS Campaign has been organized by M. Bevis and F. Taylor, and includes numerous contributors whose assistance is greatly appreciated. The authors are grateful to DMA for providing the data from their sites.

REFERENCES

Abusali, P. A. M., B. E. Schutz, H. Fliegel and A. Liu, Coordinate Reference Frame Compatibility Between VLBI/SLR Systems and WGS-84, Proceedings of Fifth International Geodetic Symposium on satellite Positioning, Las Cruces, NM, March 13-17, 1989.

Boucher, C. and Z. Altamimi, The Initial IERS Terrestrial Reference Frame, IERS Technical Note No. 1, 1989.

Decker, B. L., World Geodetic System 1984, Proceedings of Fourth International Geodetic Symposium on Satellite Positioning, Austin, TX, April 28-May 2, 1986.

Defense Mapping Agency, Department of Defense World Geodetic System 1984, DMA Tech. Report 8350-

2-B, September, 1987.

Ray, J., J. Ryan, C. Ma, T. Clark, B. Schutz, R. Eanes, M. Watkins and B. Tapley, Comparison of VLBI and SLR Geocentric Site Coordinates, *Geophysical Research Letters*, to appear, 1990.

Schutz, B., C. Ho, P. Abusali and B. Tapley, Precision Orbit Determination for GPS, Proceedings of the Second International Symposium on Precise Positioning with GPS (GPS '90), Ottawa, Ontario, September 3-7, 1990.

White, H. L., B. L. Decker and M. Kumar, World Geodetic System 1984: A Modern and Accurate Global Reference Frame, Proceedings of the Fifth International Geodetic Symposium on Satellite Positioning, Las Cruces, NM, March 13-17, 1989.

TABLE 3. WGS-84 to VLBI/SLR

Direct Comparison:

Component	RMS (m)
x	1.211
y	1.033
z	0.894

Seven Parameter Transformation:

Component		Std. Error
Origin x (m)	- 0.094	0.12
Origin y (m)	0.281	0.12
Origin z (m)	- 0.436	0.12
Scale (ppm)	- 0.222	0.02
Rotation x (mas)	- 6.018	4.40
Rotation y (mas)	2.279	5.22
Rotation z (mas)	31.700	4.67

Comparison after Transformation:

Component	RMS (m)
x	0.446
y	0.212
z	0.107

To appear in the proceedings of the Fifth International
Symposium on Satellite Positioning

COORDINATE REFERENCE FRAME COMPATIBILITY BETWEEN VLBI/SLR SYSTEM AND WGS 84

P.A.M. Abusali and Bob E. Schutz
Center for Space Research
The University of Texas
Austin, Texas 78712

Henry Fliegel and Anthony Liu
Aerospace Corporation
2350 East El Segundo Boulevard
El Segundo, CA 90245

ABSTRACT

The tracking sites of the Cooperative International GPS Network (CIGNET) are located near VLBI antennas, hence the coordinates of the GPS receiver antennas can be established in a VLBI reference frame. Since the GPS dynamics are described in a center of mass system, ties between the VLBI and SLR frames are used to define the reference frame. Precise ephemerides of GPS satellites, computed using CIGNET data, are then described in the VLBI/SLR frame which results in estimated user positions referred to this frame. Some GPS users, as in surveying applications, would prefer to compute geodetic quantities in the WGS 84 reference frame. Hence, transformations between these two reference frames are needed.

The Operational Control Segment (OCS) of GPS operates five globally distributed permanent tracking sites whose coordinates have been determined in the WGS 84 frame. Processing of tracking data from these sites in conjunction with data from the CIGNET stations facilitates the establishment of the transformation between the WGS 84 and VLBI/SLR reference frames. Pseudo-range data from OCS stations and CIGNET stations were processed separately and the orbits of all satellites differ by less than eleven meters in an RMS sense, which is partly due to the inconsistency between the reference frames. The data sets from the two networks were combined and one set of stations were estimated with respect to the other set. Using the estimated and a priori coordinates of one set of stations, a seven parameter transformation between the two systems was computed. The results indicate that there is a small longitude shift in the orientation of the two frames.

INTRODUCTION

In late 1986, the University of Texas Center for Space Research (CSR) under contract from the U.S. Geological Survey (USGS) Menlo Park, California, established a regional GPS tracking network in collaboration with the National Geodetic Survey (NGS) and the Texas State Department of Highways and Public Transportation (SDHPT). The tracking sites were at Mojave, California, Westford, Massachusetts, and Austin, Texas and used TI–4100 dual-frequency receivers. The receiver at Mojave is owned by CSR and has been operated by NGS, the receiver at Westford is owned and operated by NGS and the receiver at Austin is owned and operated by SDHPT. The data have been routinely processed at CSR, and precise ephemerides of the GPS satellites have been computed weekly. These ephemerides have been distributed to the participating agencies and other interested institutions.

Since early 1987, several other stations have been added to the network by cooperative agreements with NGS in an effort to develop a global network. NGS installed its own receivers at additional U.S. sites and made collaborative arrangements with foreign agencies to collect GPS data from their stations. The network is known as the Cooperative International GPS Network (CIGNET) and the currently contributing stations and the operating agencies are listed in Table 1. Data from these stations have been processed by CSR to produce precise ephemerides. All the tracking data and computed ephemerides have been archived at NGS.

The CIGNET antennas were installed in the vicinity of already existing or newly established very long baseline interferometry (VLBI) sites. Consequently, the coordinates of the CIGNET antennas were determined with respect to the VLBI site coordinates using conventional survey methods and GPS techniques [*Mader*, 1987a,b]. Since the VLBI determined station coordinates are insensitive to the Earth's center-of-mass location, whereas satellite laser ranging (SLR) determined station coordinates are influenced by the center-of-mass location, the reference frame adopted for the GPS antenna coordinates is a VLBI/SLR-defined frame, determined by the procedure outlined by Murray et al., [1988]. As a result, the precise ephemerides computed using these station coordinates are described in the same VLBI/SLR reference frame. Further, the gravity field and the Earth's polar motion and UT1 used in orbit computations at CSR are those determined using analysis of laser range data from Lageos satellite and reported to the International Earth Rotation Service.

The GPS satellites broadcast ephemeris messages referred to the WGS 84 system [*Decker*, 1986], and hence, the users of these ephemerides determine their coordinates in the WGS 84 system. If the precise ephemeris computed by CSR is used in determining station locations, then the solutions are referred to the VLBI/SLR frame. In some geodetic applications, as in surveying for example, users would prefer to determine coordinates of sites in WGS 84. As a consequence, there is a need to find the relation between the WGS 84 and the VLBI/SLR reference systems. An attempt has been made to establish a transformation between these two frames.

REFERENCE FRAME COMPARISON METHOD

One method of comparing two different coordinate systems is to compare satellite orbits determined using data collected from sets of stations referred to the individual reference frames. These results will be dependent on the associated force and kinematic models. The nature and level of orbit differences would reflect differences that may exist in the reference frames. However, it is difficult to quantify the specific differences using this approach. Another method to compare and quantify the differences between two reference frames is to find a set of seven parameters – three describing the origin, three describing the directional orientation and one denoting the scale difference of one frame with respect to other. Such a set of seven parameters can be determined, given two sets of cartesian coordinates for a globally distributed set of stations specified in the individual frames. This procedure was used to investigate the differences between the WGS 84 and the VLBI/SLR systems.

DATA USED IN OBTAINING RESULTS

The set of CIGNET stations listed in Table 1 does not have a completely global distribution, since the sites are concentrated in Europe and North America. A globally distributed set of stations is preferred for reference frame characterization. For this reason, a data set from one of the special global tracking campaigns of GPS satellites was chosen. The Jet Propulsion Laboratory helped organize a North Andes–Western Caribbean GPS Experiment in which data were collected from a set of globally distributed stations for a duration of about three weeks (1/17/88 to 2/5/88). This

campaign was named the CASA UNO [*Kellogg et al.*, 1989] and stations in Australia, New Zealand and America Samoa augments the CIGNET stations.

In order to be consistent with the number of stations considered in the WGS–84 frame, only five stations were chosen from among the total of thirteen fiducial stations which participated in the CASA UNO experiment. Coordinates of these five stations were determined in the VLBI/SLR system as listed in Table 2 and shown in Figure 1. The VLBI/SLR system coordinates are described by Schutz et al., [1989]. Although Ft. Davis and Canberra are not among the regularly contributing CIGNET stations, they are referred to as CIGNET stations in this paper solely for the purpose of identifying the reference frame in which they are considered.

The Operational Control Segment (OCS) of the GPS operates five globally distributed stations which collect GPS satellite tracking data continuously. The control segment uses these data to compute satellite orbits and upload the information to the satellites. The GPS satellites then broadcast the orbit information as part of the navigation message. The coordinates of the five OCS stations are known in the WGS 84 system, and hence, the ephemerides of the GPS satellites computed by OCS and broadcast by the satellites are in the WGS 84 system. The OCS stations and their coordinates [*Smith*, 1986] are listed in Table 3 and shown in Figure 1. GPS satellite tracking data from these stations for the duration of three weeks coinciding with the CASA UNO Experiment were provided to UT/CSR by the Aerospace Corporation for the purpose of a reference frame comparison study. However, contiguous OCS data were available for only four days in GPS week 419 (1/17/88 to 1/21/88) and five days in week 421 (2/2/88 to 2/7/88). This set of data will be referred to here as the OCS data in this paper.

The OCS stations operate STI communications receivers which collect dual-frequency, pseudo-range and carrier phase measurements. The pseudo-range measurements are smoothed using the carrier phase, and ionospheric-corrected range measurements are provided at fifteen-minute intervals. The CIGNET stations operate TI-4100 dual-frequency receivers which record pseudo-range and carrier phase at some specified intervals. Data are usually collected at thirty-second intervals. Since data are processed at CSR in batches of one week arc lengths, the number of measurements from five stations for all the GPS satellites is very large. Hence, the 30-second interval pseudo-range data set from the CIGNET was compressed by computing "normal points" in fifteen-minute bins at a preprocessing stage where erroneous observations are flagged and the ionospheric correction is applied. Thus, the OCS and CIGNET data sets are approximately comparable in that they both are ionospheric-corrected pseudo-range measurements at fifteen-minute intervals collected from individual sets of globally distributed stations.

ORBIT COMPARISON

GPS satellite orbits were computed in batches of one-week arcs. As mentioned earlier, since the concentration of OCS data was in Weeks 419 and 421, only these two weeks were analyzed. Orbit determinations of six of the seven GPS Block I satellites currently operational were performed simultaneously in a multi-satellite data processing mode. The satellites considered were PRN–3, –6, –9, –11, –12 and –13. PRN–8 was not used because of the variations observed in its on-board clock. A multi-satellite orbit determination version of UTOPIA [*Schutz*, 1980] software system was used in the University's dual Cyber 170/750 computer system. The following set of force models were used in all the orbit determination runs:

- Earth gravity model
  - — truncated (8 × 8) GEM-L2 [*Lerch et al.*, 1985] when VLBI/SLR frame is referenced
  - — truncated (8 × 8) WGS 84 used when WGS 84 frame is referenced
- Third body perturbation due to sun and moon using DE200 JPL ephemerides [*Standish*, 1982]
- ROCK4 model for solar radiation perturbation [*Porter*, 1976]
- y–bias acceleration [*Fliegel et.al.*, 1985]
- solid earth tide perturbation
- relativistic perturbation

For the kinematic model, polar motion and UT1 determined by Lageos long arc solution was used including the short period variations in UT1. Geometric variations on the station location due to solid Earth tides were taken into account.

The parameter estimation state vector consisted of the position and velocity components of each satellite, one scale parameter for each satellite for the ROCK4 model, one parameter for the y–bias force on each satellite and two parameters of a clock model for each of the passes defined individually for all satellites and stations. The number of these passes depended on the data distribution and the clock stability. One of the satellite clocks or a ground station clock was held fixed as reference and was not estimated. In addition to these parameters, coordinates of appropriate ground stations were estimated in some cases.

Orbit determination experiments were performed using the above mentioned force and kinematic models and the tracking data from the two sets of stations. The data were processed in batches of one week arcs for the GPS weeks 419 and 421. In each case a solution was obtained using the least squares approach which estimated the states of all the satellites and other dynamic parameters for the epoch. First, individual orbit solutions were obtained by processing the data from the OCS stations and CIGNET stations separately. To be consistent with the station coordinates, the respective gravity fields, namely, WGS 84 for OCS data and GEML2 for CIGNET data were used. The amount of data from both the sets of stations were about comparable for Week 421, whereas for Week 419 OCS had almost twice the amount of data compared to CIGNET. For this reason the orbits of the GPS satellites determined for the Week 421 were compared in Figure 2 and the comparison is summarized in Table 4. It can be observed from these figures and the table that the orbits of all the satellites computed using the two sets of data are within about 22 meters of each other in all components and within 11 meters in an RMS sense. Further, there is a mean difference of about 1.3 meters in the radial components of all satellites. This is believed to be due to the difference in the value of GM used in the two different fields, namely, 398600.5 km^3/sec^2 for WGS 84 and 398600.4404 $km^3/\ sec^2$ for GEML2. The negative mean in the along-track components of all satellites is also due, in part, to the different GM values. Several other factors, such as the difference in station coordinates, atmospheric correction applied to the data, remaining clock error, difference in the amount of data and the geometry of coverage may contribute to the overall differences between the two sets of orbits compared here. Further, any difference between the reference frames would also contribute to the orbit differences since the comparison is done in the J2000 nonrotating frame.

Data from both sets of stations were then combined and orbits of all the satellites were determined simultaneously by processing data from 10 stations. The orbit experiments and the results relevant to the discussion here are listed in Table 5. Only in Case–4 and Case–5 were the indicated station coordinates estimated and in all other cases only the satellite states and other parameters were estimated. Comparing the results of Case–3 with those of Case–6 and Case–7 shows that the

observation residual RMS is greater for Case–3 than that for either Case–6 or Case–7. This result indicates that there is an inconsistency between the two frames in which the two sets of stations are referenced. Note that in Case–3 the station coordinates are not in one consistent frame, whereas in all other cases they are. Although the improvement in residual RMS from Case–3 to Case–6 or Case–7 is small, the fact that there is an improvement is an indication of coordinate reference frame difference.

REFERENCE FRAME COMPARISON

In an attempt to quantify the difference between the reference frames and to find a transformation between these orbit determination experiments were performed in which coordinates of stations referenced in one frame were estimated while fixing the coordinates of stations in the other. These experiments are Cases–4 and –5 in Table 5. The estimated adjustments to the station coordinates for each of these cases are shown in Table 6 and in Table 7. The formal standard error corresponding to all these station coordinate estimates were less than 25 centimeters except for the Canberra estimate in Week 419 which had about 41 centimeters. The pseudo-range data from Canberra during Week 419 exhibited systematic behavior compared to other data sets believed to be caused by clock variation. The data were subdivided into a large number passes for clock model parameter estimation which caused the higher formal standard error.

Although the results shown in Table 6 and Table 7 do not reveal a definite pattern in all the coordinates, the longitude adjustments show some regularity which can be interpreted as a longitude orientation difference between the two reference frames. While interpreting these results it should be noted that the pseudo-range data used in obtaining these results have a noise RMS of about 1.5 meters. Further, the station coordinates themselves in either frame may have some uncertainty. While the uncertainty of the CIGNET station coordinates are believed to be a few centimeters based on estimates of the VLBI and SLR coordinates, the accuracy of OCS coordinates is unknown. Nevertheless, the orbit comparison results and the station estimation results indicate that there is a small difference between the two reference frames.

A transformation between the two frames which will minimize the difference can be obtained in terms of a seven parameter set consisting of three parameters for translation to make the origins coincide, three for rotation to make the direction parallel and one to make the scales equal in both the frames. Such a set is obtained as a least squares solution using as observations the differences between the estimated and a priori coordinates of the stations referred to one frame. Thus when the CIGNET station coordinates are estimated fixing the OCS stations, the estimated CIGNET coordinates are with respect to the WGS 84 frame. Since the a priori coordinates of these stations are in the VLBI/SLR frame using these two sets of coordinates for the same set of stations the seven parameter transformation can be obtained. Table 8 and Table 9 show the transformation parameters obtained using the results of Case–4 and Case–5 respectively. In Tables 8 and 9, ΔX, ΔY, ΔZ correspond to the origin translation, ΔL corresponds to scale and $\Delta\omega$, $\Delta\psi$, $\Delta\varepsilon$ correspond to rotation of one frame to the other. The quantities RMSX, RMSY and RMSZ are the RMS values of the differences between the a priori and the estimated coordinates of one set of stations, in the X,Y,Z directions respectively. The subscripts B and A refer to the RMS values before and after the transformation is applied to the station coordinates. The transformation is applied as follows:

$$\begin{bmatrix} x \\ y \\ z \end{bmatrix} = \begin{bmatrix} \Delta X \\ \Delta Y \\ \Delta Z \end{bmatrix} + (1 + \Delta L) \begin{bmatrix} 1 & \Delta\omega & -\Delta\psi \\ -\Delta\omega & 1 & \Delta\varepsilon \\ \Delta\psi & -\Delta\varepsilon & 1 \end{bmatrix} \begin{bmatrix} X \\ Y \\ Z \end{bmatrix}$$

where X,Y,Z are the coordinates of a station in one reference frame and x,y,z are the transformed coordinates of the same station referred to the new frame. It can be seen from the Tables that the differences between the station coordinates are reduced by applying the transformation thereby indicating that the computed transformation parameters are meaningful and have significance. However the values do have some uncertainties and it is difficult to arrive at one set of parameters with increased level of confidence using the current results.

CONCLUSION

Pseudo-range observations of GPS satellites obtained from two sets of global stations referred to VLBI/SLR and WGS 84 systems, were processed in order to check for compatibility between the two systems. Comparison of the satellite orbits computed in the individual systems indicates that there are small differences in gravity fields and in the orientation of the reference frames. Major effect of gravity field differences appears to be due to the differing values of GM.

The relation between the two reference frames was considered in terms of the seven parameter transformation. Estimated values of the seven parameters, except for longitude rotation, appear to be somewhat random in nature but the variations are within the noise level of the measurements processed. However, the longitude rotation from one frame to the other ($\Delta\omega$) exhibits consistency although the magnitude has some uncertainty. From the results presented here one can determine that there is a longitude shift of about 60 milliarc seconds with an uncertainty of about 15 milliarc seconds, between the two frames, the sense of rotation being eastwards from WGS 84 to VLBI/SLR frame. It should be noted that this value of longitude shift is within the uncertainty (200 milliarc seconds) assigned to the WGS 84 X-axis orientation [*DMA*, 1987].

REFERENCES

Decker, B. L., "World Geodetic System 1984," Proceedings, Fourth International Geodetic Symposium on Satellite Positioning, Austin, Texas, April 28-May 2, 1986.

Department of Defense World Geodetic System 1984, DMA Technical Report 8350-2-B, The Defense Mapping Agency, September, 1987.

Fliegel, H. F., W. A. Feess, W. C. Layton and N. W. Rhodus, "The GPS Radiation Force Model," Proceedings, First International Symposium on Precise Positioning with the Global Positioning System, NOAA, Rockville, Maryland, 1985.

Kellogg, J., T. Dixon and R. Neilan, "Central and South America 1988 GPS Geodesy Campaign–CASA UNO," To appear in *EOS*, 1989.

Lerch, R. J., S. M. Klosko, G. B. Patel, and C. A. Wagner, "A Gravity Model for Crustal Dynamics (GEM-L2)," Journal of Geophysical Research, 90 (B11), September 30, 1985.

Mader, G. L., "GPS Antenna Connections to VLBI Reference Points at Kokee Park and Westford," IOM, NGS, Rockville, Maryland, July 17, 1987a.

Mader, G. L., "GPS Antenna Connections to VLBI Reference Point at Mojave and the Position of Austin, GPS, "IOM, NGS, Rockville, Maryland, October 13, 1987b.

Murray, M. H., and R. W. King, "SV3 Coordinates of GPS Receivers," MIT Internal Memorandum, Cambridge, Massachusetts, April, 1988.

Porter, W. W., "Solar Force-Torque Model for the GPS Space Vehicle System," Rockwell

International, Space Division, Downey, California, January 15, 1976.
Schutz, B. E. and B. D. Tapley, "UTOPIA: University of Texas Orbit Processor," Center for Space Research, The University of Texas at Austin, 1980.
Schutz, B. E., B. D. Tapley, C. S. Ho, H. J. Rim and P.A.M. Abusali, "GPS Orbit Determinations: Experiments and Results," paper in this proceedings.
Smith, G. N. (Colonel, USA), "WGS 84 Coordinates of the GPS Monitor Stations," Letter to HQ USAF Space Division, (Dr. William Stein), October 17, 1986.
Standish, E. M., "Orientation of the JPL Ephemerides, DE200/LE200, to the Dynamical Equinox of J2000," Astron. Astrophys. 114, 297-302, 1982.

TABLE 1. CIGNET GPS TRACKING SITES

Location	Receiver	Clock	Agency
Austin, Texas	TI-4100	Cesium	TSDHPT
Westford, Massachusetts	TI-4100	H-Maser	NGS
Mojave, California	TI-4100	H-Maser	CSR
Yellowknife, Canada	TI-4100	Cesium	CGS
Richmond, Florida	TI-4100	H-Maser	NGS
Wettzell, West Germany	TI-4100	H-Maser	IFAG
Onsala, Sweden	TI-4100	H-Maser	NMA
Tromso, Norway	TI-4100	Cesium	NMA
Hawaii	TI-4100	H-Maser	NGS

Note: IFAG — Institut fuer Angewandte Geodaesie
NMA — Norwegian Mapping Agency
CGS — Canadian Geodetic Survey

TABLE 2. CIGNET STATION COORDINATES (VLBI/SLR FRAME)

Station	X (M)	Y (M)	Z (M)
Yellowknife	-1224064.5070	-2689832.9950	5633432.550
Kauai/Casa	-5543839.2480	-2054587.7500	2387810.0510
Fort Davis	-1324192.4360	-5332061.1350	3232044.3480
Wettzell	4075546.3550	931825.4590	4801599.1700
Canberra	-4461015.8080	2682720.5220	-3674299.5410

TABLE 3. COORDINATES OF OCS STATIONS (WGS 84 FRAME)

Station	*X* (M)	*Y* (M)	*Z* (M)
Kwajelein	-6160885.9700	1339851.3000	960843.2700
Diego Garcia	1917032.7500	6029784.3700	-801376.5400
Hawaii/OCS	-5511982.9600	-2200250.1500	2329482.1700
Ascension	6118525.3700	-1572350.9600	-876464.4400
Falcon AFB	-1248597.0200	-4819434.1000	3976501.1400

TABLE 4. SUMMARY OF ORBIT DIFFERENCES EPH(OCS) – EPH(CIGNET)						
	PRN–3	PRN–6	PRN–9	PRN–11	PRN–12	PRN–13
MEAN (m)						
Radial	1.311	1.446	1.378	1.282	1.307	1.352
A–Track	–7.475	–1.496	–2.926	–3.316	–4.730	–9.998
C–Track	0.084	–0.071	0.114	0.016	–0.168	0.012
RMS (m)						
Radial	1.677	1.519	1.417	1.693	1.521	1.622
A–Track	7.866	8.341	3.677	4.498	5.356	10.412
C–Track	8.313	5.421	3.807	2.130	6.940	0.224

TABLE 5. ORBIT DETERMINATION EXPERIMENTS			
Case	Comments	RMS (M)	No. OBS
WEEK 419			
Case–1A	OCS data only (WGS 84)	1.111	3034
Case–2A	CIGNET data only (GEML2)	1.972	1771
Case–3A	(OCS + CIGNET) data (GEML2)	1.602	4805
Case–4A	Fix OCS and Estimate CIGNET (WGS 84)	1.557	4805
Case–5A	Fix CIGNET and Estimate OCS (GEML2)	1.540	4805
Case–6A	OCS + Estimated CIGNET Coordinates (WGS 84)	1.557	4805
Case–7A	CIGNET + Estimated OCS Coordinates (GEML2)	1.540	4805
WEEK 421			
Case–1B	OCS data only (WGS 84)	1.677	3675
Case–2B	CIGNET data only (GEML2)	1.212	2702
Case–3B	(OCS + CIGNET) data (GEML2)	1.615	6377
Case–4B	Fix OCS and Estimate Cignet (WGS 84)	1.590	6377
Case–5B	Fix CIGNET and Estimate OCS (GEML2)	1.556	6377
Case–6B	OCS + Estimated CIGNET Coordinates (WGS 84)	1.590	6377
Case–7B	CIGNET + Estimated OCS Coordinates (GEML2)	1.556	6377

TABLE 6. ESTIMATED ADJUSTMENTS (METERS) OF CIGNET COORDINATES FIXING OCS STATIONS						
	Week 419 (Case–4A)			Week 421 (Case–4B)		
Station	Ht	Lat	Lon	Ht	Lat	Lon
Yellowknife	–0.822	–0.714	0.459	–1.855	0.189	0.003
Kauai/CASA	–1.386	–0.097	1.787	–1.849	–0.454	1.212
Ft. Davis	–2.690	–0.501	1.228	–1.127	–0.509	1.447
Wettzell	–2.071	0.074	0.821	–1.273	–0.301	0.878
Canberra	–0.195	0.851	2.175	0.987	0.939	1.221

TABLE 7. ESTIMATED ADJUSTMENTS (METERS) OF OCS COORDINATES FIXING CIGNET STATIONS

Station	Week 419 (Case-5A)			Week 421 (Case-5B)		
	Ht	Lat	Lon	Ht	Lat	Lon
Kwajalein	–0.086	0.529	–0.646	–1.422	0.374	–0.823
Diego Garcia	1.014	1.003	–2.084	–0.232	0.851	–3.102
Hawaii/OCS	–1.402	0.548	–1.745	–1.256	0.828	–1.143
Ascension	–0.354	0.499	–0.411	–1.226	0.770	0.396
Falcon-AFB	–1.869	0.769	–1.728	–1.282	0.714	–1.769

TABLE 8. SEVEN PARAMETER TRANSFORMATION FROM VLBI/SLR TO WGS-84

Parameter	Week 419	Week 421
ΔX (m)	–0.783	–0.413
ΔY (m)	0.178	0.646
ΔZ (m)	–0.204	–0.611
ΔL (ppm)	–0.248	–0.128
$\Delta\omega$ (rad)	–0.075	–0.063
$\Delta\psi$ (rad)	–0.014	–0.015
$\Delta\varepsilon$ (rad)	–0.021	–0.018
$RMSX_B$ (m)	1.606	1.573
$RMSY_B$ (m)	1.398	0.799
$RMSZ_B$ (m)	1.235	1.093
$RMSX_A$ (m)	0.522	0.753
$RMSY_A$ (m)	0.530	0.519
$RMSZ_A$ (m)	0.421	0.288

TABLE 9. SEVEN PARAMETER TRANSFORMATION FROM WGS 84 TO VLBI/SLR

Parameter	Week 419	Week 421
ΔX (m)	0.374	0.585
ΔY (m)	0.877	0.495
ΔZ (m)	0.404	0.664
ΔL (ppm)	–0.081	–0.171
$\Delta\omega$ (arc sec)	0.041	0.040
$\Delta\psi$ (arc sec)	0.008	0.014
$\Delta\varepsilon$ (arc sec)	–0.009	–0.003
$RMSX_B$ (m)	1.236	1.718
$RMSY_B$ (m)	1.466	1.247
$RMSZ_B$ (m)	0.569	0.599
$RMSX_A$ (m)	0.628	0.784
$RMSY_A$ (m)	0.767	0.675
$RMSZ_A$ (m)	0.248	0.255

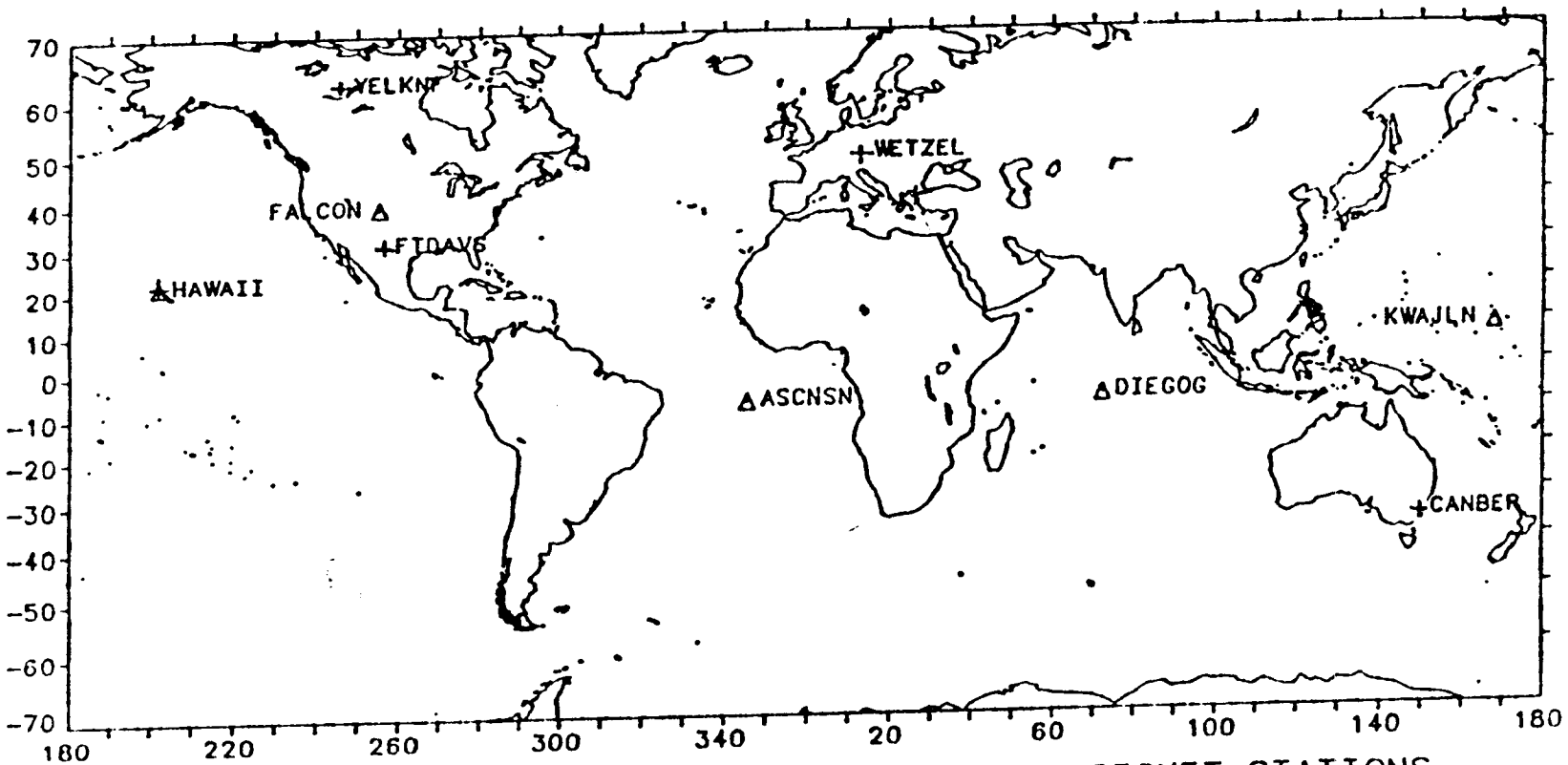

LOCATIONS OF THE OCS STATIONS AND CIGNET STATIONS CONSIDERED FOR REFERENCE FRAME TRANSFORMATION

Δ OCS

Figure 1

+ CIGNET

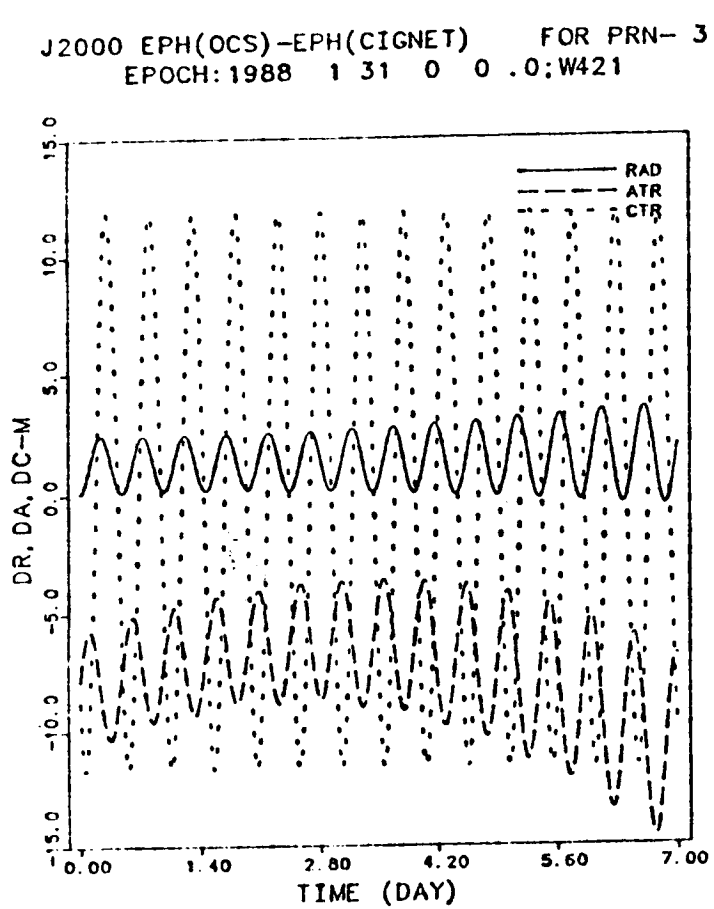

Figure 2A

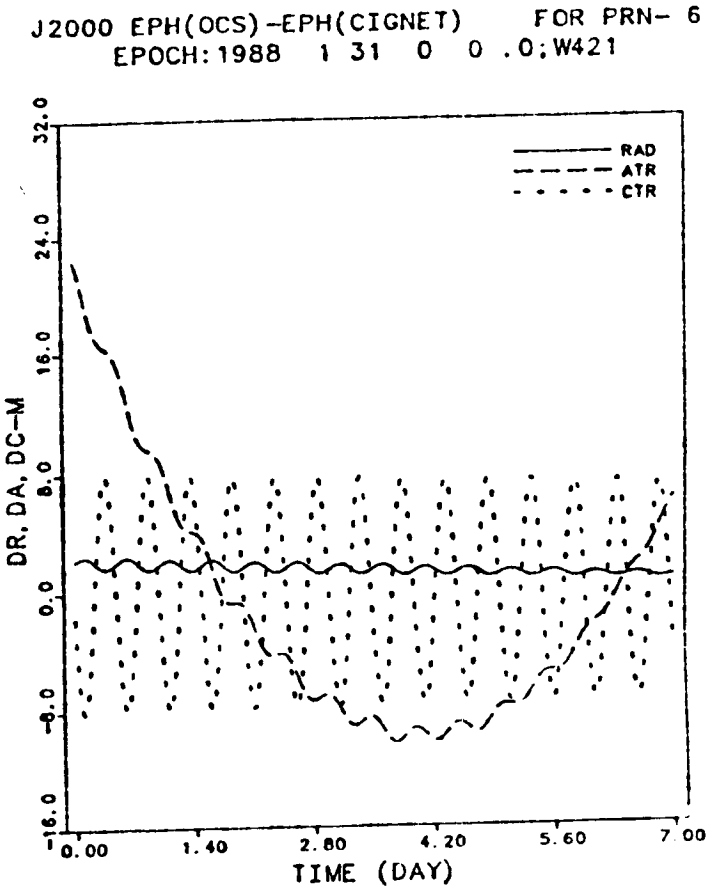

Figure 2B

The theoretical definition of the terrestrial reference system which is realized by IERS through a conventional terrestrial reference frame formed by SLR, LLR, VLBI and GPS stations is presented. In particular its origin, scale, orientation and evolution with time are reviewed, taking into account relativistic and deformation effects.

The various realizations of the IERS Terrestrial Reference System (ITRS) are also discussed, in particular the reference frames obtained by individual techniques or the combined adjustment performed by the IERS/CB in 1990 (ITRF 89).

G32A-2 1350h

The Consistency of Global Geocentric Station Coordinates Determined by SLR and VLBI Techniques

J.R. Ray (Interferometrics Inc./GSFC, Code 926.9, Greenbelt, MD 20771; 301-286-9589; SPAN CDDIS::GSFCVLBI)
C. Ma, J.W. Ryan, & T.A. Clark (NASA/GSFC, Code 926.9, Greenbelt, MD 20771; SPAN CDDIS::GSFCVLBI)
R.J. Eanes, M.M. Watkins, B.E. Schutz, & B.D. Tapley (Univ. of TX, CSR/WRW402, Austin, TX 78712; SPAN UTSPAN::UTCSR::<last name>)

NASA's Crustal Dynamics Project has devoted a significant portion of its mobile SLR and VLBI observing programs to collocation activities. These permit a direct comparison of the geocentric coordinates determined by the two independent techniques. A SLR solution (rms residual 4.4 cm) was produced at CSR using 16 months of Lageos full-rate data spanning 1988. A VLBI solution (rms residual 1.4 cm) was generated at GSFC using all data from 1979 through 1989; site coordinates and velocities were adjusted as global parameters. The coordinates for 18 pairs of collocated stations were compared using local survey ties to translate the VLBI reference points to the matching SLR points. The lengths of the local ties range from about 14 m to 387 km. Formal standard errors were used for weighting all quantities, including the ties.

After allowing a seven-parameter frame transformation, the weighted rms differences are: 17.5 mm, 26.4 mm, and 23.3 mm for X, Y, and Z components, respectively. The most significant outlier is Medicina, Italy (residual of 189 mm), for which there are only 11 mobile SLR passes. The overall reduced chi^2 is 11.7 which implies that the formal errors for each technique should be increased by a factor of 2.4, assuming an equal distribution of the errors and no added contribution by the local survey ties. However, it is likely that the survey ties are a significant source of discrepancy for at least a few of the comparison sites.

The scale of the VLBI frame is fractionally smaller than that of the SLR frame by about 10 ppb. Formally, the scales of each system are thought to be accurate to about 2 ppb. The observed scale difference cannot be accounted for by any known or suspected defect in either technique.

G32A-3 1405h

The VLBI Terrestrial Reference Frame of the Crustal Dynamics Project

C. Ma (Geodynamics Branch, NASA/Goddard Space Flight Center, Greenbelt, MD 20771; 301-286-3992)

The terrestrial reference frame realized by the Crustal Dynamics Project using VLBI data through the end of 1989 includes 80 points in North America, Europe, Africa, Asia, the Pacific and Australia. The origin of the frame is within 1 mm of the origin of ITRF89, the orientation agrees with ITRF89 within 2 mas, but the scale is determined by the VLBI models. 3-dimensional positions and velocities have been determined. The distribution of root-sum-squared 1-sigma formal errors in Cartesian position at 1990.0 is: < 1 cm = 14 sites, 1-3 cm = 45 sites, 3-10 cm = 17 sites, > 10 cm = 3 sites. Comparison with SLR positions suggests that the formal errors are perhaps too small by a factor of 2-3. The distribution of 1-sigma formal errors in horizontal velocity is: < 1 mm/yr = 20 sites, 1-3 mm/yr = 22 sites, 3-10 mm/yr = 9 sites. The remaining sites have insufficient data to compute meaningful velocities. The reference frame positions and associated earth orientation time series are available electronically through the Crustal Dynamics Project Data Information System and will be updated periodically.

G32A-4 1420h INVITED

SV5: A Terrestrial Reference Frame for Monitoring Crustal Deformation with the Global Positioning System

MARK H. MURRAY, ROBERT W. KING (Dept. of Earth, Atmospheric, and Planetary Sciences, MIT 54-521, Cambridge, MA 02139; 617-253-6389; mhm@benioff.mit.edu), and
PETER J. MORGAN (School of Applied Science, University of Canberra, Belconnen, A.C.T. 2616, Australia)

We have developed a conventional terrestrial reference frame—designated SV5—for the analysis of Global Positioning System (GPS) observations. The reference frame adopts the geocentric origin and scale defined by the CSR8902 adjustment, provided by the University of Texas at Austin Center for Space Research, of eleven years of satellite laser ranges (SLR) to Lageos. The precise relative locations of 80 sites that primarily realize the SV5 frame are derived from the GLB659 global adjustment, provided by Goddard Space Flight Center, of eleven years of very long baseline interferometric (VLBI) group delays. The coordinates of sixteen sites with well-determined local vector ties between collocated VLBI and SLR reference points are used to estimate a seven-parameter similarity transformation that makes the VLBI coordinate system commensurate with the SLR system; the sites are globally distributed, including nine in North America, three in Europe, and one each in China, Australia, Hawaii, and Kwajalein. The weighted root mean square of the estimated coordinate differences is 18 mm. A significant, and unexplained, scale difference of 6±2 parts in 10^9 must be applied to the VLBI system to agree with SLR. SV5 improves upon our previous SV systems by estimating the temporal evolution and uncertainties of the coordinates from VLBI and geophysical observations; we will discuss methodologies for systematically combining space-geodetic, geophysical and geological information, such as global plate tectonic motion models and seismic moment release. Also, a rigid-body rotation is estimated to align the orientation of the SV5 axes with the IERS terrestrial reference frame ITRF89. Data from the 1988 GOTEX global GPS campaign have been used to estimate the SV5 coordinates for sites that are not collocated with SLR or VLBI systems, and to improve estimates of the transformation parameters between SV5 and WGS84. We will compare SV5 with WGS84 and ITRF89, and discuss the sensitivity of GPS-derived baseline vectors to the parameters that define SV5.

G32A-5 1440h

COMPARISON OF SLR/VLBI AND WGS-84 REFERENCE FRAMES

P.A.M. Abusali (Center for Space Research, The University of Texas at Austin, Austin, Texas 78712)
B. E. Schutz and B. D. Tapley

The CIGNET tracking data, combined with data collected during the Southwest Pacific Campaign (summer 1989) from the field sites and a few additional sites collocated near SLR/BLVI sites, provide a global set of GPS data. Coordinates of these stations are known (some are estimated) in the SLR/VLBI reference frame. GPS data collected by the Defense Mapping Agency (DMA) at the five DMA sites, whose coordinates are known in the WGS-84 frame, are combined and processed with the data from augmented CIGNET data. The two reference frames mentioned above exhibit inconsistencies between them at a level of about 1 m as determined by earlier analyses. A 7-parameter transformation betwen the two frames is determined using the above data set and compared with earlier results. Several issues are addressed in regard to unifying the various reference frames.

G32A-6 1455h INVITED

Combining and Comparing GPS Global Results with Other Space Geodetic Techniques

S M Lichten and T P Yunck (both at Jet Propulsion Laboratory, California Institute of Technology, Pasadena, CA 91109; 818-354-1614)
S C Pogorelc (University of Colorado, Dept. of Aerospace and Engineering Sciences, Boulder, CO, 80307)

The Global Positioning System (GPS) will ultimately include 24 satellites in six orbital planes with 12-hr periods. Presently more than a dozen GPS satellites are in orbit and available for tracking. Even with only a partial constellation and limited ground coverage, present-day GPS solutions for global parameters such as earth orientation and intercontinental baselines are showing consistency with VLBI at the level of ~ 5 cm. Our studies indicate that by early 1991, GPS-based estimates for these global parameters are expected to improve to the few-cm level. With the full GPS constellation and global ground network, accuracy should eventually reach the 1-cm level.

GPS data can be used to refine estimates of the geocenter, earth orientation, global and regional baselines, as well as provide a high-accuracy low-earth orbiter tracking system for missions such as TOPEX/POSEIDON. GPS will offer certain unique capabilities in determination of these parameters, including high temporal resolution (~ hrs). However the most powerful tool for studying global geophysical earth processes will be the combined system of SLR, VLBI, and GPS. The International Earth Rotation Service (IERS) will soon face the task of combining these different data and defining a unified reference frame.

We have studied these issues both with recent GPS field data and with covariance analyses. Our recent GPS results are, in fact, consistent with the covariance analyses for present-day expected performance. However expected accuracy enhancements in the near future will require a better understanding of the relationship between global estimates obtained from different space geodetic techniques. GPS results have often incorporated a priori model constraints from VLBI and/or SLR. We will discuss issues to be resolved when some constraints are relaxed so that the full strength of these different geodetic techniques can be realized through their combination.

G32A-7 1530h

GPS-Derived Earth Orientation Parameters Based on Both Block I and Block II Satellites

E R Swift (Space and Geodesy Branch (K12), Naval Surface Warfare Center, Dahlgren, VA, 22448-5000; 703-663-7200)

From 1987 through 1989 Earth orientation estimates were produced as a byproduct of the GPS precise ephemeris computations for Block I satellites. In order to provide more accurate estimates for 1990, the Naval Surface Warfare Center has started solving for Earth orientation on a weekly basis using up to twelve satellites - 6 Block I satellites and the first 6 Block II satellites. Starting values for the two pole coordinates and UT1-UTC are obtained using the Defense Mapping Agency's predictions generated the previous week. Constant and rate corrections for the week for the two pole coordinates and for the rate of change of UT1-UTC are being estimated along with all satellite orbits and clocks and all station clocks simultaneously. This estimation procedure uses smoothed pseudorange data collected at a global network of ten tracking stations. The daily GPS pole coordinates and the weekly UT1-UTC rates are compared against the final IERS values for the data available so far this year. Earth orientation estimates based on four-day and two-day fit spans for a five-week period in early 1990 are also compared against final IERS and NEOS values.

G32A-8 1545h

Gravity Probe B as an Opportunity to Compare GPS and Laser Reference Frames

M.B Tapley (Hansen labs GP-B, Stanford University, Stanford CA 94305-4080; (415)-725-5697; bitnet TAPLEY%RELGYRO@STANFORD)

The Gravity Probe B (GP-B) mission, an experiment in basic physics, will fly in the mid 1990's. It will carry a GPS receiver and a set of laser retroreflectors aboard a drag-free platform in a 600 km. altitude polar Earth orbit. We show that GP-B will allowa good comparisonand strengthening of the laser and GPS tracking systems and coordinate frames.

Because of the drag-free system, the dynamics of GP-B's motion can be modeled to a high degree of accuracy. By moving along a well-defined trajectory from one set of stations to another, GP-B allows precise determination of the station's relative positions; and since it carries both tracking systems, it allows this determination in both coordinate systems. This is why represents an excellent opportunity to compare the laser and GPS tracking systems and reference frames.

As a preliminary step in the evaluation of this opportunity, we conducted a numerical evaluation of the accuracy with which least-squares solutions can determine ground stations' positions. We simulated a one-month arc of data, with laser ranges from ground stations to the satellite and with GPS positions for both the satellite and the ground station. We assumed colocated laser and gps receivers at the ground stations. We generated least squares solutions for the orbit elements of the satellite, the positions of the ground stations, and a few geodetic parameters. In some cases we used only laser data, in some cases we used only GPS data, and in some cases we used both. In all cases where we used GPS data, we also adjusted the orbits of the GPS satellites. Generally the combined solution is signifigantly better than either data set alone; part of this is due to the increased number of measurements, but part is due to the fact that the measurements are somewhat complementary. We present results and suggestions for further research.

G32A-9 1600h

The Doris System : Status and Prospects

J P Chassaing (CLS, 18 av. E. Belin, Toulouse France), A Auriol (CNES, 18 av. E. Belin, Toulouse, France), C Boucher (IGN, 2 av. Pasteur, St Mandé, France), M. Dorrer (CNES), M Lefebvre (CNES), F Nouel (CNES).

Doris is a new precise orbit determination system developed by CNES to meet the high accuracy -10 centimeters or better- required for oceanographic altimetric missions. The system is based upon a worldwide network of ground beacons transmitting on 2 frequencies, onboard Doppler receiver and a ground segment to control the system and coputer the orbit. Baseline tracking system for TOPEX/POSEIDON (1992) DORIS is flown on SPOT2 (launched Jan 22/90) and is operational with an actual network of 36 stations. The paper describes the system/principle, the actual status and prospects. Emphasis will be put on the inflight assesment and will adress the system evaluation : instrument performances, Doppler precision, link budget, ultra stable oscillator stability, technological parameters, disponibility data quality and availability -propagation models improvments (ionosphere, troposphere) with DORIS overall system performances : control center, data bank, network management. Explicit relationships to IERS are requiral and made through volocations. Lifetime, accuracy and flexibility will allow to contribute to densify IERS and to case the access from remote sites.

APPENDIX VII

1. Cook, R. A., "The Effects of Thermal Imbalance Forces on Simple Spacecraft," Masters thesis, The University of Texas at Austin, May 1989 (Abstract; Conclusions and Recommendations)
2. Vigue, Y., "Thermal Imbalance Effects on GPS Satellites," Masters thesis, The University of Texas at Austin, May 1990 (Abstract; Conclusions and Recommendations)
3. "Thermal imbalance force modelling for a GPS satellite using the finite element method," paper AAS 91-188, AAS/AIAA Spaceflight Mechanics Meeting, Houston, Texas, February 1991

THE EFFECTS OF THERMAL IMBALANCE FORCES ON SIMPLE SPACECRAFT

by

Richard Andrew Cook, B.S.

THESIS

Presented to the Faculty of the Graduate School of

The University of Texas at Austin

in Partial Fulfillment

of the Requirements

for the degree of

Master of Science in Engineering

THE UNIVERSITY OF TEXAS AT AUSTIN

May, 1989

ABSTRACT

THE EFFECTS OF THERMAL IMBALANCE FORCES

ON SIMPLE SPACECRAFT

by

Richard Andrew Cook, B.S.

Supervising Professor: Dr. Bob.E. Schutz

The increased orbital accuracy requirements of modern space missions have prompted the need to study more subtle forces that perturb the motion of a satellite. One such perturbation is due to the reradiation of energy from an asymmetrically heated spacecraft. The purpose of this investigation is to obtain some fundamental insights into this thermal imbalance effect . Unfortunately, modeling this phenomena for a real satellite can be quite difficult because the complete temperature distribution within the spacecraft must be determined. Consequently, this discussion concentrates on a number of simple spacecraft models that are somewhat easier to model. These models are similar to real satellites, but do not require an enormous amount of thermal analysis. Each case is investigated to determine the maximum impact of the thermal force on the satellite orbit. Some attention is also spent on understanding what material properties of a spacecraft are significant in this phenomena, and how these parameters can be determined through an estimation process.

Chapter 6

Conclusions and Recommendations

The objective of this investigation was to study the influence of the thermal imbalance force on geometrical figures representing simple spacecraft. In a broader sense, however, the work has entailed a study of two distinctly different subjects. The thermal imbalance effect is unique because it combines heat transfer theory with satellite orbit dynamics and determination through the thermal force, which is the result of heat exchange between a satellite and the surrounding space. It has been shown that the rate of this energy transfer is dependent upon the temperature distribution of the body. Chapter 3 uses a flat plate model to demonstrate this distribution in a simple geometric object. The advanced models in Chapter 4 show some of the problems that arise in the study of three dimensional bodies. Thermal analysis of actual spacecraft is much more complex than the examples considered in this investigation. In fact, determining the temperature behavior of different geometrical bodies is a significant topic in itself. There are numerous books dedicated to this subject with no mention any of the possible space applications. It was very tempting to spend all of this report discussing the temperature behavior of increasingly complex satellites.

A concerted effort was made to not acquiesce to this temptation. After all, the prime emphasis of this study was to determine the orbit behavior of a satellite subject to this perturbation. In order to do this, the simple thermal models have

each been implemented into an orbit computation program. These programs are specifically set up to determine the worst case influence of the thermal force. The assertion made here is that the simplified thermal models and orbit assumptions do not obscure the fundamental physics of the effect. Fortunately, this contention is supported by the results. In addition to the specific examples treated, an entire chapter is specifically devoted to discussing how to use this effect to improve the force model for a real satellite. Obviously, the thermal model for such a satellite will be extremely complex, but there are some key implementation aspects that are common for every situation. The result of this work is a basic introduction to all aspects of the thermal imbalance effect. The study was split almost evenly between orbital mechanics and thermal analysis. As a result, neither topic is covered completely , but significant progress in the interdisciplinary aspects has still been made.

Section 6.1 Conclusions

There are a few significant conclusions that can be made from this investigation. First, it is apparent that the thermal imbalance force can have a measurable effect on earth orbiting satellites. This effect is observed regardless of the satellite model or thermal analysis techniques that are used. The significance of this perturbation depends on the application. It is definitely important for projects that require precise orbit determination. Worst case results indicate that meter level radial errors can be generated in fourteen days. The estimation of other force model parameters can probably absorb some of this, but differences greater than 10 cm can still occur. This is obviously a problem for the TOPEX mission, with desired

radial accuracies of about 10 centimeters. The transverse orbit effect due to this perturbation can range into the tens of meters, which may be significant for some applications.

The thermal imbalance effect can also vary significantly depending on what type of satellite is being modelled. The results in Chapter 3 indicate that the thermal force generated by a solar panel can be quite important. The temperature imbalance in such an object is sizable because one side receives all of the incident radiation. In addition, the heat capacity is small because the mass is assumed to be small. The thermal imbalance effect is most significant when the heat capacity is small. The discussion in Section 3.5 indicated that the temperature in a body with high heat capacity is nearly constant. This implies that the thermal forces generated by heavy objects is probably negligible. If the main body of a satellite is represented as a single thermally connected object, then it does not have to be included in the thermal model. On the other hand, if there are thermally isolated objects like antennas or retroreflectors, then these objects must all be modelled independently.

The particular thermal analysis technique used to determine the temperature distribution of a satellite is also important. One of the most significant problems encountered in this study was how to simultaneously solve the heat equation and the satellite equations of motion. Coupled partial and ordinary differential equations are especially difficult to treat numerically, and every solution method has to use some type of approximation. The strength of the coupling determines the usefulness of a particular technique. The method introduced in Chapter 3 is useful for cases where the equations are closely related. Unfortunately, this method is slow because the ordinary differential equations describing the temperature

variations have to be numerically integrated. In addition, the method is not easily extendable to more complicated systems. The finite difference method is generally more useful for weakly coupled systems because of its speed. However, it is not as useful for strongly coupled equations because of stability limitations. This method can be used for multi-dimensional bodies, although the computational requirements are excessive.

The discussions in Section 3.5 and Chapter 5 underscore the role of the material properties of the body. Both the magnitude and direction of the thermal force are dependent upon the values of the model parameters. The emissitivity is important because the size of the force depends directly on the emissitivity imbalance. The thermal conductivity partly determines the size of the temperature imbalance, so it is also significant. The values of these parameters can be obtained by estimation, but the amount of computations is significant. It is possible to use the scale factor method introduced in Section 5.1, but only as a check on the accuracy of the entire model.

Section 6.2 Recommendations

This report has been a general introduction to the thermal imbalance effect. As a result, it is more a work of breadth rather than of depth. There are still many aspects that need to be studied in more detail. It is important, though, to not spend too much time investigating subjects that are insignificant. The following recommendations are observations about those particular areas that deserve future attention. The first order of business in future research should be to use the simple models from this report to learn more about the realistic influence of this

perturbation. All of the work in this report has been directed towards determining the largest possible influence of the thermal force. In order to accomplish this, several rather unrealistic assumptions were made. If the sun, earth, and satellite are all allowed to move in a more natural way, then significant information would be gained concerning the long-term behavior of a real satellite perturbed by thermal forces.

Future research into the thermal behavior of more complex objects is probably not warranted. Most real satellites can be separated into a main body and extended solar panels. The results in this report indicate that the thermal force generated by the main body is negligible. The thermal imbalance force can be completely determined by the force on the solar panels. Of course, the assumption here is that the satellite body is one thermally continuous body. If a particular satellite has isolated components that have significant temperature variations, then they probably should also be modelled. Parts like this will vary from satellite to satellite, so developing thermal models for them should wait until a specific spacecraft is discussed.

This is not to say however, that there should not be time spent developing more sophisticated thermal analysis techniques. Both solution methods used in this discussion give reasonable results, but they do have some limitations. Emphasis in this area should be placed on developing fast and accurate approaches that can be used on a regular basis. The finite difference method has the most potential, but the stability of the results must be improved. There also exist more advanced ways to solve partial differential equations that are not discussed here, and they may prove to be more useful. Special consideration should probably be given to modern finite

element approaches. If the study of a more complex body is warranted, then these methods should definitely be studied. The finite difference technique is applicable to multi-dimensional bodies, but the computational requirements are excessive.

Finally, there should also be some effort made to determine accurate values for the parameters used in the thermal imbalance model. One way that this can be done is by extensive research into the material properties of a specific satellite. In addition, instrumentation on the satellite may be able to provide direct measurements of some quantities. Unfortunately, however, some values may be difficult to obtain and will only be valid for that one satellite. Consequently, more time should be devoted to developing the tools required to estimate these parameters from real observational data. This again relates back to the need for faster and more accurate solution techniques. The results in Chapter 5 should be closely studied before deciding which parameters to estimate.

THERMAL IMBALANCE EFFECTS ON A GPS SATELLITE

by

YVONNE VIGUE

Center for Space Research

The University of Texas at Austin

May 1990

CSR-TM-90-01

ABSTRACT

THERMAL IMBALANCE EFFECTS ON
A GPS SATELLITE

by

Yvonne Vigue, B.S.A.E.

In recent years, the Global Positioning Satellite System orbit estimation and prediction requirements have prompted studies in non gravitational orbit perturbations which were previously considered insignificant. One of these perturbations, the thermal imbalance force, is believed to be caused by an unequal temperature distribution throughout the satellite. This discussion concentrates on obtaining an accurate thermal force model for a GPS satellite in orbit using the Finite Element Method to solve the transient heat transfer problem. Two Finite Element Method programs are used to determine satellite temperatures and thermal forces which are important in the force modelling used in the satellite prediction problem. The results are compared with those from previous studies which used finite differencing techniques to solve the transient satellite heating problem.

Chapter 4

Conclusions and Recommendations

The purpose of this study was to determine the effect of the thermal imbalance force on the orbital behavior of a GPS satellite. This investigation used the techniques known as the Finite Difference Method and the Finite Element Method to determine the satellite surface temperatures which are used to compute the thermal imbalance force. It has been shown that the thermal imbalance force is caused by the exchange of thermal energy between the satellite and its surroundings and is dependent upon the satellite's temperature distribution. Heat transfer theory combined with satellite dynamics and statistical estimation theory has been used to develop a simulation test case of the problem of satellite heating and cooling by radiation. Although the main focus of this thesis is the GPS satellite, a TOPEX satellite model was used as a basis in order to compare results with several previous studies where the Finite Difference Method was used to determine the satellite temperature distribution on a TOPEX solar panel [Cook, 1989, Rosborough, et. al., 1989, Dennehy, et. al., 1990]. Although several assumptions have been made and the satellite thermal model has been simplified, the underlying physics of the problem remains unchanged.

Section 4.1 Conclusion

The result of this investigation compares well with that of the work conducted by Cook [1989] wherein the finite difference technique was used. In this study, two independent techniques, finite element and finite difference, have been used to determine the effects of the thermal imbalance force on a GPS satellite. It is clear that the thermal imbalance force can have a measurable effect on orbits of satellites like GPS and TOPEX for which orbit accuracy requirements are very stringent in order that they may be used for geophysical applications. The results indicate that centimeter level radial errors and meter level transverse errors could result from this perturbation in a one week arc for a GPS satellite. The estimation of parameters such as the solar radiation reflectivity can absorb some of this error.

Clearly the thermal analysis technique used to determine the temperature distribution of the satellite solar panel is important. Under certain conditions, the results may vary by as much as an order of magnitude when such variables as time step is varied. Both the finite difference approximation and the finite element method are adequate heat transfer solution techniques. Either of these could be used for solving satellite solar panel surface temperatures. Both methods have advantages and disadvantages. Speed and stability are two advantages of the finite difference approximation method. However, a finite element method is probably more appropriate for the following reason. This method is capable

of implementing varying material properties as a function of nodal spacing. This is highly favorable since satellite solar panels are composed of different layers of materials with different material properties such as thermal conductivity. When comparing the models used in this investigation, the author has a preference of the PDE/Protran finite element model over the finite difference method. The software developed by Sewell [1985] has undergone extensive testing and verification. It also has a system of checks which notifies the user when such variables as time steps are not acceptable to the algorithm. For small enough time steps, this method should be very accurate. A major difficulty in including the thermal imbalance perturbation in orbit computation is the need to solve the coupled partial differential and ordinary differential equations simultaneously.

Section 4.2 Recommendations for Further Studies

An effort should be made to determine the correct material properties for a GPS satellite solar array, or the specific satellite of interest. Cook [1989] determined that the material properties such as surface emissivity and thermal conductivity will have a significant influence on the temperature distribution. The thermal imbalance force is directly related to ε, the surface emissivity imbalance, and the heat equation is largely dependent on the thermal conductivity, K. Also, as Cook [1989] mentioned, instrumentation on board the spacecraft may provide direct measurement of some quantities

such as panel surface temperature. All these factors should be considered when implementing the thermal imbalance force into the general force model of a satellite. An accurate model of the thermal imbalance force for a particular satellite will be useful in reducing the orbit estimation errors where a precise orbit is critical for mission success.

PAPER AAS 91-188

Thermal Imbalance Force Modelling for a GPS Satellite Using the Finite Element Method

Yvonne Vigue
Jet Propulsion Laboratory
California Institute of Technology
Pasadena, California

Bob E. Schutz
University of Texas at Austin
Center for Space Research
Austin, Texas

AAS/AIAA Spaceflight Mechanics Meeting

HOUSTON, TEXAS FEBRUARY 11-13, 1991

AAS Publications Office, P.O. Box 28130, San Diego, CA 92128

THERMAL IMBALANCE FORCE MODELLING FOR A GPS SATELLITE USING THE FINITE ELEMENT METHOD

Yvonne Vigue
Jet Propulsion Laboratory
California Institute of Technology
Pasadena, California

Bob E. Schutz
University of Texas at Austin
Center for Space Research
Austin, Texas

Geophysical applications of the NAVSTAR Global Positioning System (GPS) require the capability to estimate and propagate satellite orbits with high precision. An accurate model of all the forces acting on a satellite is an essential part of achieving high orbit accuracy. Methods of analyzing the perturbation due to thermal radiation and determining its effects on the orbits of GPS satellites are presented. The thermal imbalance force, a non-gravitational orbit perturbation previously considered negligible, is the focus of recent attention. The Earth's shadowing of a satellite in orbit causes periodic changes in the satellite's thermal environment. Simulations show that mis-modelling of the thermal imbalance force over several days gives meter level errors for those satellites which are eclipsing and can limit accuracy in orbit determination and in estimation of baselines used for geophysical applications.

INTRODUCTION

To study the thermal imbalance effect, it is important to understand the theoretical background and the laws of physics that govern the problem of radiative and conductive heat transfer. Radiative heat transfer between a satellite and its environment is the basis for the thermal force model. A satellite in Earth orbit is continuously showered by radiation, most of which comes from the sun. The thermal imbalance force is directly related to the temperature distribution of the satellite in its changing environment (Ref. 1). An uneven temperature distribution causes surfaces to re-radiate energy at different rates. Most of the thermal force on a satellite originates with the solar panels due to their large exposed area and low heat capacity.

The satellite's heated body re-radiates energy at a rate that is proportional to its temperature, losing the energy in the form of photons. By conservation of momentum, a net momentum flux out of the body creates a reaction force against the radiating

surface, and the net thermal force can be observed as a small perturbation that affects long term orbital behavior of the spacecraft (Ref. 2). The partial differential equations and boundary conditions describing the temperature distribution and the heat transfer between surfaces, along with the application of the finite element method are presented in this paper. A brief description of the statistical estimation technique used for studying the effect of the thermal imbalance force on GPS orbits is included.

RADIATION AND HEAT CONDUCTION FORMULATION

Two types of heat transfer that affect a spacecraft in orbit are radiation and heat conduction. The exchange of energy between the spacecraft and its surroundings is described by radiation heat transfer. Conduction is the transfer of heat by molecular motion within a solid medium. Figure 1 shows the type of heat transfer that affects an orbiting spacecraft.

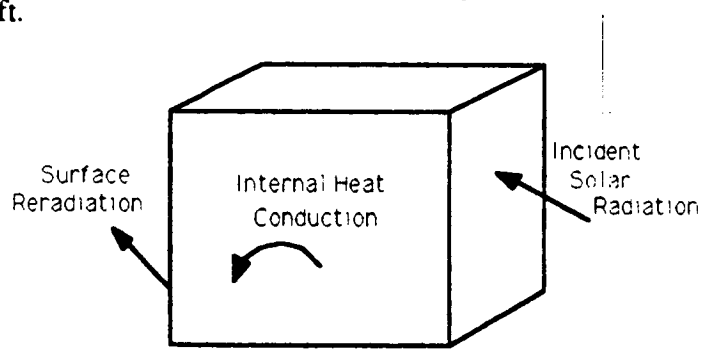

Figure 1 General Heat Transfer Diagram for a Spacecraft

The rate of radiant energy transfer for a real object is given by Stefan-Boltzmann Law (Ref. 3):

$$E_T = \varepsilon \sigma T^4 \tag{1}$$

where E_T is the energy radiated by a real body per unit area per unit time,
ε is the emissivity of the body, dependent on material properties,
σ is the Stefan-Boltzmann constant,
T is the temperature.

By conservation of momentum , the thermal force, or rate of change of momentum for a radiating surface element is expressed as (Ref. 1):

$$d\vec{F}_{thermal} = -\frac{2}{3}\frac{\varepsilon \sigma T_A^4}{c} dA\, \hat{n_A} \tag{2}$$

where t is time and c is the speed of light.

The differential force must be integrated over the entire surface to determine the complete thermal force:

$$\vec{F}_{thermal} = -\frac{2\sigma}{3c}\int_{\Omega} \varepsilon T_A^4\, dA\, \hat{n}_a \tag{3}$$

Clearly, the thermal force cannot be calculated unless surface temperatures of the spacecraft are known.

In general, the temperature at any point within a body satisfies the heat equation:

$$K \nabla^2 T = \rho C_p \frac{\partial T}{\partial t} \tag{4}$$

where K is the material thermal conductivity,
ρ is the material density and specific heat,
C_p is the specific heat,
T is the temperature,
t is the time,
and ∇ is the Laplace operator.

The solution to this second order partial differential equation requires that the coefficients K, ρ and C_p be time independent. Also, the boundary conditions must be specified. The boundary conditions are described by thermal radiation and conduction. As given by the conservation of energy principle, the total amount of energy coming into a surface is equal to the total amount of energy leaving the surface. The boundary condition for the surface of the satellite can be obtained by using this condition as

$$q_{in} = q_{out} \tag{5}$$

where q_{in} is the amount of incoming radiative energy due to external sources and internal conduction and q_{out} is the amount of radiative energy leaving the specified boundary due to re-radiation and conduction. Figure 2 shows the conservation of energy principle for the surface of a satellite solar panel.

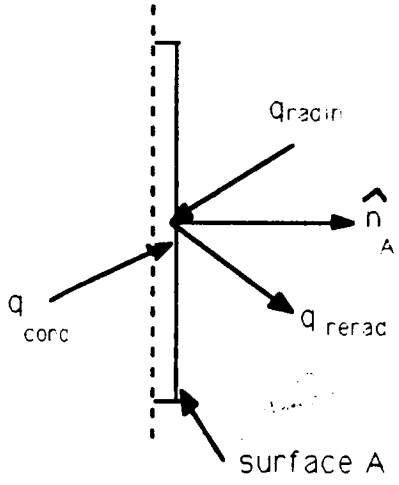

Figure 2 Conservation of Energy Diagram for a Satellite Surface

Using this concept, the boundary conditions for each surface are constructed. The incident radiative solar energy received per unit area per unit time by side A and side B of the solar panel are represented by h_a and h_b (Ref. 2):

$$KA\frac{\partial T_b}{\partial X} = \varepsilon_b \sigma A T_b^4 - h_b A \qquad (6\ a)$$

$$-KA\frac{\partial T_a}{\partial X} = \varepsilon_a \sigma A T_a^4 - h_a A \qquad (6\ b)$$

The actual amount of incident radiative energy received by the each side of the solar panel is a function of panel orientation and the orbit of the satellite. The subscript *a* represents the left boundary in local coordinates (cold side) and *b* is the right boundary (sunlight side). The term on the left side of the equal sign in equations 6a and 6b is the heat flux, energy per unit time per unit area, in the local x-direction, which is perpendicular to the solar panel face. The values used for some of the parameters described above are shown in Table 1.

TABLE 1

THERMAL AND ORBIT PARAMETERS

Model Parameter	Value
Initial orbit radius:	26,550,000 meters
surface emissivity ε_a:	0.78
surface emissivity ε_b:	0.83
surface absorptivity α_a:	0.77 - 14.1% (panel efficiency)
solar panel surface area - A:	10.832 meters square
satellite mass - m:	845 kg
initial panel temperature (t = 0) :	300 degrees Kelvin
Stefan-Boltzmann constant - σ:	5.6699 E-08 Watts/m^2°K
speed of light - c:	2.998 E+08 m/s
solar constant - ψ :	1368.2 Watts/m^2
total panel thickness (8 layers):	0.01478 meters = 0.582 inches

The finite element method is used to solve the transient heat conduction and radiation problem. PDE-Protran, a finite element method program incorporates material properties to determine solar panel surface temperatures (Ref. 4). Accurate and current knowledge of physical parameters such as surface emissivity, thermal conductivity, heat capacity and material density is required. These parameters, which may change due to degradation of materials in the environment of space (Ref. 5), influence the thermal force calculations and have an effect on the prediction and propagation of the spacecraft trajectory.

ORBIT ANALYSIS TECHNIQUE

In this investigation, the equations of motion for an Earth satellite are assumed to include the two body gravitational effect and the thermal imbalance forces only, and are given in vector form by:

$$\ddot{\vec{r}} = -\frac{\mu \vec{r}}{r^3} + \frac{\vec{f}_{therm}}{m} \tag{7}$$

where $\vec{r}$ is the geocentric satellite position,
μ is Earth's mass multiplied by gravitational constant,
m is the mass of the satellite.

and thermal imbalance force perturbing the satellite, $\vec{f}_{therm}$, is computed as:

$$\vec{f}_{therm} = \frac{2\sigma A}{3c}(\varepsilon_b T_b^4 - \varepsilon_a T_a^4) \tag{8}$$

The effect of the thermal imbalance force on a satellite can be observed by comparing the perturbed orbit with the unperturbed two body orbit in time (Ref. 6). Since there is no closed form analytical solution for the perturbed equations of motion, a numerical integration technique is necessary to solve the ordinary differential equations of motion. The perturbed and unperturbed orbits can be set with the same initial conditions and then the displacement between them at a given time can be observed. A least squares estimation technique (Ref. 7) is used to determine the state of the satellite in its orbit at a specified epoch. The initial conditions of one orbit can be adjusted at a given time to eliminate the secular divergence between the perturbed and unperturbed orbits to observe the periodic behavior.

DISCUSSION OF RESULTS

In order to determine the direction and magnitude of the thermal force, the surface temperatures were calculated using a finite element method program. Several simulations were tested. The data input that was required for the satellite solar panel is shown in Table 2. This table lists the material properties for a Block II GPS satellite solar panel (Refs. 5, 8, 9, 10, 11, 12).

TABLE 2

GPS BLOCK II SOLAR PANEL PROPERTIES

Panel Layer Composition	Thickness (meters)	Density (kg/m^3)	Specific Heat (J/kg°K)	Conductivity (Watts/m°K)
fused silica coverglass	0.00749	2186.622	753.624	1.417
adhesive	0.00005	1079.472	1256.04	0.116
solar cell	0.00025	2684.84	711.756	147.994
interconnect cell adhesive	0.00018	1051.793	1256.04	0.116
Kapton cocured	0.000076	1162.508	1130.436	0.1506
graphite epoxy	0.00019	2186.622	1373.27	0.8706
aluminum core	0.00635	2491.088	1046.7	250.966
graphite epoxy	0.00019	2186.622	1373.27	0.8706

The satellites of the Global Positioning System are distributed in six evenly spaced orbit planes. The proposed final constellation will consist of 24 satellites at an orbit altitude of 20,000 km and orbit period of 12 hours. These satellites are inclined in their orbits such that the spacecraft will experience an eclipsing season for only a few weeks every year. At all times, there is at least one orbit plane in eclipse mode. Eclipsing has a strong effect on the solar radiation environment those satellites. This is evident in the temperature of a GPS satellite solar panel over one orbit shown in Figure 3. The steady state temperature for the sun-facing side is approximately 317 degrees Kelvin and the shaded side is 313 degrees Kelvin. These values compare well with the approximate value of 313 degrees Kelvin which was measured on the cold shaded side of the solar panel for a GPS satellite (Refs. 8,9). The face exposed to the sun was not directly measured and therefore the temperature difference between surfaces is not well known, but is believed to be approximately 5 degrees Kelvin (Ref. 9, 10, 11). The eclipse period shows a slow decline to an panel equilibrium temperature of approximately 253 degrees Kelvin.

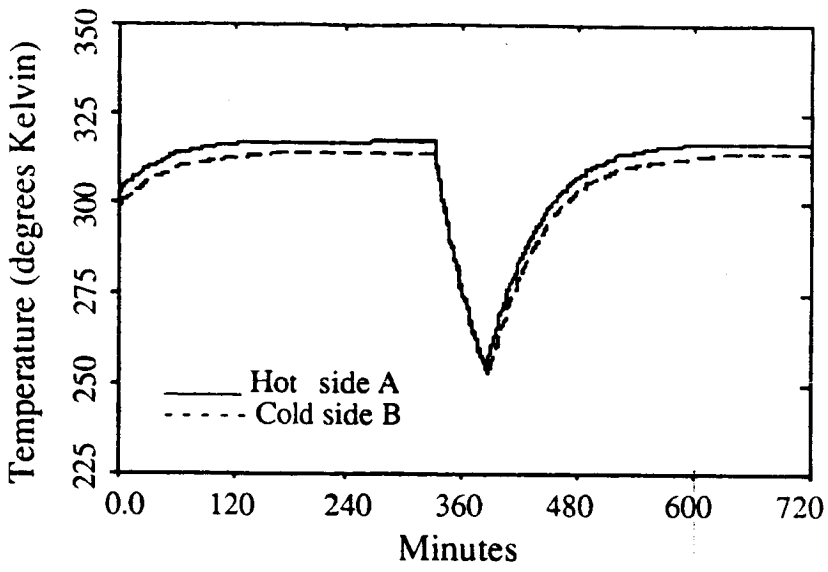

Figure 3. Temperature history simulation for a GPS solar panel

Modelling the coverglass surface on the sun-facing side accurately has been difficult during this study since that information was not readily available. The thermal conductivity of the fused silica coverglass is much lower than any of the other 7 solar panel stack layers (Ref. 10). This layer contributes most of the temperature imbalance because of its low thermal conductivity and high thickness as compared to the other solar panel layers. For example, two simulations were performed using identical solar panel parameters except for different thermal conductivities for the coverglass. The results shown in Table 3 describe the steady-state temperatures and thermal accelerations that were computed using the specified values for the coverglass thermal conductivity.

TABLE 3. COVERGLASS THERMAL SIMULATION

Test Case 1	Test Cast 2
K = 1.417 W/m°K	K = 0.04327 W/m°K
Hot side T_a = 317.41 °K	Hot side T_a = 340.30 °K
Cold side T_b = 313.66 °K	Cold side T_b = 285.37 °K
Thermal Acc. = **1.88 E-10 m/s^2**	Thermal Acc. = **-8.01 E-9 m/s^2**

In this paper, the reference frame that is used is the spacecraft radial and along-track components. The along-track component is sometimes referred to as the

transverse or down-track direction and is defined in the direction of the satellite velocity vector. Figure 4 shows the radial and along-track components of the acceleration due to thermal re-radiation over one orbit for an eclipsing satellite. These also compare well with studies which have shown un-modelled non-gravitational forces to cause errors of this magnitude (Ref. 11)

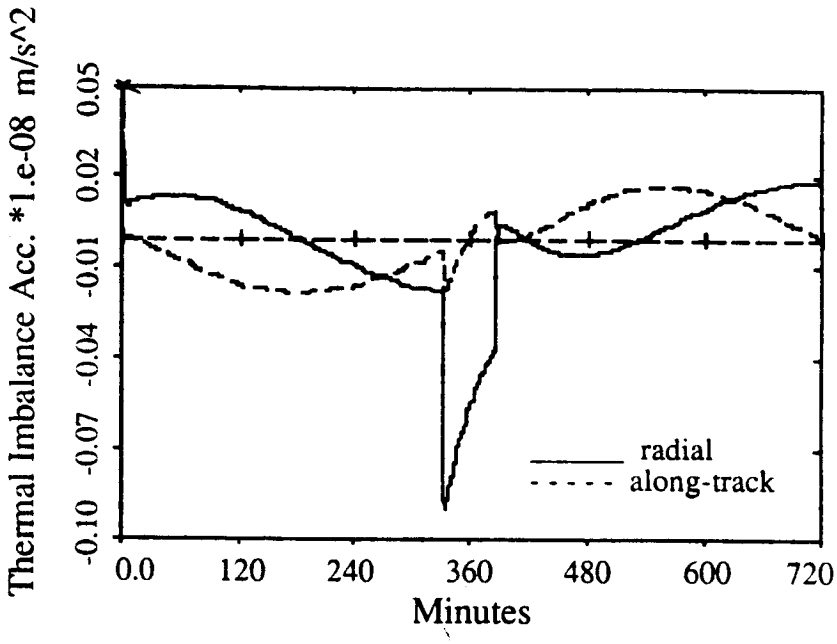

Figure 4. Radial and transverse components for the thermal force over one orbit

Figure 5 shows the differences between two orbits, one computed using two-body effects only and another trajectory was computed with two-body and thermal imbalance force for a satellite in an eclipsing orbit during one week. The radial rms is 0.5 meters and the along-track rms is 5.2 meters. These results were computed using a technique similar to the method used to predict satellite orbits based on a set of initial conditions and a complete force model of the spacecraft, which could include the solar radiation pressure and thermal imbalance force. In this case for an eclipsing satellite after seven days, the along-track components differ by approximately 13 meters.

Figure 6 also shows the differences between two orbits, one with two-body effects only and another computed using two-body and thermal imbalance force for a satellite which is not in an eclipsing plane. The radial rms is 0.5 meters and the along-track rms is 1.6 meters. It can be seen from these results that an eclipsing satellite experiences a larger perturbation in the along-track direction over the span of one week, than a satellite which is not in an eclipsing orbit plane. For the non-eclipsing satellite case, after seven days, the along-track difference is approximately 5 meters.

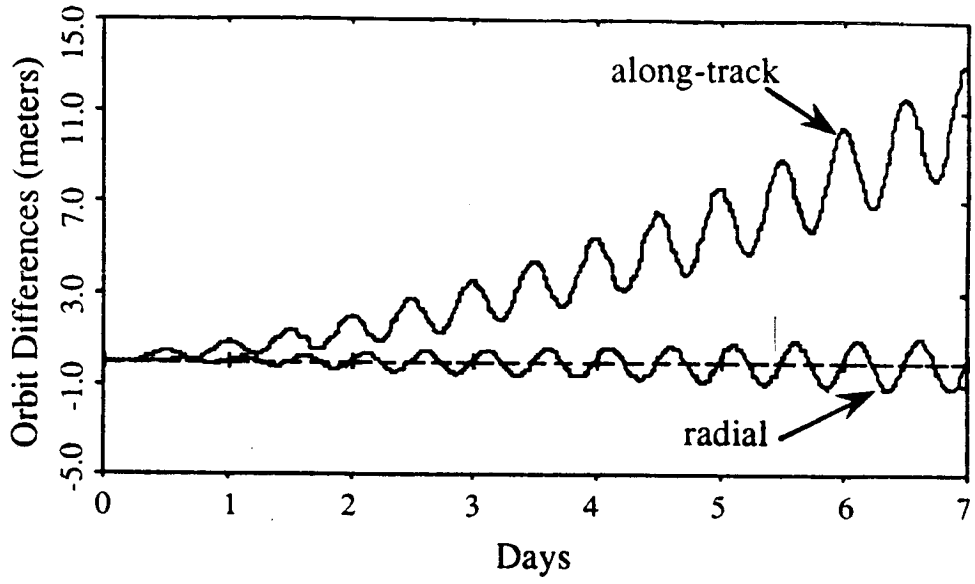

Figure 5. Radial and transverse orbit differences, eclipsing satellite

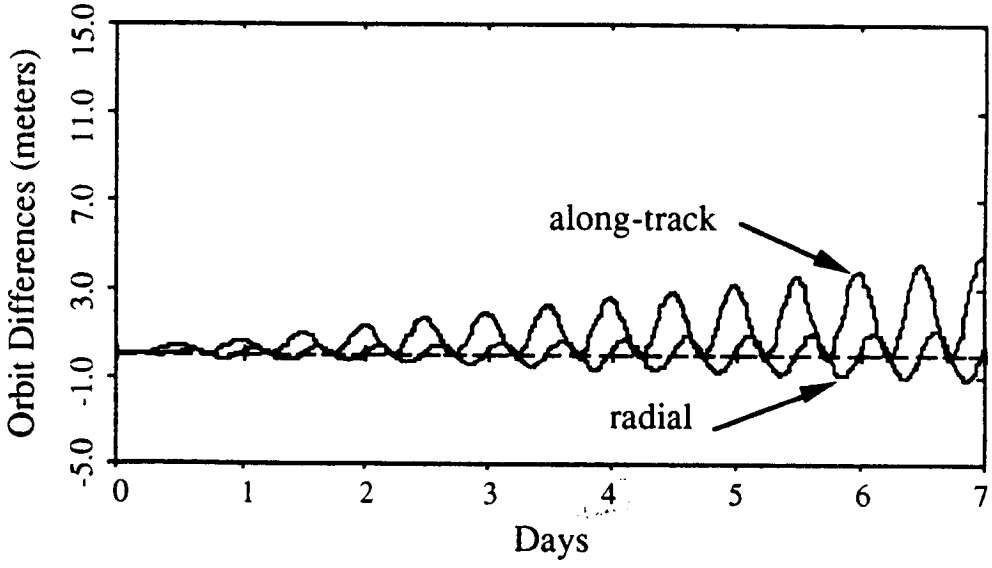

Figure 6 . Radial and transverse orbit differences, non-eclipsing satellite

The next two figures represent the results computed using a least squares estimation algorithm in which the simulated observation data contained only the two-body gravitational and thermal imbalance re-radiation forces. The force model used in the estimation algorithm contained the two-body gravitational force model with a solar radiation pressure model to observe the ability of the force model to account for thermal imbalance forces which have been difficult to model but exist in the observations. The best estimate of the satellite epoch state, in the least squares sense, is calculated which includes the satellite position, velocity and a solar radiation pressure scale factor.

Figure 7 shows the orbit fit residuals for a satellite in an orbit plane that is regularly eclipsing. The radial rms is 5 centimeters and the along-track rms is 80 centimeters. After seven days, the along-track orbit error is almost 2 meters. These results show that the solar radiation pressure scale factor in the estimation scheme is capable of absorbing most of the orbit error due to thermal re-radiation, but not all of the orbit error, especially in the along-track direction.

Figure 8 also shows orbit fit residuals for a GPS satellite, the same estimation technique, but the satellite is in a non-eclipsing orbit plane. The radial rms is 9 mm and the along-track rms is 17 centimeters. After seven days, the along-track orbit error is approximately 40 centimeters. Clearly, the eclipsing of the satellites has an influence on the orbit errors, when a thermal re-radiation force is not included in the estimation force model. Larger orbit errors are calculated when the satellite is in an eclipsing orbit plane.

Studies have shown that, for eclipsing satellites, the quadratic-like growth in the along-track direction can give errors as large as 50 meters after a one week prediction (Ref. 13). A one week prediction can be made using the satellite state computed for the best least squares estimate in Figure 7 and compared to the best least squares estimate for that predicted week. Although that specific test was not computed for this paper, errors of this magnitude are possible.

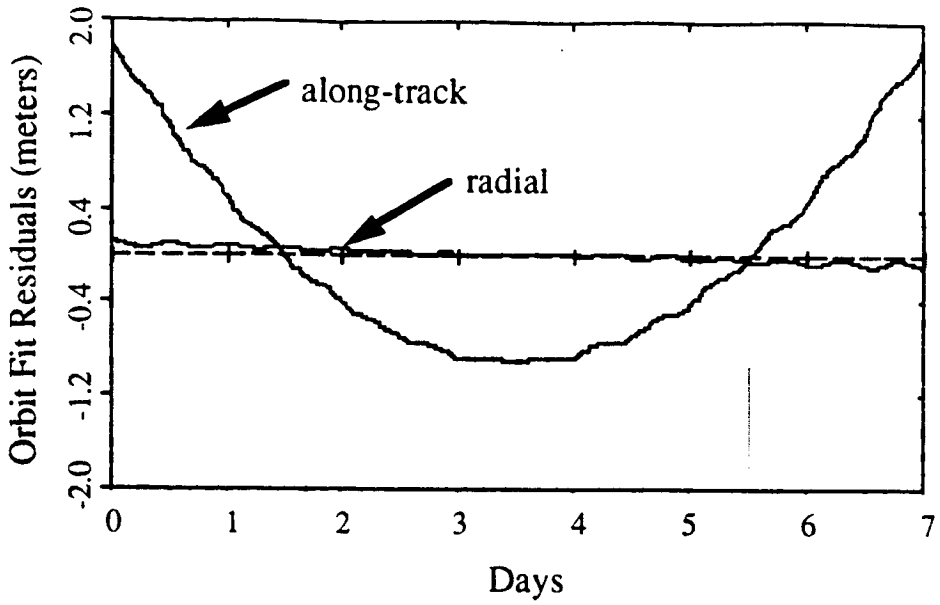

Figure 7 Orbit fit residuals, with a solar radiation pressure scale factor, eclipsing satellite

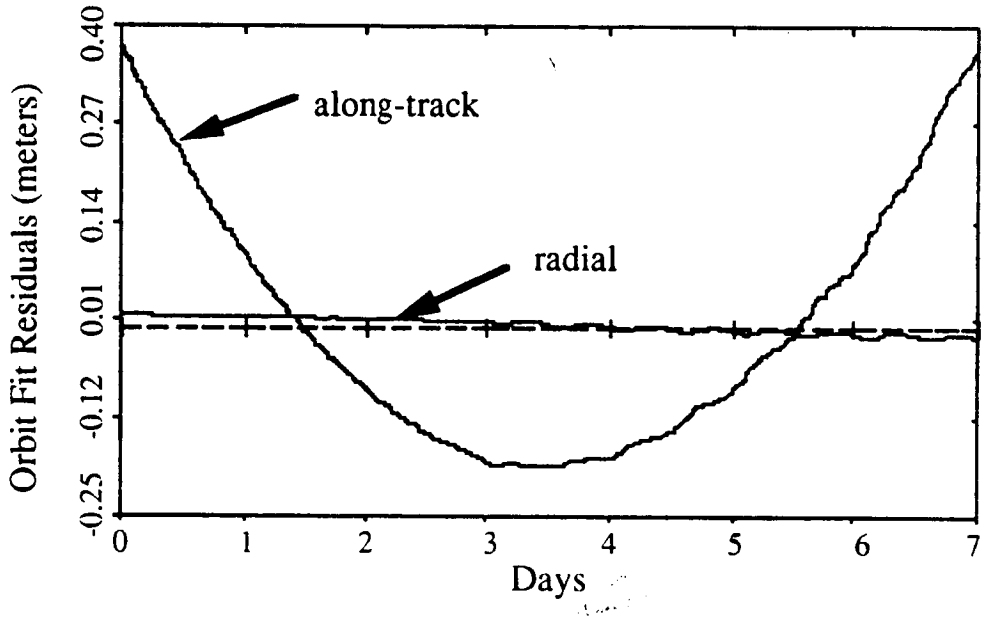

Figure 8 Orbit fit residuals, with a solar radiation pressure scale factor, non-eclipsing satellite

CONCLUDING REMARKS

The current analysis has shown that orbit errors larger than 10 meters occur when mismodelling non-gravitational forces such as the thermal imbalance force presented here. A finite element method technique has been used to calculate satellite solar panel temperatures which are used to determine the magnitude and direction of the thermal imbalance force. Although this force may not be responsible for all of the force mismodelling, conditions may work in combination with the thermal imbalance force to produce such accelerations on the order of 1.e-9 m/s^2. One possible contribution which is currently being studied is the solar panel misalignment, acting together with the thermal imbalance force which may account for much of the unmodelled perturbations. If sub-meter accurate orbits and centimeter-level accuracy for geophysical applications are desired, a time-dependent model of the thermal imbalance force should be used especially when satellites are eclipsing, where the observed errors are larger than for satellites in non-eclipsing orbits. This force has been observed for years, even on such satellites as LANDSAT and is still not completely understood. Forces such as the thermal imbalance force are dependent on the space environment and especially on such parameters as the satellite mass, cross-sectional area and material composition. Unfortunately, these parameters can change or degrade with long-term exposure in space. The results obtained using the finite element model used in this study agree with the work of others who have conducted studies for various spacecraft such as TOPEX and LANDSAT using the finite difference technique to determine spacecraft temperatures.

ACKNOWLEDGEMENT

The work described in this paper was carried out by the Jet Propulsion Laboratory, California Institute of Technology, under contract with the National Aeronautics and Space Administration. The University of Texas at Austin Center for Space Research and Center for High Performance Computing provided the computers and CPU time to perform this study. The authors would like to thank Lt. Randy White of the United States Air Force Global Positioning System Joint Program Office in Los Angeles, California, for his assistance.

REFERENCES

1. Cook, R., "The Effects of Thermal Imbalance Forces on a Simple Spacecraft", Thesis, University of Texas at Austin, Austin, Texas, 1989.
2. Vigue, Y., "Thermal Imbalance Effects on a GPS Satellite", University of Texas Center for Space Research Technical Memorandum 90-01, Austin, Texas, 1990.
3. Chapman, A. J., Heat Transfer, Macmillan Publishing Company, New York, N.Y., 1984.
4. Sewell, G., Analysis of a Finite Element Method: PDE/PROTRAN, Springer-Verlag, New York, 1985.

5. Lam, Tung T., Aerospace Corporation, Private Communication, 1990.

6. Abusali, P. A. M., University of Texas Center for Space Research, Private Communication, 1990.

7. Tapley, B. "Least Squares Estimation Algorithm", Course Notes, Statistical Estimation Theory, University of Texas at Austin, Austin, Texas, 1972.

8. Pence, W., Rockwell International, Private Communication, 1990.

9. Albeck, J., Spectrolab Corporation, Private Communication, 1990.

10. Marvin, D., Aerospace Corporation, Private Communication, 1991.

11. Fliegel, H.F. and T.E. Gallini, "Radiation Pressure Models for Block II GPS Satellites", Aerospace Corporation Interoffice Memorandum, El Segundo, California, 1989.

12. Rauschenbach, H. S., Solar Cell Array Design Handbook, Van Nostrand Reinhold Company, New York, 1980.

13. Schutz, B. and C.S. Ho, P.A.M. Abusali, B.D. Tapley, "Casa Uno GPS Orbit and Baseline Experiments", Geophysical Research Letters, Volume 17 No. 5, pages 643-646, 1990.

APPENDIX VIII

1. "Accuracy assessment of GPS satellite orbits," *Advances in Space Research, 11*(6), (6)189–(6)192, 1991
2. Feulner, M. R., "The Numerical Integration of Near Earth Satellite Orbits Across SRP Boundaries Using the Method of Modified Back Differences," Masters thesis, The University of Texas at Austin, August 1990 (Introduction; Conclusions)
3. "Improving the numerical integration solution of satellite orbits in the presence of solar radiation pressure using modified back differences," paper AAS 91-187, AAS/AIAA Spaceflight Mechanics Meeting, Houston, Texas, February 1991

Adv. Space Res. Vol. 11, No. 6, pp. (6)189 – (6)192, 1991
Printed in Great Britain.

0273-1177/91 $0.00 + .50

ACCURACY ASSESSMENT OF GPS SATELLITE ORBITS

B. E. Schutz, B. D. Tapley, P. A. M. Abusali and C. S. Ho

Center for Space Research, The University of Texas at Austin, Austin, TX 78712, U.S.A.

ABSTRACT

Global Positioning System (GPS) orbit determination using data collected by the civilian tracking network CIGNET have been used in a variety of experiments, along with data collected from special campaigns to augment the global tracking data. These experiments have been used to investigate the fidelity of the satellite force and kinematic models with the goal of improving the GPS ephemeris accuracy. Software has been developed for the preprocessing of GPS pseudo-range and phase measurements, including procedures for cycle slip correction. A multi-satellite orbit determination program, MSODP, allows for satellite-dependent force models, including high-low satellite constellations. Assessments of orbit accuracies derived from measurements collected in campaigns with nearly global networks have been performed with a variety of techniques, including determination of baselines known from SLR or VLBI, the computation of long, multi-week arcs and the comparison of predicted ephemerides with determined ephemerides. These results have provided indications of inadequacies in the force models, especially with the nongravitational forces, particularly those aspects associated with eclipsing.

INTRODUCTION

The importance of accurate GPS orbits has been widely acknowledged by an abundance of papers /1, 2/. The required orbit accuracy is dependent on the particular application and is further complicated by the fact that orbit accuracy does not always map into comparable accuracy in terms of geodetic parameters, such as interstation baseline vectors. While the orbit accuracy can be described in terms of, for example, the positional accuracy in an adopted reference frame, the more commonly used measure of accuracy is the ability of an orbit, or ephemeris, to support geodetic parameter estimation. The latter application describes the accuracy in terms of the baseline length, such as 1 part in 10^8 or 1 cm on a 1000 km baseline.

The positional accuracy of an orbit is dependent on a variety of factors, including the quality of the force and kinematic models as well as the precision and geographical distribution of the measurements used to determine the orbit. The quality of the models interacts in a complex way with the measurement quality and distribution over the interval of time selected for the orbit determination.

This paper examines the GPS orbit accuracy using several evaluation procedures. The data used for the study is drawn from the CASA Uno experiment /3/. Furthermore, this paper provides additional detail to the results published in /4/.

DATA

The CASA Uno experiment was conducted from January 18 through February 5, 1988, using a tracking network based on the CIGNET, but augmented with several additional sites in the Pacific. The complete network of stations is given in Table 1, which consisted of TI-4100 receivers. Most of the sites were located near VLBI or SLR sites and the position vectors of the GPS receiver reference point with respect to the VLBI/SLR reference points has been documented (e.g., /4/). For all of the studies described in this paper, ionospherically corrected measurements were used.

In Table 1, a few sites could not be satisfactorily specified a priori with respect to SLR and VLBI reference points as noted with the asterisk. These sites were treated as unknown and estimated during the solution process. In addition, a few sites were selected to be estimated for the purpose of aiding in orbit accuracy assessment even though their coordinates are accurately known with respect to the SLR/VLBI systems.

All data were processed in the orbit determination program as double difference phase, a formulation which removes most of the contribution of clock errors. Preliminary editing and correction of cycle slips were accomplished prior to the orbit determination. The data were collected at 30-second time intervals on satellites PRN 3, 6, 8, 9, 11, 12 and 13, all Block-I satellites.

TABLE 1 Sites Used in Solution

CIGNET	Augmentation
Mojave, CA	American Samoa *
Onsala, Sweden	Black Birch, NZ *
Richmond, FL	Ft. Davis, TX *
Tromso, Norway *	Kokee Park, HI
Westford, MA	Owens Valley, CA *
Wettzell, FRG	Tidbinbilla, Australia
Yellowknife, NWT	

* denotes sites estimated in simultaneous solution with orbit

FORCE AND KINEMATIC MODELS

The force models used differed from the International Earth Rotation Service (IERS) Standards /5/ as follows. The adopted gravity field was GEM-L2, truncated at degree and order 8, instead of the IERS field, GEM-T1. Experiments have shown that the difference between these two fields has little effect in the orbit determination process. The solar radiation pressure model was ROCK4 with an estimated scale parameter and a *y*-bias parameter /6/. A zenith delay was estimated to account for tropospheric variations. The zenith delay was further divided into 3-hr parameters for each station.

The adopted coordinates of the tracking sites were based on the orientation and scale of a University of Texas SLR solution known as CSR 8901. Since several of the tracking sites were located in close proximity to VLBI sites, the Goddard Space Flight Center GLB484 was adopted. Using a set of common sites between SLR and VLBI, the VLBI system was translated, rotated and scaled into the SLR system /7/.

The orbit determination software, MSODP, is a multi-satellite derivative of the single satellite software used at CSR for processing of SLR data, UTOPIA. Data screening, editing and cycle slip corrections are accomplished in a separate suite of programs designed for efficient and interactive operation with graphical displays to facilitate examination of the data.

ORBIT RESULTS

The fidelity of the models used were examined by determining the GPS orbits in one week arcs in two consecutive weeks, namely, GPS Weeks 419 and 420 during the CASA Uno experiment. In these experiments, the estimated parameters in Week 419 were used to predict the ephemeris into Week 420. This predicted ephemeris was directly compared with the ephemeris determined from the tracking data. Two classes of results were observed as illustrated in Figs. 1 and 2. The characteristics illustrated by Fig. 1 were shared by satellites with PRN identity of 3, 8, 11 and 13 whereas the characteristics in Fig. 2 were common to PRN 6, 9 and 12. The element of commonality shared by these two groups of satellites is that PRN 3, 8, 11 and 13 orbits were experiencing eclipsing, whereas PRN 6, 9 and 12 were not. As is suggested by Figs. 1 and 2, the eclipsing satellites exhibit a quadratic-like error growth in the prediction, whereas the non-eclipsing satellite differences are bounded to about ± 5 m.

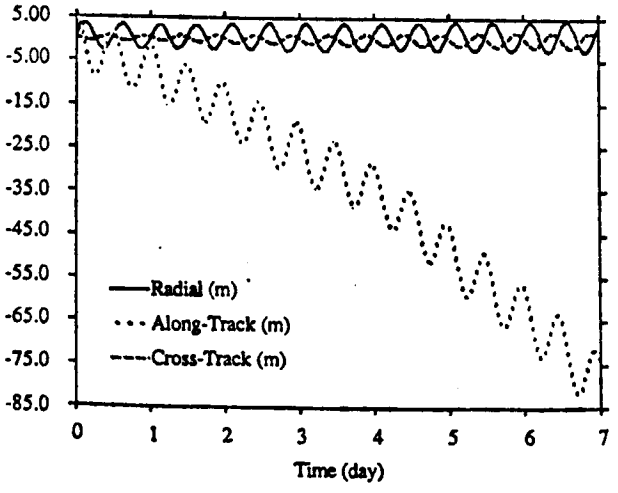

Fig. 1. Comparison of Orbits: Week 420 estimated solution vs. Week 419 predicted solution for SV13

CONCLUSIONS

For the CASA Uno data set examined in this paper, the existence of unmodeled effects, presumably in the force model, have been shown to exist that correlate with eclipsing of the sun. These effects are pronounced in ephemeris predictions and can be regarded as a limiting effect on the prediction accuracy. In spite of the existence of these unmodeled effects, the ability to obtain geodetic results that show an accuracy of 1–2 parts in 10^8 or better has not been diminished. The possibility that such unmodeled effects are constraining the ability to reach a few parts in 10^9 is under investigation.

ACKNOWLEDGMENTS

This study was supported, in part, under NASA Grant No. NAG5-940. The use of University of Texas System Center for High Performance Computing facilities is gratefully acknowledged. The assistance of H. J. Rim is appreciated.

REFERENCES

1. Proceedings of the Fifth International Geodetic Symposium on Satellite Positioning, Las Cruces, NM, 1989.
2. Special issue on CASA Uno, *Geophys. Res. Lett., 17*, March and April, 1990.
3. J.N. Kellogg and T.H. Dixon, Central and South America GPS Geodesy – CASA UNO, *Geophys. Res. Lett.* 17, # 3, 195–198 (1990).
4. B.E. Schutz, C.S. Ho, P. Abusali and B.D. Tapley, CASA UNO GPS orbit and baseline experiments, *Geophys. Res. Lett.* 17, # 5, 643–646 (1990).
5. D. McCarthy, Ed., IERS Standards, *IERS Tech. Note* 3, Observatoire de Paris (1989).
6. H. Fliegel, W. Fees, W. Layton and W.W. Rhodus, The GPS radiation force model, Proceedings of First Internat. Symp. on Precise Positioning with the Global Positioning System, NOAA, Rockville, Maryland, 1985.
7. J. Ray, J. Ryan, C. Ma, T. Clark, B. Schutz, R. Eanes, M. Watkins and B. Tapley, Comparison of VLBI and SLR geocentric site coordinates, to appear *Geophys. Res. Lett.* (1990).
8. M. Feulner, The numerical integration of near-Earth satellite orbits across SRP boundaries using the method of modified back differences, Master's thesis, Univ. of Tex. at Austin (1990).
9. Y. Vigue, Thermal imbalance effects on a GPS satellite, Master's thesis, Univ. of Tex. at Austin (1990).

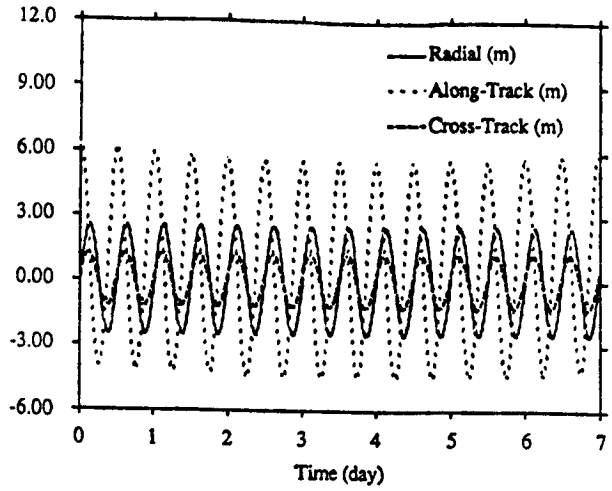

Fig. 2. Comparison of Orbits: Week 420 estimated solution vs. Week 419 predicted solution for SV06

The effects of eclipsing have been recently examined in two areas. First, the proper accounting of eclipsing in the numerical integration of the differential equations of motion requires care with a fixed step integrator when crossing the shadow boundary. A detailed study of this effect by Feulner /8/ showed that, while a significant effect was observed, it did not account for the observed effects in Fig. 1.

In a second study, Vigue /9/ solved the partial differential equations for heat conduction and radiation for simplified models of a GPS-type solar panel simultaneously with the orbit. When the modeled satellite passed into shadow and the panel begins to cool, the solar panels were found to be at distinctly different temperatures, giving rise to a "thermal imbalance" or a net force due to the radiation properties. The study did show that this effect could have a significant (meter or tens or meter) effect on the orbit, however, additional work is in progress.

It should be noted that the RMS of double differenced phase data for the cases examined were typically about 3 cm or less. While this RMS is a measure of the orbit accuracy, it cannot be implied that the orbit accuracy is comparable to the double difference RMS. In fact, because of cancellations of parameters other than clocks in the formation of the double difference measurement, the 3 cm RMS may differ from the actual orbit accuracy by an order of magnitude or greater.

GEODETIC RESULTS

The determination of geodetic quantities, such as vector baselines, are an important measure of the sensitivity to orbit accuracy. Selected relative position vectors for the sites estimated in Table 1 are given in Table 2 in terms of the week to week repeatability, an indication of the precision of estimates. Comparison of the average values with SLR or VLBI shows the differences given in Table 3. It is particularly important to note that the Onsala/Tromso result was obtained before the VLBI measured baseline was available, thus constituting a "blind test" of GPS. In general, the comparison with independently determined results from SLR and VLBI provide a measure of the accuracy of the results with space techniques. From these comparisons, the GPS results have an accuracy of 1–2 parts in 10^8 or better.

TABLE 2 Week-to-Week Estimate Repeatability, RMS about Mean (m) Over Three Weeks

Baseline	*dx*	*dy*	*dz*	*dl*
Tidbinbilla/American Samoa	0.044	0.144	0.101	0.177
Tidbinbilla/Black Birch	0.005	0.072	0.020	0.066
Onsala/Tromso	0.023	0.029	0.026	0.011
Kokee Park/Ft. Davis	0.024	0.047	0.022	0.048
Mojave/Owens Valley	0.012	0.033	0.026	0.007

TABLE 3 Comparison of Estimates with SLR or VLBI (m)

Baseline	Longitude	Latitude	Height	Length
Mojave/Owens Valley	–0.014	–0.007	0.004	0.000
Kokee Park/Ft. Davis	–0.013	–0.008	0.017	0.012
Onsala/Tromso	–0.019	–0.025	0.030	0.026

This report was prepared with the support of

Contract NAG5-940 and CRAY Research, Inc.

under the direction of

Bob E. Schutz and J. B. Lundberg

The Numerical Integration of Near Earth Satellite Orbits Across SRP Boundaries Using the Method of Modified Back Differences

by

Matthew Roger Feulner, B.S.

Thesis

Presented to the Faculty of the Graduate School of

The University of Texas at Austin

in Partial Fulfillment of the

Requirements for the

Degree of

Master of Science in Engineering

The University of Texas at Austin

August, 1990

Chapter 1
Introduction

The modeling of forces for the numerical integration of near Earth satellites is an important aspect of the orbit determination procedure. In applications using satellites such as Lageos, Topex, or the Global Positioning System (GPS), orbits must be known very precisely to obtain the most benefit from each satellite. To recover the orbits, many small perturbing forces must be modeled correctly within the numerical integration portion of the orbit determination procedure. This study is an investigation of one of the important perturbing forces, the solar radiation pressure (SRP) and its modeling when a fixed-mesh/fixed-order class II general formulation multistep numerical integrator is used to propagate the orbit.

There are two important aspects of the SRP force and its modeling: (1) the shadow model and (2) the nature of the numerical integration algorithm in which the SRP force is to be modeled. For most applications, the shadow of the Earth can be modeled as a cylinder extending behind the Earth, with respect to the Sun, enclosing the region of total shadowing, the umbra. In this model, there is no region of partial shadowing (penumbra), thus a true step function in the force model is caused by the SRP when satellites pass into and out of the Earth's shadow. For more precise applications, the shadow can be modeled as two cones, one extending inward behind the Earth enclosing the umbra and the other extending outwards enclosing the penumbra. The partial shadow region, the penumbra, provides a smooth transition from total sunlight to total shadow.

Multistep numerical integrators are frequently used in the orbit determination procedure because of their efficiency relative to single step methods [Lundberg, 1981]. A general formulation multistep integrator is derived assuming the forcing function f of the problem

$$\frac{d^2y}{dt^2} = y^{(2)} = f(t, y, y^{(1)}) \tag{1-1}$$

is smooth and continuous so that the integrals of f can be approximated by integrating an *m-1* order polynomial formed using m nodes, where the time step between each node is referred to as the *step size*. If the second integral of the polynomial is formed explicitly, as opposed to reducing the second order differential equations into twice as many first order equations, the integrator is referred to as a *class II* integrator. When the the conical model is used in the numerical integration, the SRP force appears smooth and continuous as long as the step size is small enough to sample the penumbra more than a few times. However, the force model may have an apparent discontinuity which violates the assumption of a smooth, continuous function of the numerical integrator. This discontinuity may occur if (1) the step size is longer than the time satellites spend in the penumbra, meaning the numerical integrator can step at most once in the penumbra, or (2) a cylindrical model is used. Thus, the polynomial does not accurately represent the forcing function and the integrator does not step correctly across the shadow boundary. GPS satellites which pass through the shadow take on the order of 60-100 seconds to cross the penumbra. However, to reduce the computational load, it is desired to use a 500 second numerical integration step size in the orbit determination process. Consequently, GPS

satellite orbits are good candidates for studying the effect that this problem has on the numerical solution for the orbits and techniques that can be used to alleviate this problem.

One possible solution to this problem is to reduce the step size used by the numerical integrator, but as was mentioned previously, it is desired to have a larger step size to reduce the computational load. Another possible solution is to integrate up to the boundary of the cylindrical model and restart the integrator at the boundary using the new level of the SRP force. This solution increases the computational load to a lesser degree than decreasing the step size, but it also introduces errors in the restarting process and is not an appropriate alternative when a conical shadow model is used.

The *modified back differences* (MBD) method, proposed by Hubbard, and described by Anderle (1973), corrects for most of the error by introducing modifications to the state at the leading node and modifying the back differences of the forcing function so the polynomial approximation is again valid. Lundberg (1985) also presents some results of this method. Modifications to the MBD method will also be examined including a new approach to the leading node state modifications.

Two types of tests were performed to analyze the MBD methods: (1) Numerical integration tests were performed using different step sizes, shadow models and numerical precision to analyze the direct effect of the MBD method on the propagation of the state given true initial conditions; (2) Batch filter estimations were performed to analyze the effects of the MBD method on the prediction of GPS orbits.

Chapter 2 discusses the numerical integrator, the orbit determination procedure, and the two applications to be used in the evaluation of the MBD method. Chapter 3 describes the Global Positioning System, including the orbits of the satellites and some of the data types available for orbit determination. Chapter 4 discusses the MBD method proposed by Hubbard as well as proposed modifications to this approach. Chapter 5 presents results from integration tests and batch filter estimations using both simulated and real data. Finally, Chapter 6 contains a discussion of the major conclusions and some suggestions for future work.

Chapter 6
Conclusions

The purpose of this work was to investigate solutions to the problem of integrating across the step function-like solar radiation pressure boundaries when large integration step sizes are used. Two shadow models were examined: the cylindrical model, which has true step function boundaries between full sunlight and full shadow, and the conical model, which has a smooth transition from full sunlight to full shadow only when the penumbra is sampled at least a few times per crossing. In the orbit determination of GPS satellites, it is desired to use an integration step size of at least 5 times as long as it takes the satellite to cross the penumbra, so the conical shadow model will appear in some cases to be a step function. Only when an integration node happens to lie near the middle of the penumbra will the step function nature be lessened, although the state at the next node will still not be correct.

Hubbard's original MBD method was the basis for most of the algorithms used to alleviate this problem at large step sizes. The following were proposed modifications to the original MBD method: the extension of the method to the conical shadow model, including two different approximations to the fractional acceleration in the penumbra; the interpolation method for leading node state corrections; and corrections due to the point mass term. The other method examined to alleviate this problem was restarting the integrator at each cylindrical shadow boundary crossing.

In Sections 5.1.1 and 5.1.2, it was found that Hubbard's MBD method with

integral leading node state corrections is effective in reducing the error. Furthermore, the proposed point mass term corrections at the leading node are necessary to obtain an accurate solution. Also from Sections 5.1.1 and 5.1.2, it was found that the MBD method with the proposed interpolated leading node state corrections is the most effective algorithm in reducing the error. Again, the point mass term corrections were found necessary for an accurate solution but the choice of penumbra approximations does not affect the results. Section 5.1.3 showed that restarting the integrator at each cylindrical shadow model boundary was very effective in reducing the error, but from Table 5-1, significant additional computer time was required to restart the integrator. Also from Section 5.1.3, it was found that the cylindrical shadow model, when the MBD method with interpolated leading node state corrections was applied, was an accurate approximation to the conical model.

Section 5.2 showed how the magnitude of the errors incurred by estimating trajectories with no special action taken at the shadow boundaries could be reduced by using the MBD method with interpolated leading node state corrections applied to either shadow model or to a lesser degree, the MBD method with integral leading node state corrections applied to the cylindrical model. Table 5-5 showed that the character of crossing the shadow boundaries with no special action has RMS values of less than 1 m in the radial and normal directions and up to 20 m in the transverse direction.

Section 5.3 applied the MBD method to actual observations to reduce the prediction errors. Table 5-7 showed that the RMS values in the radial and normal directions were as large as 4 m indicating that there is still mismodeled or

unmodeled force(s) in the GPS force model causing errors at least as large as that of crossing the shadow boundaries with no special action. Possible error sources include: (1) modeling the Y-bias acceleration as a constant for satellites which passed through the shadow, including the satellites which were shut down during periods of eclipse, (2) Earth radiation or albedo pressure, (3) the use of a constant area model instead of a variable area model or (4) inclusion of the Moon's shadowing effect.

Additional unanswered questions or possible improvements have arisen in the course of this study. The first one would be modeling the Earth as a nonspherical body. The effective radius of the Earth used in this study, 6371.0 *km*, is within about 7 *km* of the true radius of the Earth everywhere, but this can result in crossing times which are off by as much as 2-3 seconds. The implications of this was not examined. Second, the shadowing effect of the Moon's shadow should be included. Although MSODP has an option to include the Moon's shadow in the variable area model, the constant area model does not. At the Earth's distance, the Moon's umbra has almost vanished, so the MBD method should not have to be used. Finally, it might be worth while to actively check for sunlight/penumbra/sunlight crossings which might be skipped in the numerical integration. If the value of $\theta+\alpha_s+\alpha_e$ is saved at the past three integration nodes, a second order polynomial can be formed using these values. For example, if it is assumed the satellite is in sunlight and a boundary crossing has not been detected, the penumbra may have been crossed if the minimum value of the polynomial is both less than 0 and between the nodes of the polynomial. This can also be applied to the cylindrical model by monitoring the values of $r\sin\alpha$

and $\cos\alpha$.

A further application of this method could be to model impulse maneuvers. The trajectory would be integrated past the impulse by one step and interpolation would be used to find the state immediately before the maneuver. The ΔV would be added directly to the velocity at the time of the impulse and the back differences should be modified to reflect the maneuver. Finally, interpolation would be used to find the new state at the leading node.

PAPER AAS 91-187

IMPROVING THE NUMERICAL INTEGRATION SOLUTION OF SATELLITE ORBITS IN THE PRESENCE OF SOLAR RADIATION PRESSURE USING MODIFIED BACK DIFFERENCES

J. B. Lundberg, M. R. Feulner, P. A. M. Abusali, and C. S. Ho

Center for Space Research
The University of Texas at Austin
Austin, TX 78712

AAS/AIAA Spaceflight Mechanics Meeting

HOUSTON, TEXAS FEBRUARY 11-13, 1991

AAS Publications Office, P.O. Box 28130, San Diego, CA 92128

IMPROVING THE NUMERICAL INTEGRATION SOLUTION OF SATELLITE ORBITS IN THE PRESENCE OF SOLAR RADIATION PRESSURE USING MODIFIED BACK DIFFERENCES

J. B. Lundberg,* M. R. Feulner,** P. A. M. Abusali,+ and C. S. Ho++

Numerical integration techniques are frequently used to form the solution of the equations that describe the orbital motion of a satellite. The basic errors associated with numerical integration can be described in terms of round–off and truncation errors resulting from a finite number of significant digits used in the computations and the functional approximation used in deriving the numerical integration algorithm. Additional numerical integration errors can result when the time scale of some of the perturbing forces is smaller than or on the same order as the integration step size. This type of error can occur when solar radiation pressure is included in the force model and the trajectory crosses through the shadow of a planet. The method of modified back differences is a technique that significantly reduces the numerical integration errors associated with crossing shadow boundaries using a fixed–mesh multistep integrator without a significant increase in computer run time.

INTRODUCTION

Many near Earth satellite missions require the most precise trajectory solutions possible from the available tracking information and solution techniques with some orbit

* Special Research Assistant, Center for Space Research, The University of Texas, Austin, TX 78712.

** Graduate Research Assistant, Center for Space Research, The University of Texas, Austin, TX 78712 (now at the Massachusetts Institute of Technology).

+ Special Research Assistant, Center for Space Research, The University of Texas, Austin, TX 78712.

++ Graduate Research Assistant, Center for Space Research, The University of Texas, Austin, TX 78712 (now at the Institute for Aeronautics and Astronautics, National Chang-Kung University, Tianan, Taiwan 7010).

requirements ranging from a few meters to a few decimeters or less in position. Precise orbit solutions typically involve forming estimates of the orbit state parameters as well as geophysical and empirical parameters used to model the forces acting on the satellite. Any numerical errors introduced into the orbit determination process can affect the values of these estimated parameters. Since the precision orbit determination process depends upon the numerical integration of the equations of motion, it is important to have an accurate and efficient numerical integration algorithm that is compatible with the equations of motion.

Since numerical integration errors are unavoidable, the issue of how to carry out the numerical integration is reduced to selecting an algorithm in which the resulting computer costs and numerical errors are tolerable. The equations of motion for a near Earth satellite can be written as

$$\frac{d^2\bar{r}}{dt^2} = -\mu \frac{\bar{r}}{r^3} + \bar{f}_p(t, \bar{r}, \dot{\bar{r}}) = \bar{f}(t, \bar{r}, \dot{\bar{r}}) \tag{1}$$

and several important characteristics about the numerical solution of Eq. (1) have become widely accepted. First, a Class II integrator which solves this system directly is more efficient than a Class I integrator which would require writing Eq. (1) as a system of first order differential equations. Second, multistep integrators are more efficient than single step (Runge–Kutta) algorithms in solving this system. Finally, when the eccentricity of the orbit is small, the equations of motion are sufficiently smooth that step size control is not necessary to maintain the solution accuracy. Consequently, a Class II, fixed–mesh, multistep integrator of either the summed form (Second Sum, Gauss–Jackson) or the general form (Adams' type) are widely used in many precision orbit determination programs.

The multistep integrator is based upon the assumption that the right hand side of Eq. (1) is smooth and continuous and can be approximated to sufficient accuracy by a polynomial formed using a set of discrete values of $\bar{f}$ computed at the integration nodes along the trajectory. When solar radiation pressure (SRP) is included as a perturbing force, this assumption is violated when a cylindrical shadow model is used and the satellite passes from total sunlight into the umbra. This assumption is also violated when a conical shadow model is used in combination with a fixed–mesh algorithm in which the step size is large enough that the penumbra is sampled only once or twice at most per revolution. These violations can lead to appreciable numerical integration errors for arc lengths of only a few tens of revolutions.

Various modifications to the fixed–mesh, multistep integrator can be employed to reduce or negate the errors incurred when crossing shadow boundaries. However, the method of modified back differences can be used with either the cylindrical or conical shadow models, does not require any alteration of the multistep integrator's mesh or step size, and can be carried out with only a slight increase in computer run time. To begin this discussion of the method of modified back differences, the original method, as proposed by Hubbard and described by Anderle,[1] is discussed. Improvements to

Hubbard's approach for the case involving a cylindrical shadow model will be offered. The extension of the modified back difference approach to cases using a conical shadow model will also be demonstrated.

The integrator to be used in this investigation is a general formulation (Adams') Class II integrator of the form

$$y_{n+s} = y_n + (sh)\,\dot{y}_n + (sh)^2 \sum_{j=1}^{m} \alpha_{j,s} \nabla^{j-1} f_n \qquad (2)$$

$$\dot{y}_{n+s} = \dot{y}_n + (sh) \sum_{j=1}^{m} \beta_{j,s} \nabla^{j-1} f_n$$

where h is the step size, $\nabla^{j-1} f_n$ are the back differences of the force, $f(t, y, \dot{y})$, formed at t_n, and $\alpha_{j,s}$ and $\beta_{j,s}$ are the coefficients used in the prediction (s=1), correction (s=0), or interpolation (s<0) stages of the integrator. Given a value for s, the coefficients are computed using a recursive algorithm.[2,3] The selection of the general formulation integrator instead of the summed formulation was arbitrary; the method of modified back differences is applicable to either formulation.

HUBBARD'S METHOD

The method of modified back differences as proposed by Hubbard is an attempt to reduce the numerical errors associated with the crossing of the cylindrical shadow model boundary between sunlight and shadow which introduces a step function change in the forcing function. In the cylindrical model, a satellite is assumed to be in shadow when $\cos \varepsilon < 0$ and $(r \sin \varepsilon) \leq R_e$ are satisfied where ε is the angle between the Earth–satellite and the Earth–sun lines, r is the radial distance of the satellite from the origin, and R_e is the effective radius of the Earth. The method of modified back differences consists of three steps.

Step 1

To begin the application of the method of modified back differences, it is necessary for the numerical integrator to detect the crossing of a shadow boundary and to solve for the time and state at the boundary crossing. Although a shadow boundary is crossed, the integration should be propagated across the boundary as if there were no boundary. This will assure that the integrated solution up to the time of the shadow boundary crossing is correct. After the crossing, the trajectory will have errors that are proportional to the difference between the actual SRP model and the value used to form the integrated solution. If the last three integration nodes are taken to be t_1, t_0 and t_{-1} with t_c, the time of crossing, in the interval $[t_0, t_1]$, the shadow boundary can be found by using a quadratic approximation of the function $T(t) = r(t) \sin\alpha(t)$ where $T(t_c) = R_e$. By evaluating the

function T(t) at the nodes, the shadow boundary crossing is found by evaluating the expression

$$\delta t = \frac{h}{2\nabla^2 T_1}\left\{2\nabla T_1 + \nabla^2 T_1 - \beta\left[(2\nabla T_1 + \nabla^2 T_1)^2 - 8\nabla^2 T_1 (T_1 - R_e)\right]^{1/2}\right\} \quad (3)$$

where $\nabla T_1 = T_1 - T_0$, $\nabla^2 T_1 = T_1 - 2T_0 + T_{-1}$, $\beta = 1$ for $\nabla T_1 > 0$, $\beta = -1$ for $\nabla T_1 < 0$, and from this $t_c = t_1 - \delta t$. The accuracy of t_c is dependent on the spacing between the nodes, i.e. the integration step size, because of the the second order polynomial approximation. If a more accurate solution is desired, t_o is taken to be the last solution of the boundary crossing time, the range $[t_{-1}, t_1]$ is reduced, the trajectory is interpolated at t_{-1}, t_o, and t_1 to evaluate T(t), and δt is recomputed using Eq. (3). This algorithm can be iterated until the value of t_c converges.

Step 2

At this point, the back differences, $\nabla^i f_n$, represent the forcing function evaluated at the level of SRP before the boundary crossing. To avoid the step function nature of the cylindrical shadow model boundary, it is necessary to modify the back differences to be consistent with the new level of SRP at the leading node, t_n. To accomplish this, the back differences of the SRP are formed at the leading node, $\nabla^j \bar{f}_{SRP,n}$, where the SRP has been evaluated at each node as if the satellite were in full sunlight. The SRP back differences are added to (subtracted from) the back differences of the total forcing function when the satellite is passing out of (into) the shadow.

Step 3

Since the state at the leading node ($\bar{r}_n$, $\dot{\bar{r}}_n$) is in error, the integrated effect of the SRP from t_o to t_n must be used to modify the state at the leading node. If the SRP is assumed to be constant over one integration step, corrections of

$$\delta\bar{r} = \frac{1}{2}\gamma (t_n - t_c)^2 \bar{f}_{SRP,n}$$

$$\delta\dot{\bar{r}} = \gamma (t_n - t_c) \bar{f}_{SRP,n}$$

must be applied to the position and velocity at the leading node, respectively, where $\bar{f}_{SRP,n}$ is the SRP evaluated at the leading node and γ is +1 (-1) if the satellite is moving out of (into) shadow.

The modified back differences algorithm is represented in Fig. 1 where the solid line represents the actual trajectory, the dashed line represents the trajectory if there were no boundary, and the dotted line represents the new "past" trajectory after the method of

modified back differences is applied. The technique of using an approximate integral of the SRP to correct the state at the leading node will be referred to as the *integral method.*

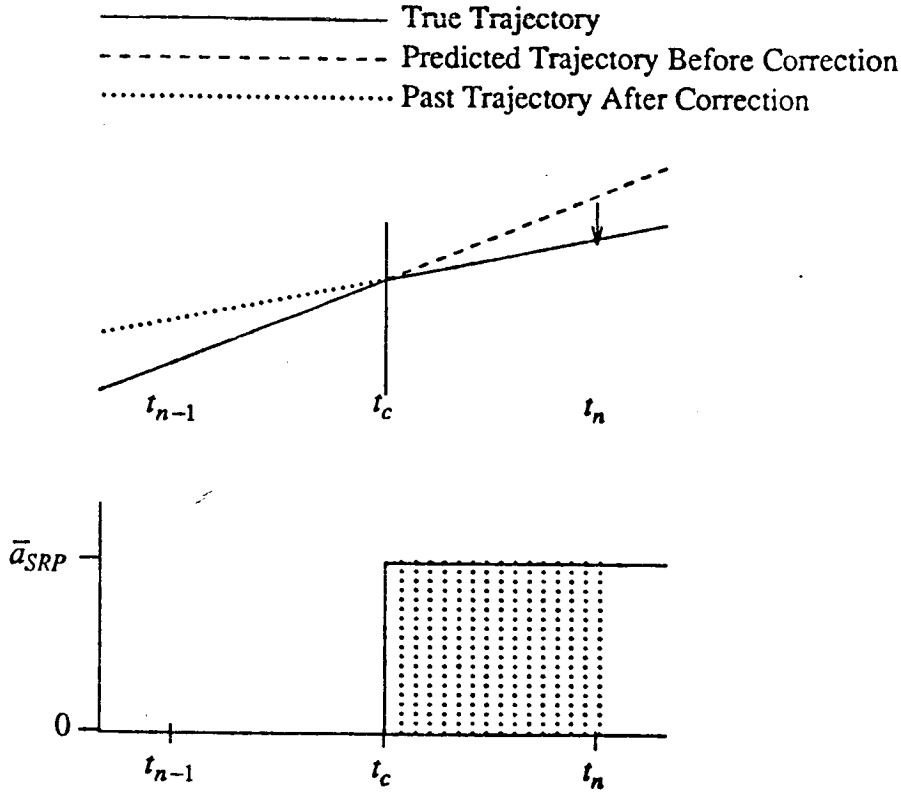

Fig. 1 Cylindrical SRP Force Model with Trajectory
Representation of the Method of Modified Back Differences

MODIFICATIONS TO HUBBARD'S METHOD

Two important modifications to Hubbard's method have been identified. The first comes as a result of the leading node state correction. Once the leading node state correction is made, the force at the leading node, $\bar{f}_n$, is no longer consistent with the state. Since the leading node state correction is small, the only important force to re–evaluate is the point mass term (PMT) of the geopotential. Using the corrected state, the PMT is re–evaluated and is used to update $\bar{f}_n$. However, since $\bar{f}_n$ has been altered, the state should be corrected for this small change in the force function. If the difference in the PMT is assumed linear with a value of zero at the shadow boundary crossing to the value of the computed difference at the leading node, the force can be integrated to yield the leading node state corrections

$$\delta\bar{r} = \frac{1}{6}(t_n - t_c)^2 \delta\bar{f}_{PMT,n}$$

$$\dot{\delta\bar{r}} = \frac{1}{2}(t_n - t_c)\ \delta\bar{f}_{PMT,n}$$

where $\delta\bar{f}_{PMT,n}$ is the difference in the PMT evaluated at the leading node. Since another leading node state correction has been made, the PMT should be re–evaluated once more. This second re–evaluation can then lead to another leading node state correction, so this process can be iterated more than once.

The second important modification to Hubbard's method is how the leading node state corrections are made. Since the integral corrections are only valid over short intervals, an alternative method is needed to increase the accuracy at larger integration step sizes. After iterating to find the boundary crossing time and state and correcting the back differences of the force function for the change in SRP, the state at the boundary crossing can be used in this interpolation equations of numerical integrator to solve for the state at the leading node. Selecting $t_{n+s} = t_c$, Eq. (2) can be written as

$$\dot{y}_n = \dot{y}_c - (t_n - t_c) \sum_{j=1}^{m} \beta_{j,s} \nabla^{j-1} f_n \tag{4}$$

$$y_n = y_c - (t_n - t_c)\, \dot{y}_n - (t_n - t_c)^2 \sum_{j=1}^{m} \alpha_{j,s} \nabla^{i-1} f_n$$

where y_c and $\dot{y}_c$ are the position and velocity at t_c, respectively, and $s = (t_c - t_n)/h$. This technique for correcting the state at the leading node will be called the *interpolation method.* To apply the point mass term corrections to the interpolation method, it is only necessary to update the back differences with the new PMT, then solve for the new leading node using Eq. (4).

APPLICATION TO THE CONICAL SHADOW MODEL

The conical shadow model is more representative of the Earth's shadow than the cylindrical model. The angular parameters used to describe the conical model can be expressed using the following equations

$$\alpha_s = \tan^{-1}\frac{R_s}{r_s}, \qquad \alpha_e = \tan^{-1}\frac{R_e}{r_e}, \qquad \theta = \cos^{-1}\frac{\bar{r}_e \cdot \bar{r}_s}{|\bar{r}_e|\ |\bar{r}_s|}$$

where R_s is the effective radius of the sun, $\bar{r}_s$ is the vector from the satellite to the sun, R_e

is the effective radius of the Earth, and $\bar{r}_e$ is the vector from the satellite to the Earth. The satellite is assumed to be in the region of partial shadowing, the penumbra, when $(\alpha_e+\alpha_s) > \theta > (\alpha_e-\alpha_s)$ and in the full shadow, the umbra, when $\theta < (\alpha_e-\alpha_s)$.

To implement the method of modified back differences with the conical model, the time and state at both the sunlight/penumbra and umbra/penumbra boundaries must be found. By defining the function T(t) as $T(t) = \theta - \alpha_e - \gamma\alpha_s$, where γ is +1 for the sunlight/penumbra crossing and -1 for the umbra/penumbra crossing, then the boundary crossings satisfy the condition that $T(t_c) = 0$. The times of the boundary crossings can then be found by writing Eq. (3) in the form

$$\delta t = \frac{h}{2\nabla^2 T_1}\left\{2\nabla T_1 + \nabla^2 T_1 - \beta\left[(2\nabla T_1 + \nabla^2 T_1)^2 - 8\nabla^2 T_1 (T_1)\right]^{1/2}\right\}$$

where $\beta = 1$ for $\nabla T_1 > 0$, $\beta = -1$ for $\nabla T_1 < 0$, and $t_c = t_1 - \delta t$ as before. As in the case of the cylindrical shadow model, the numerical integration is carried out assuming that the satellite is in full sunlight (shadow) until both of the shadow boundaries are crossed and the satellite is in full shadow (sunlight).

At this point both shadow boundary crossing times are found and the corrections to the state at the leading node are applied. To extend Hubbard's integral approach to the conical model, the fractional SRP encountered in the penumbra as well as the appropriate SRP from the second boundary crossing to the leading node must be modeled. If the SRP in the penumbra is modeled as a linear function with a value of 0 at the umbra/penumbra boundary to a value of $\bar{f}_{SRP,n}$ at the penumbra/sunlight boundary, the leading node corrections can be written as

$$\delta\bar{r} = \gamma\left[\frac{1}{2}(t_n - t_{c2})^2 + \frac{1}{6}(t_{c2} - t_{c1})^2\right]\bar{f}_{SRP,n}$$

$$\delta\dot{\bar{r}} = \gamma\left[(t_n - t_{c2}) + \frac{1}{2}(t_{c2} - t_{c1})\right]\bar{f}_{SRP,n}$$

where t_{c1} and t_{c2} are the times at which the boundaries, umbra/penumbra or sunlight/penumbra, were crossed and γ is +1 (-1) if the satellite is passing out of (into) shadow.

If the interpolation method is used, an integral correction is applied to the state at the second boundary crossing, and this corrected state is used in the interpolation equations to solve for the leading node state. The integral corrections applied to the state at the second boundary crossing are

$$\delta\bar{r} = \frac{1}{6}\gamma(t_{c2}-t_{c1})^2\,\bar{f}_{SRP,n}$$

$$\dot{\delta\bar{r}} = \frac{1}{2}\gamma(t_{c2}-t_{c1})\,\bar{f}_{SRP,n}$$

if a linear model of the penumbra is used where γ is +1 (-1) if the satellite is passing out of (into) shadow. After the integral correction is used to update the state at the leading node, the PMT corrections to the state and force at the leading node are iteratively applied.

To investigate the accuracy of using a linear model for the shape of the solar radiation pressure in the penumbra, a nonlinear model was derived by assuming that in the neighborhood of the solar disk the Earth's limb is linear and the satellite's velocity is nearly constant. Under these conditions, the fractional SRP can be written as

$$f_{SRP} = \frac{\cos^{-1}(1-2s)}{\pi} - \frac{2}{\pi}(1-2s)\,(s-s^2)^{3/2}$$

where s is a nondimensional parameter such that $s = 0$ at the umbra/penumbra boundary and $s = 1$ at the sunlight/penumbra boundary. For this nonlinear model, the integral correction for the penumbra effect becomes

$$\delta\bar{r} = \frac{5}{32}\gamma(t_{c2}-t_{c1})^2\,\bar{f}_{SRP,n}$$

$$\dot{\delta\bar{r}} = \frac{1}{2}\gamma(t_{c2}-t_{c1})\,\bar{f}_{SRP,n}$$

However, this model did not provide any significant improvement over the linear model. Consequently, only results using the linear model are given.

TEST RESULTS

Two types of tests were performed to evaluate the modified back differences algorithm. First, it was necessary to use numerical integration comparisons to identify the best variation of the modified back difference algorithm. Then, the best variations were used in batch filter estimation tests to determine the effect of the algorithms on the orbit solutions. The orbital parameters to be used in this investigation are representative of those in the GPS constellation.

Algorithm Comparison

The numerical integration comparisons were done in two groups, one using a cylindrical shadow model and one using a conical shadow model. The initial conditions were the same for all tests:

semimajor axis	=	26,000 km	ascending node	=	0°
eccentricity	=	0.01	argument of perigee	=	0°
inclination	=	55.0°	mean anomaly	=	0°

The time span of the tests was taken to be two weeks or 28 orbital revolutions. The dynamical force model included only a constant area SRP model and a geopotential model including terms through degree and order eight. For the SRP model reflectivity coefficient (η) was 0.22, the effective radius of the Earth (R_e) was taken to be 6371.0 km and the effective radius of the Sun (R_s) was taken to be 696000.0 km. The Sun was assumed to be in the equatorial plane with the Earth–Sun direction initially in line with the line of nodes of the satellite. The number of function evaluations represented in the back difference table (m in Eq.s 2 and 4) was 14. These test were performed on a dual Cyber 170/750 computer utilizing a 60 bit word with a 48 bit mantissa.

To evaluate the various permutations of the modified back difference algorithm, reference trajectories were computed for each shadow model. The reference trajectory for the cylindrical shadow model comparisons was computed using a 500 second integration step size which was restarted at each cylindrical model shadow boundary. This was chosen over a double precision integration using a 5 second step size because even at small step sizes, the solution is flawed by the step function introduced in the force model at the cylindrical shadow boundary. The reference for the conical shadow model comparisons was computed using a 5 second step size and double precision (28 significant digits) arithmetic. This integration does not suffer from a step function in the force model because it samples the penumbra more than 12 times per pass.

The transverse (alongtrack) errors for the selected algorithms involving both the cylindrical and conical shadow models are shown in Figs. 2 and 3. Only the transverse error is displayed because it is known to be much larger than the errors in the normal (crosstrack) or radial directions. For each shadow model, the interpolation method with two iterations of the PMT correction results in the best ephemeris with a maximum error of less than 3 cm when applied to the conical model and a maximum error of less than 1 cm when applied to the cylindrical model. It is also shown that the PMT corrections are important in obtaining high accuracy solutions, although it was found that no more than two PMT corrections are necessary. In comparison, the cylindrical model with no special action taken at the boundaries had a maximum transverse error of 7 m, and the conical model with no special action at the boundaries had a maximum transverse error of 20 m.

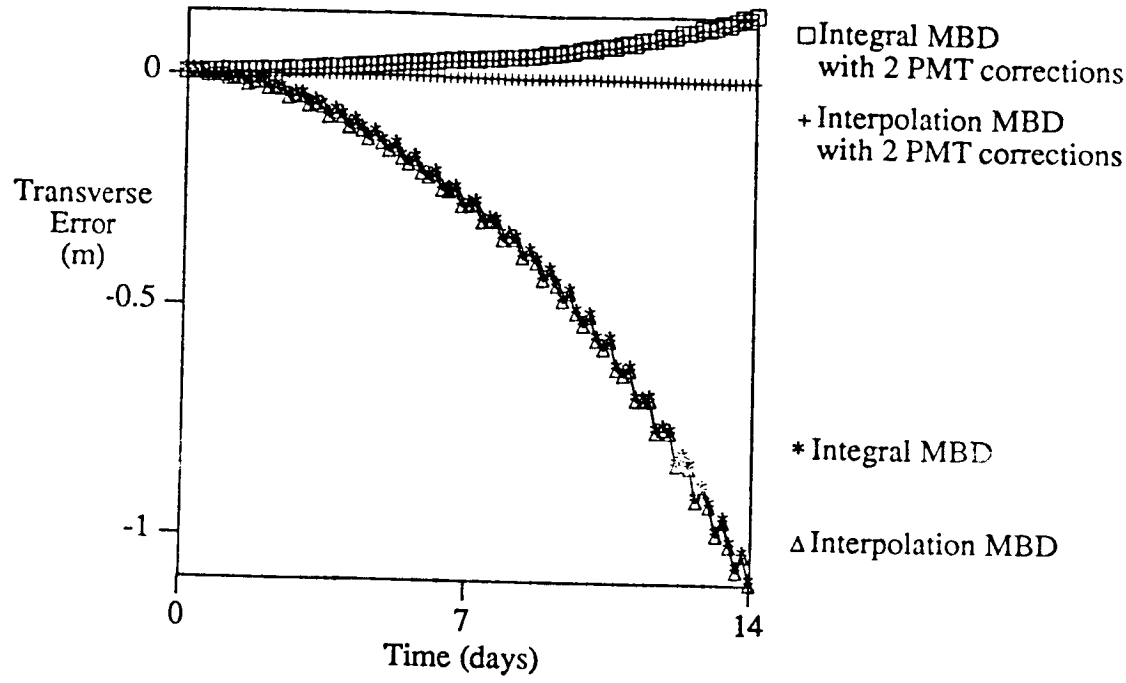

Fig. 2 Results of the MBD Algorithm
Using the Cylindrical Shadow Model

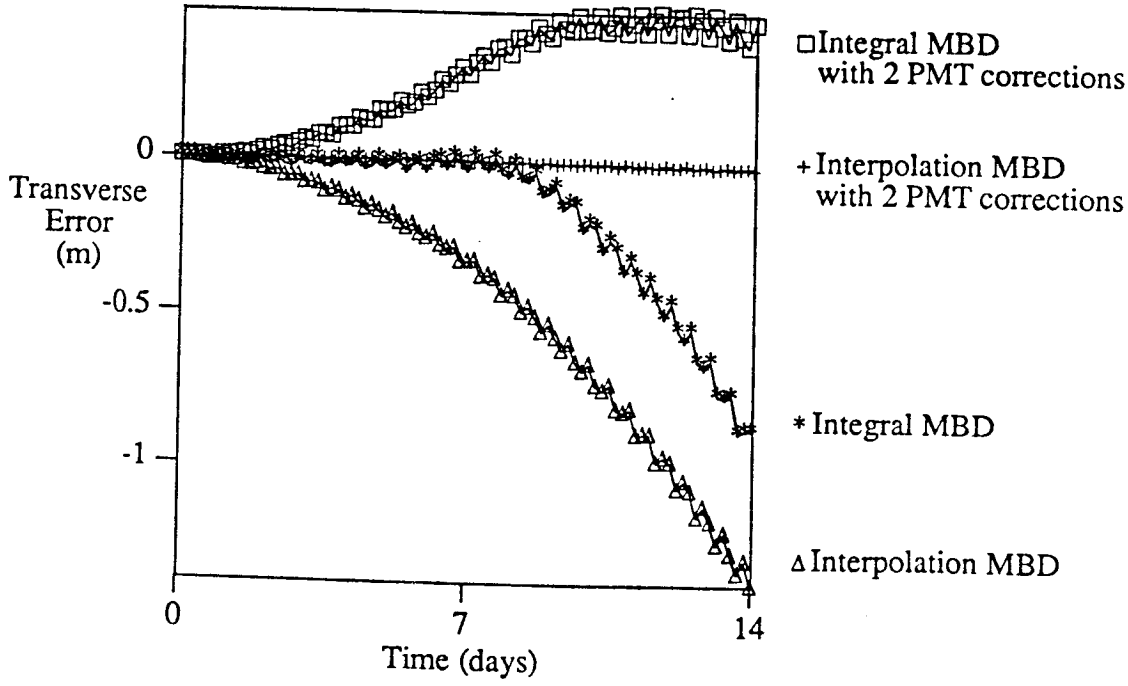

Fig. 3 Results of the MBD Algorithm
Using the Conical Shadow Model

The method of modified back differences will be an effective tool only if it can be implemented at a reasonable cost in terms of computer time. To evaluate the additional cost of using the method of modified back differences, trajectories spanning one week (14 orbital revolutions) were computed in which no special action was taken at the boundaries for both the conical and cylindrical models, and the execution time of these trajectories were used as the baseline for evaluating the method of modified back differences. As in the previous tests, the force model included only SRP and a geopotential model complete to degree and order eight. An integrator step size of 500 seconds was used for all cases. It was found that the method of modified back differences increased the execution time by about 10% for the cylindrical case and about 20% for the conical case over the baseline cases; whereas restarting the integrator at the boundary of the cylindrical model represented an increase of over 100%. The relative cost of the method of modified back differences will decrease as the complexity of the force model increases since its cost is proportional to the number of boundary crossings. The relative cost of restarting the integrator at the boundaries will remain high since it is proportional to the cost of evaluating the forcing function as well as the number of shadow crossings.

Batch Filter Tests

To measure the effect that this numerical integration error has on batch filter solutions and the extrapolation of these solutions, tests were conducted in which the only source of error is the result of using a relative large step size to cross the shadow boundary. The scenario for the batch filter tests involved the satellites PRN 3, 6, 8, 9, 11, 12, and 13 of the GPS constellation during Weeks 419 and 420 which correpsonds to the CASE UNO experiment.[4] PRN 3, 8, 11 and 13 are in one orbital plane which eclipses during these weeks, and PRN 6, 9 and 12 are in another orbital plane that is in full sunlight. The locations of the twelve ground stations involved in the experiment are shown in Table 1. The observations used in this experiment were double differenced carrier phase measurements computed along simulated "true" trajectories for the seven satellites using the time tags of the actual observations made during this two week period. Simulated "true" trajectories and noiseless observations were used 1) to remove the effect of other error sources on the batch filter solutions and 2) to provide a true solution to evaluate the technique. The time tags of the actual observations were used to provide a spatial and temporal data distribution representative of actual tracking. There were over 80,000 observations which were simulated along the true trajectory that was generated using a 20 second integration step size with a conical shadow model. The step size was chosen to have at least three steps in the penumbra per pass to avoid introducing the step function change in the SRP at the shadow boundary which occurs with larger step sizes.

The force model in all cases included a constant area SRP model and a geopotential model complete to degree and order eight. The estimated parameters in these tests included the initial conditions for each satellite in the constellation and the

Table 1

GPS GROUND STATIONS

Station	Longitude (°E)	Latitude (°N)
American Samoa	-170.7147	-14.3322
Black Birch, New Zeland	173.8056	-41.7452
Onsala, Sweden	11.9255	57.3953
Tidbinbilla, Austrailia	148.9786	-35.3976
Tromso, Norway	18.9383	69.6627
Wettzell, FRG	12.8786	49.1446
Yellowknife, Canada	-114.4689	62.4769
Ft. Davis, TX	-103.9470	30.6360
Kokee Park, HI	-159.6649	22.1263
Mojave, CA	-116.8882	35.3315
Owens Valley, CA	-118.2836	37.2320
Westford, MA	-71.4933	42.6133

reflectivity coefficient for a total of 49 parameters. The number of nodes represented in the back difference table (m) was 14. The computations were carried out on a Cray X–MP/24 using single arithmetic (64 bit word size with a 48 bit mantissa).

The MBD algorithms used in the batch filter tests are (1) the integral method as applied to the cylindrical shadow model, (2) the interpolation method as applied to the cylindrical shadow model, and (3) the interpolation method as applied to a conical shadow model. Each of these algorithm variations included two iterations of the PMT correction. For comparison, the cylindrical and conical shadow models with no special action at the boundaries were included in the tests. The batch filter tests involved estimating the trajectories using only the data from the first week of the study. The estimated trajectories were extrapolated to the second week and compared with the reference trajectory. The results from both the batch filter and the extrapolations are used to evaluate the effectiveness of the modified back differences algorithm.

Fig. 4 gives an example of the transverse orbit errors for the estimated trajectories of PRN 3 which is eclipsing and PRN 6 which is in full sunlight during week 419. These results were obtained using the interpolation method with two PMT corrections and a conical shadow model to propagate the orbit. Similarly, Fig. 5 gives an example of the orbit errors for PRN 3 and PRN 6 under the same conditions except that no special action is taken at the boundaries. These results demonstrate that the method of modified back differences can be used to reduce the effect of this numerical integration error on the batch filter solutions by two orders of magnitude from about 1 m to 1 cm.

Table 2 shows the root–mean–square (RMS) of the differences between the estimated and true trajectories for the week 419 estimates. All of the MBD algorithms

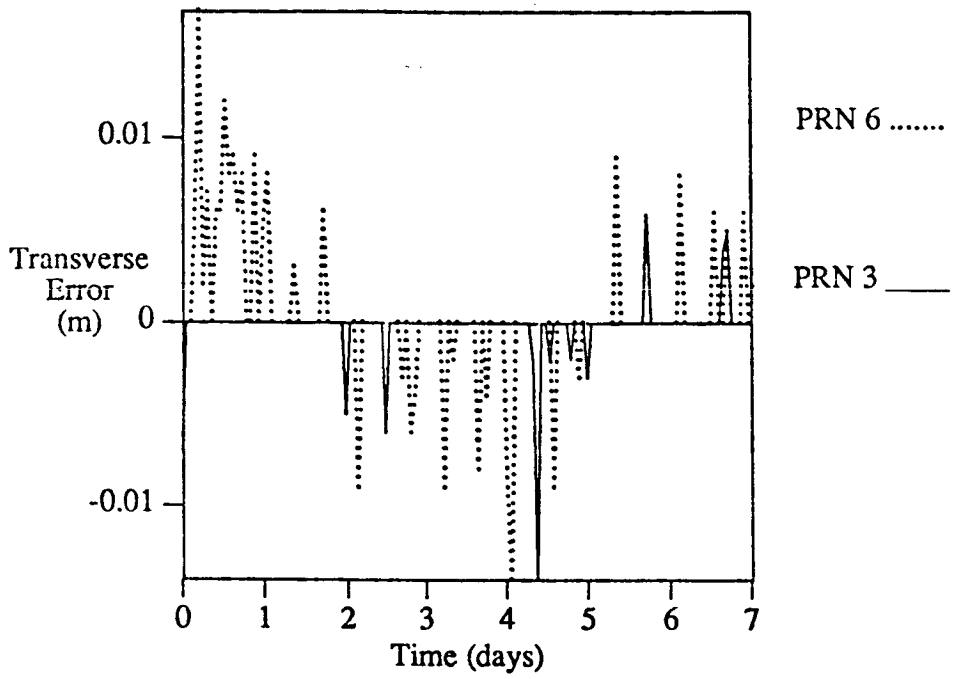

Fig. 4 Transverse Orbit Errors for the Batch Filter Solutions of Week 419 Using the Interpolation MBD Method with a Conical Shadow Model

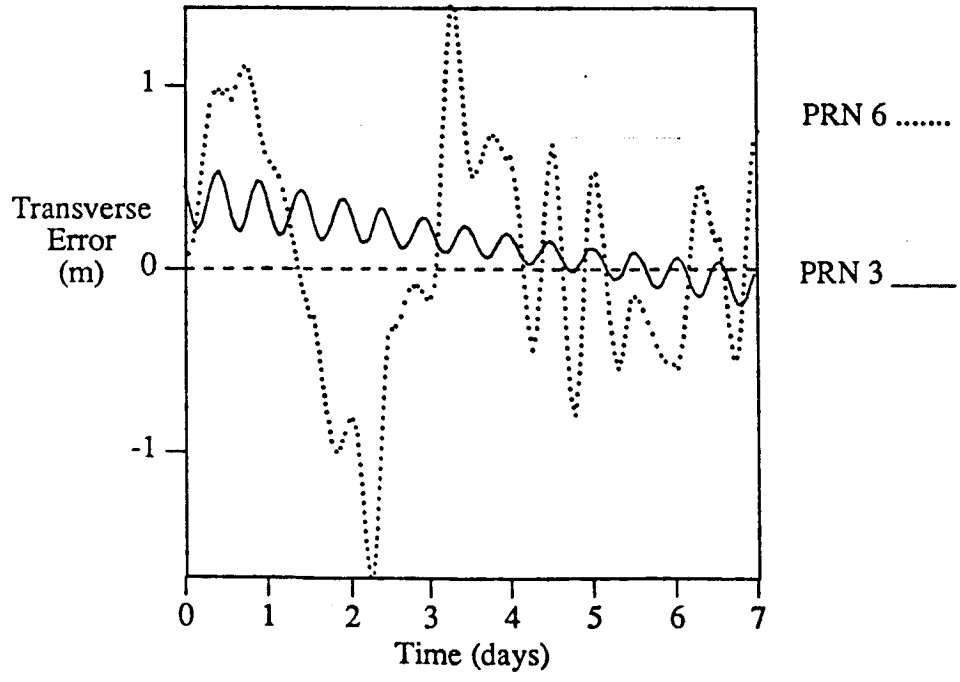

Fig. 5 Transverse Orbit Errors for the Batch Filter Solutions of Week 419 When No Special Action is Taken at the Shadow Boundaries of a Conical Model

have RMS values of less than 1 cm while some of the trajectories with no special action taken at the boundaries have RMS values greater than 1 m. Table 3 shows the RMS of the double difference measurement residuals for the week 419 estimates. All of the MBD algorithms result in RMS values of less than 3 mm while the cases in which no special action was taken at the boundaries have values greater than 7 cm. These tables suggest that the MBD method should provide a better prediction of the trajectory into week 420 than the models in which no special action is taken.

Table 2

RMS (m) OF THE DIFFERENCES BETWEEN THE ESTIMATED AND TRUE TRAJECTORIES OF WEEK 419

Model	Component	PRN 3	PRN 6	PRN 8	PRN 9	PRN 11	PRN 12	PRN 13
Cylindrical No Special Action	Radial	0.176	0.081	0.305	0.065	0.174	0.067	0.236
	Trans	1.201	0.460	2.626	0.433	0.811	0.300	0.929
	Normal	0.100	0.027	0.020	0.080	0.085	0.111	0.104
Cylindrical Integral MBD	Radial	0.001	0.002	0.003	0.002	0.002	0.002	0.003
	Trans	0.003	0.003	0.007	0.003	0.004	0.003	0.005
	Normal	0.003	0.002	0.004	0.002	0.003	0.002	0.003
Cylindrical Interpolation MBD	Radial	0.010	0.002	0.002	0.001	0.003	0.002	0.002
	Trans	0.004	0.002	0.003	0.002	0.004	0.002	0.003
	Normal	0.003	0.002	0.002	0.002	0.003	0.002	0.002
Conical No Special Action	Radial	0.154	0.090	0.183	0.099	0.151	0.008	0.171
	Trans	0.652	0.217	1.109	0.267	0.671	0.191	0.623
	Normal	0.112	0.090	0.099	0.111	0.129	0.121	0.130
Conical Interpolation MBD	Radial	0.010	0.002	0.002	0.002	0.003	0.002	0.002
	Trans	0.004	0.002	0.003	0.002	0.005	0.002	0.003
	Normal	0.003	0.002	0.002	0.002	0.003	0.002	0.002

Table 3

DOUBLE DIFFERENCE RESIDUAL RMS (m) FOR WEEK 419

Cylindrical No Special Action	Cylindrical Integral MBD	Cylindrical Interpolation MBD	Conical No Special Action	Conical Interpolation MBD
0.1341	0.0003	0.0002	0.0742	0.0002

The RMS of the differences between the extrapolated solutions from week 419 and the "true" trajectory for week 420 are given in Table 4. Table 4 shows that solutions using the MBD methods do indeed predict the trajectories much better than the solutions

without the MBD approach. Also, the interpolation method applied to either shadow model has RMS trajectory differences of less than 1 cm while the cylindrical shadow model with integral corrections has an RMS less than 9 cm. However, the orbit predictions in which no special action is taken at the boundaries have RMS values as high as 30 m for the cylindrical model and as high as 9 m for the conical model.

Table 4

RMS (m) OF THE DIFFERENCES BETWEEN THE EXTRAPOLATED AND TRUE TRAJECTORIES OF WEEK 420

Model	Component	PRN 3	PRN 6	PRN 8	PRN 9	PRN 11	PRN 12	PRN 13
Cylindrical	Radial	0.337	0.185	0.939	0.070	0.757	0.182	0.517
No Special	Trans	17.316	1.073	31.361	0.904	7.759	0.838	3.244
Action	Normal	0.098	0.027	0.018	0.079	0.095	0.111	0.107
Cylindrical	Radial	0.006	0.003	0.005	0.003	0.004	0.003	0.004
Integral	Trans	0.020	0.005	0.085	0.006	0.047	0.005	0.051
MBD	Normal	0.004	0.003	0.004	0.003	0.004	0.003	0.004
Cylindrical	Radial	0.004	0.002	0.004	0.002	0.002	0.003	0.003
Interpolation	Trans	0.016	0.003	0.007	0.003	0.003	0.005	0.009
MBD	Normal	0.004	0.002	0.004	0.002	0.002	0.003	0.004
Conical	Radial	0.285	0.088	0.459	0.078	0.202	0.081	0.242
No Special	Trans	1.700	0.420	9.471	0.290	3.796	0.353	2.648
Action	Normal	0.113	0.090	0.099	0.111	0.130	0.120	0.131
Conical	Radial	0.005	0.003	0.003	0.002	0.004	0.003	0.004
Interpolation	Trans	0.009	0.004	0.006	0.003	0.008	0.005	0.013
MBD	Normal	0.004	0.003	0.003	0.002	0.004	0.003	0.004

CONCLUSIONS

It has been demonstrated that the method of modified back differences applied to either the cylindrical or conical shadow model significantly reduces the numerical integration errors associated with the crossing of shadow boundaries. While Hubbard's integral approach can produce significant improvements to the trajectory solution, the interpolation method provides the best overall results. Also, it has been shown that iterating on the PMT correction is also important for achieving the best overall results. In addition, it has been demonstrated that the method of modified back differences can be implemented with only a small increase in execution time.

ACKNOWLEDGEMENTS

The comments and assistance of Dr. Bob Schutz and H. J. Rim are deeply appreciated. Computational support was provided by the Center for High Performance Computing at the University of Texas. This work was supported under NASA contract NAG5–940 and by a grant from Cray Research Inc.

REFERENCES

1. Anderle, R. J., "Geodetic Analysis Through Numerical Integration," **Proceedings of the International Symposium on the Use of Artificial Satellites for Geodesy and Geodynamics,** Athens, Greece, 1973.

2. Lundberg, J. B., "Numerical Integration Techniques for Satellite Orbits," Masters Thesis, The University of Texas at Austin, May, 1981.

3. Shampine, L. and M. Gordon, **Computer Solutions of Ordinary Differential Equations, The Initial Value Problem** W. H. Freeman and Company, San Francisco, 1975.

4. Schutz, B. E., C. Ho, P. A. M. Abusali, and B. D. Tapley, "CASA UNO GPS Orbit and Baseline Experiments," **Geophysical Research Letters,** Vol. 17, No. 5, April 1990, pp. 643-646.

APPENDIX IX

"GPS orbits and baseline experiments: Mini-Mac/TI comparisons," presented at the IAG General Meeting (Symposium 102, Poster 2.2.10), Edinburgh, U.K., August 1989

GPS ORBITS AND BASELINE EXPERIMENTS: MINI-MAC/TI COMPARISONS

B.E. Schutz, P.A.M. Abusali, C.S. Ho, B.D. Tapley
Center for Space Research
University of Texas at Austin, Austin, Texas 78712 USA

ABSTRACT

Major changes in the Cooperative International GPS Network (CIGNET) tracking hardware took place in 1989. Prior to 1989, the CIGNET solely consisted of TI-4100 receivers except for the Mini-Mac receiver at Tsukuba. In January, 1989, the National Geodetic Survey (NGS) installed Mini-Mac 2816AT receivers at Mojave, Westford and Richmond which, with the Tsukuba receiver, brought the network to an almost equal number of TI and Mini-Mac receivers. Simultaneous operations of TI and Mini-Mac receivers were conducted by the NGS at the three U.S. sites for a period of several weeks. Using this simultaneous data set in addition to the other CIGNET data, an investigation has been conducted into the compatibility of the all-TI and the mixed receiver configuration. The preliminary results have verified the existence of a 1 ms time tag discrepancy in the Mini-Mac data reported by others, however, a 2.5 cm unresolved discrepancy was found on the short TI to Mini-Mac baseline at Mojave. When the discrepancy in GPS time was corrected, several meter RMS orbit differences were found; however, the 1400 km test baseline between Onsala and Tromso demonstrated less than two parts in 10^8 agreement between the two cases. The results also demonstrated the existence of a change in Tromso antenna position from the location previously reported.

INTRODUCTION

Beginning in 1987, the National Geodetic Survey has been active in the development of the CIGNET. The site locations as of November 1988 are illustrated in Fig. 1 [*CSTG Bulletin*, Vol. 1, No. 3, 1988]. All site locations, except Tsukuba, consisted of TI-4100 receivers using the CORE software developed by the Applied Research Laboratory of the University of Texas (UT).

In January, 1989, Mini-Mac 2816AT receivers were installed at Mojave, Westford and Richmond. For several weeks after this installation, the TI receivers were operated simultaneously with the Mini-Mac. In addition, NGS performed local surveys to determine the position vector of the Mini-Mac antenna with respect to other geodetic markers in the vicinity of very long baseline interferometry (VLBI) systems.

Results obtained from mixed receiver types have been reported by (Gurtner et al., 1989), (Rocken et al., 1989) and (Chin, private communication, 1989). In the former case, a 1 ms time tag discrepancy with GPS time was observed when TI and Mini-Mac data were mixed. The source of the discrepancy was traced to the Mini-Mac software; however, the discrepancy is not apparent when only Mini-Mac data were used.

Because of the observed problems with mixing receiver types, the purpose of this study was to investigate the compatibility between TI and Mini-Mac in the use of CIGNET data for GPS orbit and baseline determinations, especially for longer baselines than those used in the previous studies. It was believed that this study was essential for the understanding of results obtained using CIGNET data after the TI receivers were removed and to aid in establishing historical links to prior campaigns using only TI receivers. The results presented in this paper are preliminary, and further detailed studies are planned.

DATA

The simultaneous operation of Mini-Mac and TI receivers at Mojave, Westford and Richmond began on January 30, 1989, in GPS Week 473 using Mini-Mac receiver software Version 1.49. The TI operations continued for approximately two weeks at Westford and Richmond after the Mini-Mac installation. At Mojave, the UT receiver operated until June. At all three sites, the displacement between the TI and Mini-Mac antennas was about 5 m or less.

For the preliminary analysis reported in this paper, only data from the first three days of simultaneous TI and Mini-Mac operation were used (January 30 to February 1, 1989). Since prior work had suggested that the TI data from Richmond would not be usable, these data were initially excluded from the analysis. However, further investigation showed the existence of a significant amount of usable TI data from Richmond. These data were used in some experiments, along with TI data from Kauai, Yellowknife, Wettzell, Onsala and Tromso.

PROCEDURE

The TI and Mini-Mac data at the three U.S. sites were used in two separate, but complementary analyses. First, the TI and Mini-Mac data were used for short baseline tests (<5 m) in which the TI to Mini-Mac vector baseline was determined at each of the three sites. The purpose of this test was to assess the reported time tag discrepancy and phase center of the respective antennas. Because of the very short baselines, L_1 only solutions were obtained, as well as ionospherically corrected solutions. For these analyses the orbits were fixed to a nominal ephemeris obtained from either pseudo-range or double-difference phase data. All baseline solutions were obtained with phase data.

Second, the GPS orbits were determined from double-difference phase data using a) only TI data and b) Mini-Mac data from Mojave, Westford and Richmond plus TI data from the other sites. In these cases, the typical estimated parameter set consisted of the epoch position and velocity for each satellite in the three-day arc, a scale parameter for the ROCK4 radiation pressure (Fliegel et al., 1985), a parameter for y-bias force, three-hour troposphere zenith delay, appropriate biases and selected antenna coordinates. No *a priori* constraints were used on any estimated parameters. The modeling of the GPS force and kinematic characteristics and the site coordinates are given by (Schutz et al., 1989a). In all cases, Tromso was treated as a site with unknown coordinates.

SHORT BASELINE TESTS

Analyses were performed on the short baseline between the TI antenna and the Mini-Mac antenna at each of the three U.S. sites. These analyses verified the existence of the 1 ms time tag correction required for the Mini-Mac data. In addition, a more detailed analysis was performed with the short baseline estimates at Mojave.

The orbit used for this analysis was derived from double difference phase data using only TI instruments (Case B in the next section). This orbit was fixed and the coordinates of the Mojave Mini-Mac were estimated with respect to the TI. The TI antenna at Mojave was the FRPA-2 and further information on the relative positions is given in the CSTG GPS Bulletin for May-June, 1989. The results are shown in Table 1 in which the Mini-Mac position vector is given with respect to the FRPA antenna used on the TI-4100. The Mini-Mac coordinates were obtained from the average of three individual solutions, each comprising a complete day of double differences between the TI and the Mini-Mac. This result was compared with the vector difference of positions for the respective antennas obtained on previous surveys. The resulting 2.5 cm vertical discrepancy is under investigation. No significant time tag adjustment to the Mini-Mac was obtained after application of the 1 ms discrepancy. Furthermore, the estimate was obtained with and without bias-fixing; however, both cases gave the same result to within a few millimeters.

ORBIT AND LONG BASELINE TESTS

Several cases were used for the orbit and long baseline tests. These cases were:

A. TI only data from Mojave, Westford, Richmond, Kauai, Wettzell, Onsala and Tromso,

B. Same as Case A except Richmond TI data were excluded,

C. Mini-Mac data from Mojave and Westford, no Richmond data and TI data from other sites.

The orbits that resulted from Case B and Case C are compared in Fig. 2 for PRN-9 and a tabular summary for all satellites is given in Table 2. For comparison, the tabular summary for the differences between Case A and Case B are shown in Table 3, showing the influence of Richmond TI data. Comparison of Table 2 and 3 indicates agreement between the three cases at the few meter level.

Since Tromso cannot yet be linked directly into a VLBI coordinate system (the mobile VLBI occupied a site at Tromso in July, 1989), Tromso has been treated as a site with unknown coordinates. The results obtained from the three cases considered are shown in Table 4, where the coordinates are given with respect to Onsala. The table also contains the number of double-difference measurements and the RMS of the global set of measurement residuals. All three cases give Tromso coordinates that agree to within 1.6 cm in (x, y, z) and 1.5 cm in the 1400 km baseline length, thus suggesting internal consistency at the level of a part in 10^8.

Comparisons of the Onsala to Tromso baseline with previously determined results are shown in Table 5. The previous results are given by (Schutz et al., 1989a; 1989b). While the previous results agreed with each other within about 8.5 cm in all components and in the baselines, the Week 473 results disagreed with the others by about 81 cm in height. This discrepancy prompted further investigation to identify the source. (Engen, private communication, 1989) indicated that a new pillar for the GPS antenna had been constructed at Tromso in November, 1988. The results from earlier weeks given in Table 5 were obtained with data collected prior to November, 1988, whereas the Week 473 results of this paper used data recorded after the pillar was installed. Detailed measurements of the pillar by the Norwegian Mapping Agency showed a change in height of about 81 cm, thereby justifying the conclusion that the Tromso discrepancy was caused by a change in the antenna height. This result is of further interest since the initial GPS result was obtained without knowledge of the antenna height change, thereby providing a "blind test." An additional test of the GPS determination of Tromso will be possible when the VLBI result is available at the end of 1989.

SUMMARY AND CONCLUSION

Data collected for a period of three days using the TI-4100 and the Mini-Mac 2816AT receivers collocated at Mojave and Westford were processed along with data from other CIGNET sites. Three-day orbit comparisons indicate that the impact of replacing TI-4100 with Mini-Mac on the orbits was less than four meters RMS. However, the effect on the Onsala to Tromso baseline determination was insignificant. A previously reported Mini-Mac one millisecond time tag discrepancy from GPS time was verified in the process of determining short (~5 m) baselines between the TI-4100 and the Mini-Mac antennas collocated at Mojave and Westford, however, an unresolved 2.5 cm discrepancy exists in the Mojave result. The baseline between Tromso and Onsala (~1400 km) was determined with a repeatability between three cases of 1 part in 10^8. An 81 cm change in antenna height at Tromso (due to new construction) was detected without any prior knowledge of the change. While this test can be regarded as a "blind test," an essential component of the test will be provided by the VLBI determination. Based on the analysis of three days of data, it can be tentatively concluded that TI-4100 and Mini-Mac 2816AT CIGNET receivers are sufficiently compatible for orbit determination to support a part in 10^8 baseline determinations. However, orbit differences at the few meter level require further investigation.

Acknowledgement. The data were preprocessed by D. Carroll, L. Burton and H. Rim at the Center for Space Research. The information provided by G. Mader and M. Chin at NGS for this study is gratefully acknowledged. This research has been supported by NASA.

REFERENCES

Gurtner, W.G., Beutler, G., and Rothacher, M., (1989), Combining GPS observations made with different receiver types, *Proceedings of the Fifth International Geodetic Symposium on Satellite Positioning*, Las Cruces, New Mexico, March 13-17.

Fliegel, H.F., Feess, W.A., Layton, W.C., and Rhodus, N.W., (1985). The GPS radiation force model, *Proceedings of the First International Symposium on Precise Positioning with Global Positioning System*, NOAA, Rockville, Maryland, April 15-19.

Schutz, B.E., Tapley, B.D., Ho, C.S., Rim, H.J., and Abusali, P.A.M., (1989a), GPS orbit determination: experiments and results, *Proceedings of the Fifth International Geodetic Symposium on Satellite Positioning*, Las Cruces, New Mexico, March 13-17.

Schutz, B.E., Ho, C.S., and Bevis, M., (1989b), Analysis of southwest pacific campaign data: July 1988, *Proceedings of the Fifth International Geodetic Symposium on Satellite Positioning*, Las Cruces, New Mexico, March 13-17.

Rocken, C. and Meertens, C.M., (1989), GPS antenna and receiver tests: multipath reduction and mixed receiver baselines, *Proceedings of the Fifth International Geodetic Symposium on Satellite Positioning*, Las Cruces, New Mexico, March 13-17.

Table 1. Mojave short baseline test (TI to Mini-Mac).

	Components and length (m)			
	x	y	z	l
L_1 Average of three days*	−1.197	−2.478	−4.180	−5.005
RMS of three days	0.001	0.001	0.001	0.006
Independent solution**	−1.181	−2.466	−4.196	5.008

*The three days in Week 473 were days 30, 31 and 32
**The independent solution was obtained by TI to TI and Mini-Mac to Mini-Mac local surveys at different times (*GPS Bulletin*, Vol. 2, No. 3, May-June 1989)

Difference (m) between the three-day and the independent solution		
North	East	Up
0.0013	−0.0054	0.0239

Table 2. Summary of orbit differences: EPH (C)-EPH (B).

	PRN-3	PRN-6	PRN-8	PRN-9	PRN-11	PRN-12	PRN-13
Mean (m)							
Radial	−0.026	0.007	−0.010	0.017	0.027	0.038	0.008
Along-Track	3.276	2.089	1.534	1.280	1.843	1.510	1.213
Cross-Track	−0.015	−0.013	−0.026	−0.027	−0.038	−0.003	0.006
RMS (m)							
Radial	0.957	0.922	0.890	0.298	0.165	0.497	0.251
Along-Track	3.935	2.794	2.354	1.427	2.003	2.001	1.341
Cross-Track	1.580	0.768	2.475	1.005	1.631	0.982	0.966

Table 3. Summary of orbit differences: EPH (B)-EPH (A).

	PRN-3	PRN-6	PRN-8	PRN-9	PRN-11	PRN-12	PRN-13
Mean (m)							
Radial	0.028	0.013	0.024	−0.006	0.015	−0.010	0.014
Along-Track	2.811	5.387	1.619	1.429	−0.577	−2.873	0.441
Cross-Track	−0.003	−0.024	−0.012	−0.023	−0.009	−0.017	0.001
RMS (m)							
Radial	0.519	0.902	0.083	0.317	0.297	0.727	0.280
Along-Track	3.037	5.725	1.758	1.574	0.862	3.250	0.769
Cross-Track	0.553	1.679	0.965	0.734	0.376	0.884	0.346

Table 4. GPS week 473 results.

Case	DD RMS(m)	No. of DD	Onsala to Tromso baseline (m)			
			Δx	Δy	Δz	l
A	0.021	25353	−1267718.165	9692.552	608406.658	1406187.026
B	0.019	19734	−1267718.149	9692.552	608406.661	1406187.014
C	0.019	19371	−1267718.154	9692.568	608406.647	1406187.011

DD = double differenced phase

Table 5. Onsala to Tromso baseline comparison with other results.

	Components and length (m)			
	Δz	Δy	Δz	l
Week 473 Case B	−1267718.149	9692.552	608406.661	1406187.014
Week 419 1 week soln	−1267718.396	9692.560	608405.885	1406186.900
Week 420 1 week soln	−1267718.417	9692.533	608405.862	1406186.909
Week 444 1 week soln	−1267718.414	9692.512	608405.882	1406186.915
Week 444 3 day soln w/o S. Pacific	−1267718.480	9692.566	608405.899	1406186.983

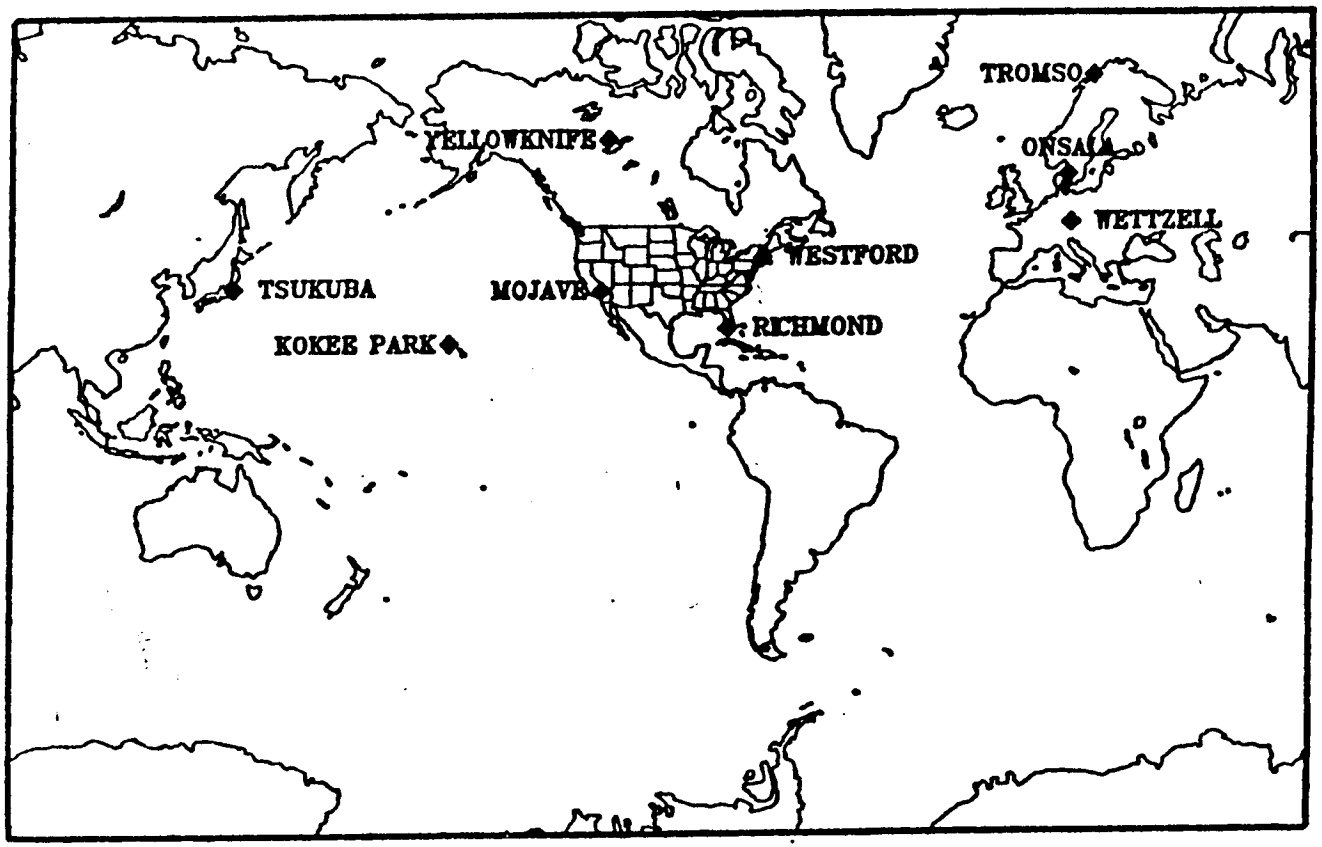

Figure 1. CIGNET Tracking Sites [CSTG GPS Bulletin]

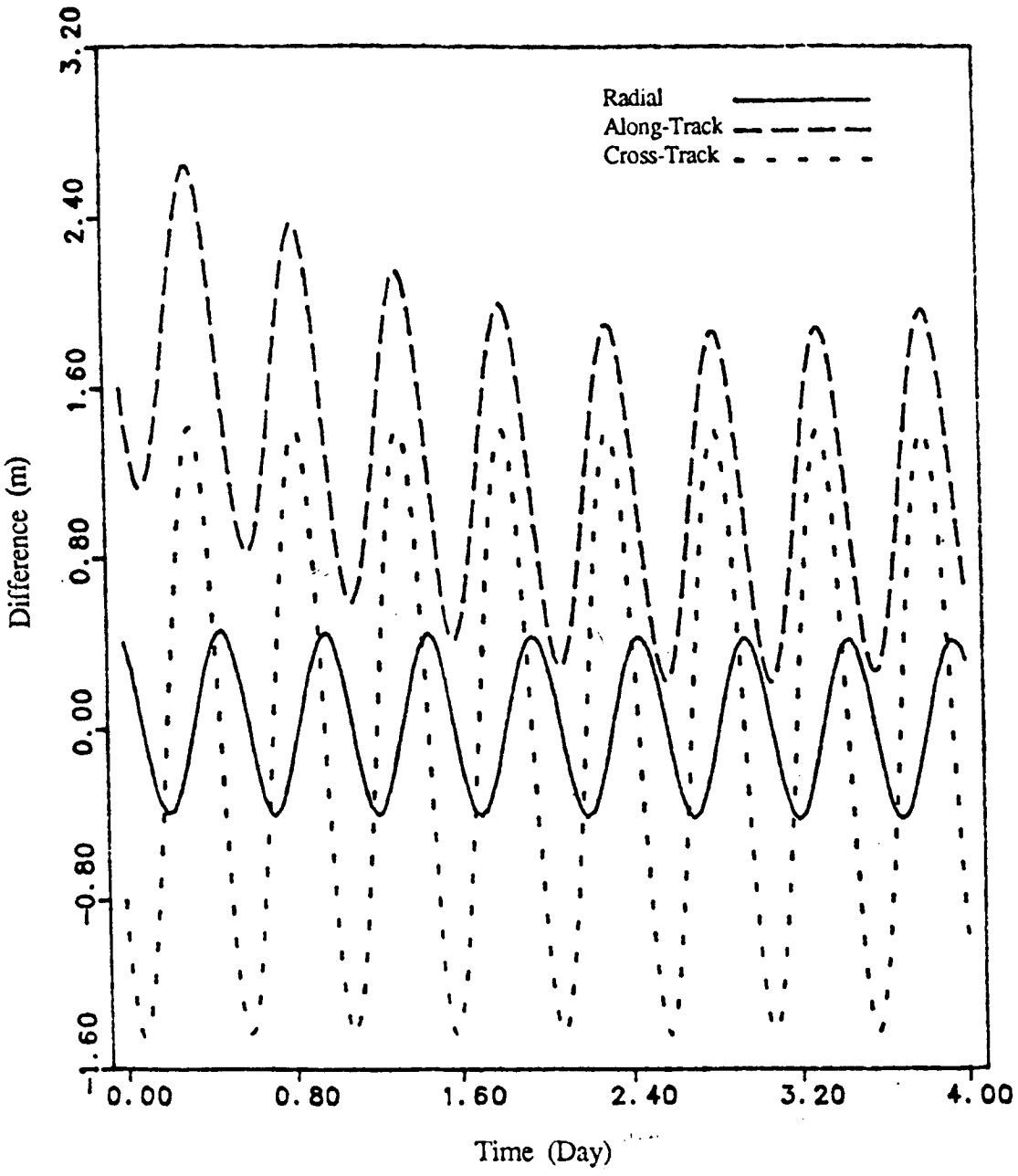

Figure 2. Comparison of solution trajectories in J2000 system for PRN-9
(Case C - Case B) Epoch - Jan.29,1989 00:00:00

APPENDIX X

"Observations of selective availability and the effect on precision geodesy," presented at the Fall Meeting of the American Geophysical Union, San Francisco, Calif., December 1990 (Abstract; Figures)

Analogy with Alaska, Chile, and Japan suggests that great earthquakes on the Cascadia subduction zone would have caused sudden lowering of land in coastal Washington. The fossil trees and grass add to previously reported evidence that such earthquakes did occur, even though none have happened in the 200 years since Europeans arrived in the Pacific Northwest.

G12B CA: 303 Mon 1440h
The Impact of Selective Availability (SA) on GPS Geodesy
Presiding: W Melbourne, Jet Propulsion Lab; K Feigl, MIT

G12B-1 1440h INVITED
An Overview of GPS Selective Availability

T P Yunck (Jet Propulsion Laboratory, California Institute of Technology, Pasadena, CA 91109)

Selective Availability, or SA, is now active nearly full time on the GPS Block II satellites, ten of which are due to be in service by December of 1990. SA is designed to degrade the real time positioning accuracy attainable by those not authorized to use the GPS Precise Positioning Service. Notably, it is within the constraints of unauthorized use that a number of scientific groups are now achieving geodetic accuracies of 1:10^8 or better over distances ranging from hundreds to many thousands of kilometers—undoubtedly the most precise GPS measurements being made in any conditions.

There is nonetheless a good deal of concern over SA among the unauthorized, a situation that has been encouraged by the rather elusive manner in which SA has been officially portrayed to the outside world. This presentation will attempt to address common SA questions by reviewing GPS signal structure, defining the two methods (data message corruption and "dithering") by which SA errors are imposed, giving quantitative examples of the effect of SA on point positioning and baseline determination, describing strategies by which SA effects can be minimized, and illustrating these topics with data and results taken from recent experiments.

G12B-2 1500h INVITED
Global Positioning System (GPS) Policies

Lt Col Jules G. McNeff, USAF (Military Assistant to the Assistant Secretary of Defense for Command, Control, Communications and Intelligence, Pentagon, Rm 3D174, Washington, DC 20301-3040, 703-695-6123) (Sponsor: Dr. William Melbourne)

This presentation will cover the overall process for radionavigation system plan and policy development which culminates in the biennial Federal Radionavigation Plan. It will highlight current plans and policies affecting the Global Positioning System (GPS). These include availability of and access to GPS services, implementation of selective availability and anti-spoofing features and requirements for access to precise GPS capabilities.

G12B-3 1515h INVITED
Ethical Considerations for the Custodians of GPS

Roger Bilham, Department of Geological Sciences and CIRES, University of Colorado, Boulder CO 80309.

Since its inception, the military architects and custodians of the Global Positioning System (GPS) have maintained a consistent policy concerning the availability of the precise positioning code to the civilian community. "Access to the code can and will be denied". Where alternative methods exist this policy has moderated the wholesale adoption of GPS geodesy, because of the financial risk of investing in the acquisition of commercial GPS receivers that may become unusable in the near future. Where alternative methods are not available because of the unique qualities of GPS positioning, the possible denial of future availability continues to alarm the scientific community. Several ongoing crustal deformation programs have as a fundamental goal the mitigation of seismic and volcanic hazards. The denial of the precise positioning code to such programs raises ethical and moral issues that were unforeseen at the time that selective availability was being designed into the GPS.

A policy to permit continued access to the GPS precise positioning code in its unencrypted original form would provide two benefits to the custodians of the GPS: it would be perceived as a generous contribution by the US to hazard mitigation in many nations of the world, and its free availability would inhibit the proliferation of alternative navigation systems by other nations who for commercial reasons would not wish to include limited access. It is clear that the GPS precise positioning code has enormous benefits to civilization beyond any military application. If the AS and SA limited access signals are implemented and cannot be successfully overcome in geodetic applications, it may be desirable for the world scientific community to launch its own satellite system for geodetic control in sea level, earthquake and volcano studies.

G12B-4 1530h
Monitoring S/A and its Effect on GPS Geodesy

Rocken C.[1]·[2] and C.M. Meertens[1]·[3]
[1]UNAVCO/CIRES, CB 216 Univ. of Colorado, Boulder, CO, 80309. [2]Colorado Center for Astrodynamics Research, CB 431 Univ. of Colorado, Boulder, CO, 80309. [3]Dept. of Geol. + Geophys., Univ. of Utah, Salt Lake City, UT, 84112.

We present a technique to monitor the level of S/A clock dithering of Block II GPS satellites. Frequency offsets due to S/A can be monitored to within ~0.1 Hz for double differences and with an uncertainty of ~0.5 Hz for single differences if a rubidium oscillator is used. We observed frequency offsets due to S/A of +/- 1.6 Hz from the nominal GPS carrier frequency (see figure below). Monitoring S/A may aid post-processing high accuracy point positioning applications. Our limited data set also shows that S/A monitoring is generally not required on any terrestrial baseline for high accuracy relative GPS geodesy. Results obtained from zero-baseline tests indicate that clock dithering causes maximum double-difference phase residuals (dd_{max}) as a function of receiver clock synchronization error of: dd_{max} = 0.04 cm/msec; and as a function of baseline length of: dd_{max} = 0.014 cm/(100 km). Since these are linear relations for maximum observed values of post-fit residuals due to S/A, the effect on the baseline will be smaller than 0.014 cm for a baseline separation of 100 km. We conclude that S/A clock dithering effects can be monitored and corrected for, but they are more conveniently neglected in double-difference processing if the GPS receivers remain synchronized to better than 10 msec.

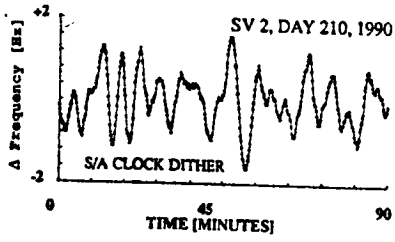

G12B-5 1545h
A Scheme for Reducing the Effect of Selective Availability on Precise GPS Carrier Phase Measurements

KURT L. FEIGL, ROBERT W. KING, THOMAS A. HERRING, AND MARKUS ROTHACHER*; MIT 54-610, Cambridge MA 02139;
(617) 253-6872 (* visiting from University of Berne)

In early 1990, the Department of Defense began dithering the carrier frequency transmitted by Block II satellites of the Global Positioning System (GPS). We can characterize the dithered oscillator frequency by differentiating the phase received at stations equipped with atomic frequency standards. It appears that the deviations from the nominal frequency of 1.5742 GHz are typically 1-2 Hz or several parts in 10^9. Moreover, these deviations vary rapidly with time, often reversing sign within a span of 5 to 10 minutes. If left unmodeled, the deviations produce quasi-periodic arches in one-way residuals with amplitude of order 100 cycles. For data sampled at the same nominal receiver time, the amplitude of the arches in double differences is small, less than 0.02 cycles for transcontinental baselines. For asynchronously sampled data, however, these arches can map into the double differences with an amplitude of up to several cycles. The magnitude of the problem is roughly proportional to the difference in sampling times between the receivers. For example, the extreme, but typical case of a Minimac 286AT (sampling at the even GPST minute) and a TI4100 (sampling 0.92 seconds earlier), produces doubly-differenced residuals with an RMS of about 0.6 cycles ("broadcast" in Figure). To estimate the frequency deviation from the nominal value, we differentiate the phase sampled at 30 second intervals by the CIGNET receiver at Mojave. At this station, the local oscillator is a hydrogen maser, but we expect that any atomic standard stable at the level of 10^{-11} would be adequate for this purpose. For convenience, we parameterize the deviation of the satellite oscillator using the same three coefficients (a_{f0}, a_{f1} and a_{f2}) as broadcast by the satellite in its navigation message. Using one set of these values every 30 seconds, we can reduce the RMS in asynchronously sampled doubly-differenced residuals by a factor of 6, to about 0.1 cycles ("modeled" in Figure). This scatter is still worse than for Block I satellites without Selective Availability, but might be improved if one of the CIGNET stations sampled more frequently. Although our approach can model most of the effect of Selective Availability on asynchronously sampled data, a simpler approach for future surveys is to program the receivers to sample the phase as close to simultaneously as possible. For consistency with the CIGNET stations in North America, this means sampling at 0.0 s after the even minute GPST.

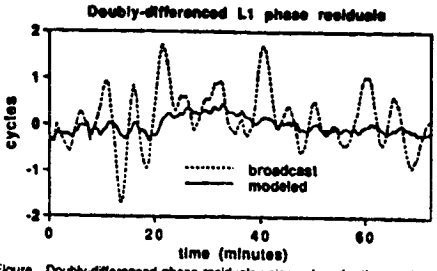

Figure. Doubly-differenced phase residuals using values for the satellite frequency as broadcast in the navigation message and as modeled at Mojave. The data were transmitted by PRN 16 (Block II) and PRN 3 (Block I) and received at Mojave and Owens Valley, California. The receivers sampled at times separated by 0.92 seconds.

G12B-6 1600h
The Impact of Recent Selective Availability on Precise Relative Positioning with Static GPS

D. Rosenblatt, Y. Bock[1], J-B. Minster and D.C. Agnew (IGPP, Scripps Institution of Oceanography, La Jolla, CA 92093;[1] also at Jet Propulsion Laboratory, California Institute of Technology, Pasadena, CA 91109)

We have examined the impact of the recent implementation of Selective Availability (SA) on Block II GPS satellites on daily three dimensional relative position estimates of the Permanent GPS Geodetic Array (PGGA) sites in California. We conclude that as long as the simultaneity of observation time tags is maintained between receivers, SA alterations of the GPS signals do not degrade positioning accuracy when using several hours of doubly-differenced phase measurements. In fact, adding observations of the SA affected Block II satellites improves baseline repeatability (even in California where Block I geometrical coverage is quite favorable).

The PGGA became operational at about the same time that the Department of Defense initiated SA. Data are collected daily at Scripps Institution of Oceanography (SIO) and the Jet Propulsion Laboratory (JPL) from three Rogue SNR-8 receivers deployed at JPL, SIO, and Piñon Flat Observatory, and from three Mini-Mac 2816AT receivers at the CIGNET tracking stations in California, Massachusetts, and Florida. In the first few weeks of operation, the time tags of the Rogue (UTC based) and Mini-Mac receivers (GPS time based) were offset by 6 seconds. The Rogue receiver time tags were subsequently modified to be GPS time based. We examined the repeatability of position determinations of JPL, Piñon and SIO relative to the fixed CIGNET sites, using five days during the initial period of time tag discrepancy and four days after the time tags were synchronized. To test the effects of SA on relative positioning within the array, we performed daily, simultaneous, orbit improved network solutions of the Rogue and Mini-Mac data with only Block I satellite observations (unaffected by SA), and with both Block I and II observations. We report on the experiments that we performed on these data using different orbit improvement schemes, and arrive at the encouraging conclusion described in the first paragraph. However, we have learned that current SA has very adverse effects on networks with non-simultaneous observations, and makes data editing more problematic, even with P-code based receivers. We also assess the effects of SA alterations in the navigation message by comparison with orbit improved solutions.

G12B-7 1615h
OBSERVATIONS OF SELECTIVE AVAILABILITY AND THE EFFECT ON PRECISION GEODESY

B. E. Schutz (Center for Space Research, The University of Texas at Austin, Austin, Texas 78712)
Y. C. Chao, R. Gutierrez, and C. Wilson

From July 15-July 22, several experiments with GPS receivers were conducted on zero length baselines at McDonald Observatory (TX), Platteville (CO), and Quincy (CA) as part of a GPS campaign in West Texas, New Mexico, and Nevada. TI-4100 and Trimble 4000ST receivers were used on the zero length baselines with recording epochs that differed by 0.92 s. The McDonald Observatory TI was connected to a cesium oscillator, while all other receivers used internal oscillators. Evidence of selective availability is apparent in the double-differenced residuals; for example, the differences between TRN 3 and 20 exhibit periodicities within rms of about 10 cm, a characteristic not observed when only Block I satellites are used. Similar characteristics were observed at two different sites. The nature of the periodicities and techniques for their removal are presented, and the influence of these characteristics on long baselines is examined.

G12B-8 1630h
The Effect of SA on Baselines from the California GPS Array in Southern California

Frank H. Webb, Ulf J. Lindqwister, Geoffrey Blewitt, and James Zumberge (All at: Jet Propulsion Laboratory, California Institute of Technology, Pasadena, CA 91109; 818-354-4670)

GPS observables are routinely collected from an array of continuously operating Rogue receivers in southern California. The receivers are located at Pinyon Flat in the Santa Rosa Mountains, Scripps Institution of Oceanography in La Jolla, and at JPL in

OBSERVATIONS OF SELECTIVE AVAILABILITY AND THE EFFECT ON PRECISION GEODESY

B. SCHUTZ, Y. CHAO, R. GUTIERREZ, C. WILSON

CENTER FOR SPACE RESEARCH

THE UNIVERSITY OF TEXAS AT AUSTIN

AGU
DECEMBER 1990
SAN FRANCISCO

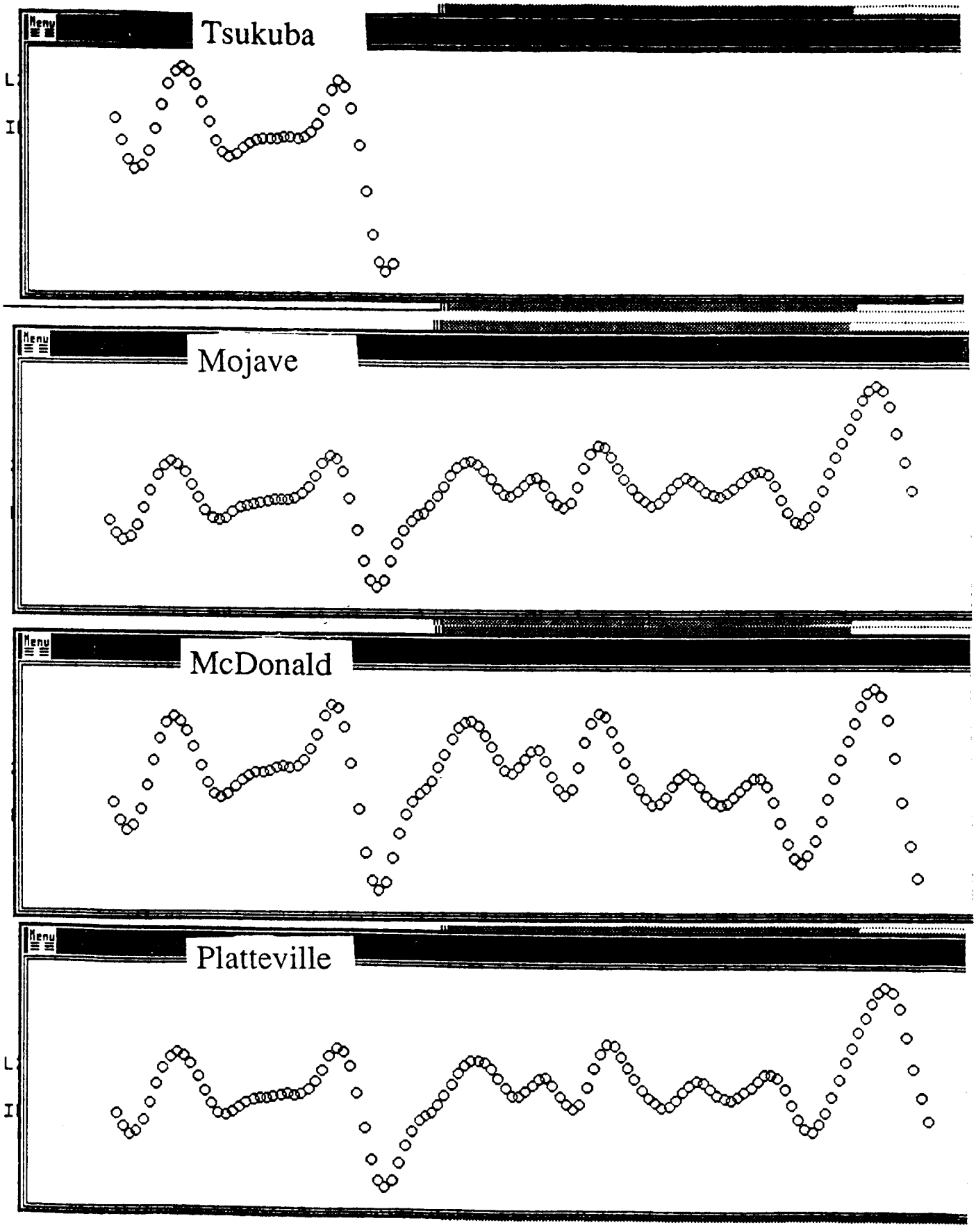

RESIDUALS, PRN 20, Week 549, 167-168 Hours

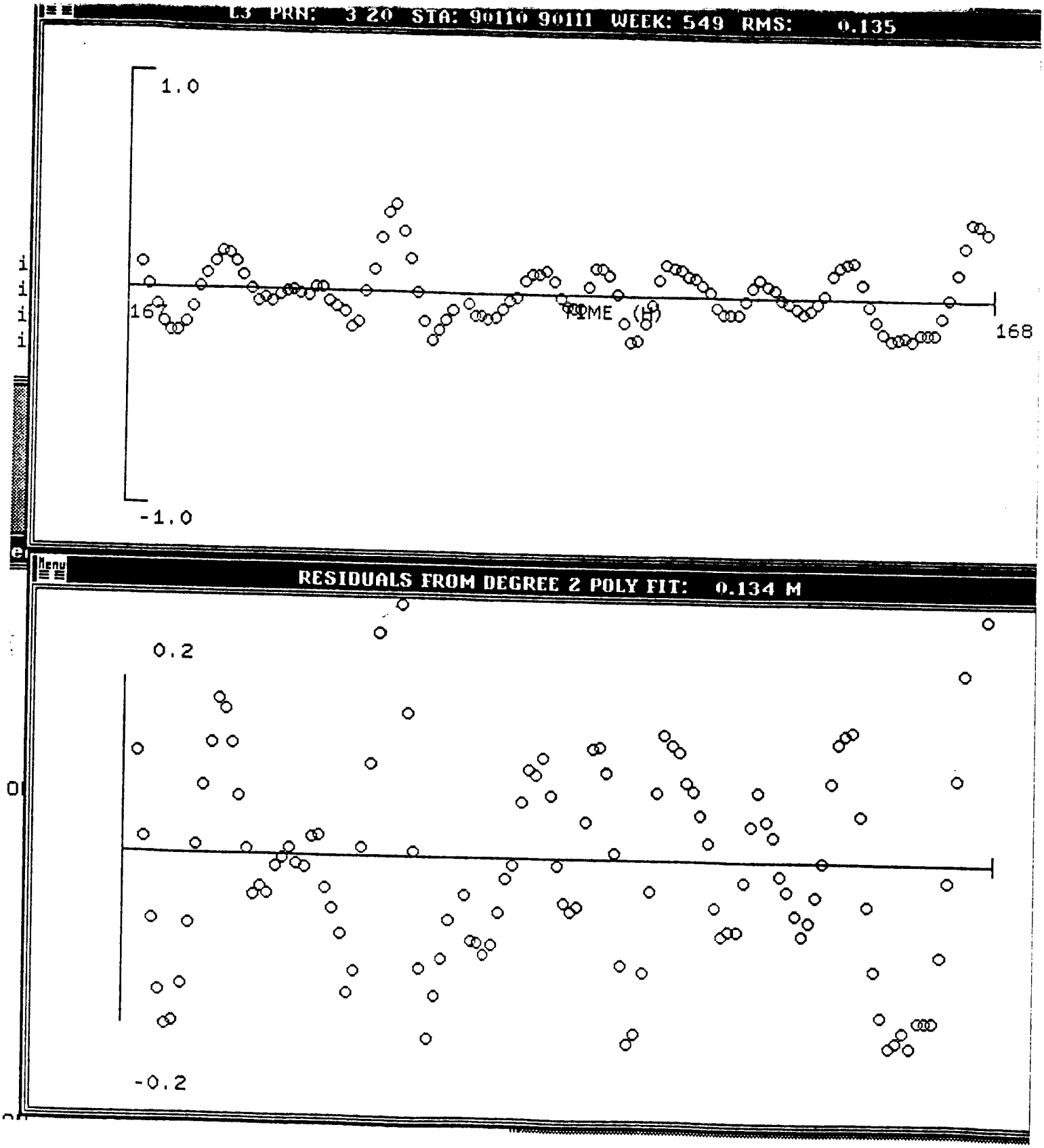

Double Difference Residuals Showing SA-Induced Effects
Caused by Nonsynchronized Receivers